



Alexander Schmon, Dipl.-Ing.

Density Determination of Liquid Metals by Means of Containerless Techniques

DOCTORAL THESIS

to achieve the university degree of
Doktor der technischen Wissenschaften
submitted to

Graz University of Technology

Supervisor

Ao.Univ.-Prof. Dipl-Ing. Dr.techn. Gernot Pottlacher

Institute of Experimental Physics

AFFIDAVIT

I declare that I have authored this thesis independently, that I have not used other than the declared sources/resources, and that I have explicitly indicated all material which has been quoted either literally or by content from the sources used. The text document uploaded to TUGRAZonline is identical to the present doctoral thesis.

Date

Signature

Abstract

Density is a fundamental thermophysical quantity for describing the behaviour of metals and alloys in the liquid phase. The high temperature and intense reactivity of metallic melts pose a challenge for creating investigation settings and determining properties of the specimen material.

This thesis deals with density determination using two very different investigation methods. A fast resistive pulse-heating technique based on the approach to avoid interactions of the liquid specimen material with its environment by extremely reducing the experimental duration; and an electromagnetic levitation setup preventing interactions with the environment by creating non-contact conditions through levitating the specimen material.

The pulse-heating setup at TU Graz provides the investigation of liquid metals by performing short-term studies. Wire shaped specimens are resistively self-heated as part of an electrical discharge circuit. Heating rates up to $10^8 \text{ K} \cdot \text{s}^{-1}$ lead to experimental durations of about $60 \mu\text{s}$. This short process enables the investigation of vertical aligned liquid metal columns maintaining their shape until the boiling point is reached.

The electromagnetic levitation setup at TU Graz is based on heating and levitating a specimen by a levitation coil generating high-frequency electromagnetic fields. Induced eddy currents heat the specimen material in its liquid phase and electromagnetic forces hover the specimen toward regions of lower field strength.

In the course of this work the radial thermal expansion measurement approach of the pulse-heating method at TU Graz was used to render possible reliable density determinations up to temperatures of about 5500 K. The comparison of the quasi-containerless method of pulse-heating and the containerless method of electromagnetic levitation shows the individual limitations of the techniques regarding density determination, as consequence of their different experimental approaches.

Liquid phase densities as function of temperature for nickel, copper, aluminium, Manganin ($\text{Cu}_{86}\text{Mn}_{12}\text{Ni}_2$) and TiAl6V4 were determined and are presented.

Kurzfassung

Die thermophysikalische Größe Dichte ist ein wichtiger Parameter um das Verhalten von flüssigen Metallen und Legierungen zu beschreiben. Ihre Ermittlung erweist sich jedoch als besondere Herausforderung, da sich flüssige Schmelzen üblicherweise durch sehr hohe Temperaturen und besonders ausgeprägte Reaktivität auszeichnen. Diese Arbeit beschäftigt sich mit der Dichtebestimmung flüssigen Metalls unter Verwendung zweier unterschiedlicher Untersuchungsmethoden. Eines ohmschen Pulsheizaufbaus, darauf basierend Interaktionen zwischen Probenmaterial und Umgebung durch extreme Verkürzung der Untersuchungszeit zu verhindern. Sowie einer elektromagnetischen Levitationsanlage, die Interaktionen vermeidet indem kontaktfreie Untersuchungsbedingungen durch Schweben des Probenmaterials hergestellt werden.

Der Pulsheizaufbau an der TU Graz ermöglicht die Untersuchung von flüssigem Metall im Rahmen von Kurzzeitexperimenten. Dabei werden drahtförmige Proben als Teil eines elektrischen Entladungskreises, bei Heizraten von bis zu $10^8 \text{ K} \cdot \text{s}^{-1}$, von der festen bis zur beginnenden Gasphase innerhalb von $60 \mu\text{s}$ aufgeheizt. Die innerhalb dieses kurzen Zeitfensters vertikal ausgerichteten flüssigen Metallsäulen können bezüglich ihrer thermophysikalischen Eigenschaften untersucht werden.

Die elektromagnetische Levitationsapparatur an der TU Graz nutzt eine Levitationspule um Metallproben mittels hochfrequenter elektromagnetischer Felder in einen Schwebезustand zu versetzen. Induzierte Wirbelströme heizen das Probenmaterial in die flüssige Phase.

Im Rahmen dieser Arbeit wurde der Pulsheizaufbau der TU Graz verwendet um zuverlässig Dichtemessungen bis zu Temperaturen von 5500 K zu ermöglichen. Der Vergleich der quasi-gefäßfreien Methode des Pulsheizens mit der tatsächlich gefäßfreien Methode der elektromagnetischen Levitation zeigt die verschiedenen Vorzüge und Limitierungen der beiden Untersuchungsmethoden bezüglich Dichtebestimmung, die sich aufgrund ihrer unterschiedlichen experimentellen Herangehensweisen ergeben.

Für Kupfer, Nickel, Aluminium, Manganin ($\text{Cu}_{86}\text{Mn}_{12}\text{Ni}_2$) und TiAl_6V_4 wurden die Dichten als Funktion der Temperatur in der flüssigen Phase ermittelt und werden in dieser Arbeit präsentiert.

Contents

1	Introduction	1
2	Experimental Methods	4
2.1	Archimedean	4
2.2	Pycnometric	6
2.3	Dilatometer	7
2.4	Bubble Pressure	8
2.5	Sessile Drop	10
2.6	Levitation	11
2.7	Radiation	13
3	Pulse-Heating	16
3.1	Exerimental setup	17
3.2	Measured quantities	20
3.2.1	Electrical quantities	20
3.2.2	Thermal radiance	21
3.2.3	Thermal radial expanding	24
3.3	Data evaluation	28
3.3.1	Enthalpy and isobaric heat capacity	30
3.3.2	Electrical resistivity	31
3.3.3	Temperature	32
3.3.4	Thermal conductivity and thermal diffusivity	35
3.3.5	Thermal radial expansion and density determination	36
4	Levitation	46
4.1	Electromagnetic levitation	47

4.2	Experimental setup	49
4.2.1	Experiment atmosphere	53
4.2.2	Temperature	54
4.2.3	Levitation coil construction	55
4.2.4	Image acquisition system	56
4.3	Density determination	57
4.3.1	Experimental procedure	58
4.3.2	Evaluation procedure	59
5	Measuring Results	67
5.1	Nickel	68
5.2	Copper	73
5.3	Aluminium	78
5.4	Manganin - Cu ₈₆ Mn ₁₂ Ni ₂	83
5.5	TiAl ₆ V ₄	88
6	Uncertainties	92
6.1	Pulse-heating	93
6.2	Levitation	97
7	Discussion	98
8	Outlook	104
9	Publications	105
	Bibliography	129
	List of Figures	136

1 Introduction

In understanding and describing the behaviour of metals and alloys in the liquid phase, knowledge of thermophysical basic properties, such as density, surface tension, viscosity ect., is an essential requirement.

Beside the fundamental interest in scientific knowledge, understanding the mechanisms in metallic liquid phases is of direct practical importance, as the majority of metallic work pieces is produced by manufacturing processes of melting and casting.

In the last two decades numerical simulations of solidification, casting and welding processes have become established methods for improving modern production routines. The lack of reliable data of thermophysical properties, particularly in the high temperature range, poses a limiting factor for the quality of computer based modelling results.

The quantity density is of primary importance as it is input parameter in the determination of most other basic quantities (as surface tension, viscosity) of liquid metals. Density is required as parameter for example in mass balance calculations, descriptions of convection, simulations of solidification, fluid flow behaviour and heat flow descriptions. Considered from a general point of view, density is required to constitute the radial distribution function describing a structure model of a liquid.

The scarcity of thermophysical data for commercially used high-melting alloys above their liquidus temperatures reflects the difficulties to handle and investigate metals in this temperature range. Challenging factors that need to be dealt with are the very high temperature (usually above 1000 K) and the intense reactivity of metallic high temperature liquid phases. This demands investigation settings preventing contaminations of the sample material under investigation

and problems with heat transfer, loss of mechanical strength and evaporation have to be taken into account.

Essentially following approaches are possible to handle the high temperatures and to isolate the investigated liquid metal from potential reactants:

- Usage of inert crucibles. This means that materials used for contact areas between the liquid metal and containment should be selected carefully to avoid chemical reactions between the sample and its environment. In case of liquid metals commonly ceramics (e.g sapphire, boron nitride) or graphite are used as isolating material. The temperature of arising chemical reactions between crucible material and liquid sample determines the upper temperature limit of investigation as the composition of the investigated sample is changed.
- Reduction of experimental duration. This approach is based on the idea to minimize interactions with the environment and to extend the temperature range up to higher temperatures by reducing the investigation time to the subsecond-range. Pulse-heating techniques have been developed, heating and investigating a sample in time regimes of milliseconds (primarily used for investigating the solid phase) and microseconds (for investigating the liquid phase). Outstanding feature of these techniques is the possibility to reach temperatures of several thousand Kelvin and thereby to investigate the entire liquid phase of a sample material. Problems with containment interactions are avoided but the short-term investigation restricts the accuracy of the measurement.
- Evade containment by levitating the specimen. Interactions with the environment are minimized by establishing non-contact conditions. The specimen is hovered and suspended by an external force and is investigated using non-contact diagnostics as well. Techniques based on aerodynamic, acoustic, electrostatic and electromagnetic levitation have been developed. This approach enables the investigation of highly reactive specimens and provides the opportunity for undercooling a melt because of the absence of containment-wall initiated heterogeneous nucleation.

Depending on the material to be investigated, the amount of material available, the temperature range in question and the accuracy needed various investigation methods have been developed based on the mentioned approaches; some common used methods are described in chapter 2.

This thesis deals with density determination using two very different investigation techniques. On the one hand a fast resistive pulse-heating setting was employed enabling investigations of metals in the liquid state within reduced experimental time-regimes of about $50 \mu\text{s}$. On the other hand an electromagnetic levitation apparatus was built up, as cooperation project of Dipl.-Ing. Kirmanj Aziz and the author of this thesis, based on the approach to create a containerless investigation setup and thereof allowing the investigation of highly reactive metallic melts in a several minutes time-regime.

The workgroup of thermophysics and metalphysics (formerly workgroup of sub-second thermophysics) at the Institute of Experimental Physics at TU Graz has applied pulse-heating experiments for about 35 years. Setups working in the μs time-range and below were build up to create a so called 'quasi-containerless' investigation environment, with the objective to investigate thermophysical properties of the liquid phase of metals and alloys. Uprightly fixed wire specimen are resistive self-heated from room temperature up to the end of the liquid phase by a large current pulse (about 10000 A). Heating rates in the order of $10^8 \text{ K} \cdot \text{s}^{-1}$ entail short-term experimentations of vertically aligned liquid metallic columns with preserved geometry in the entire liquid phase until the boiling point is reached.

Purpose of this thesis was to focus on the pulse-heating density determination to exploit the potential to determine density in a temperature range unattainable for most other investigation techniques (up to temperatures of about 5500 K). The results obtained are compared to density results received employing the concurrently built-up containerless electromagnetic levitation apparatus.

2 Experimental Methods of Density Determination

Several methods have been developed to determine the density of liquid metals and alloys. Based on the different approaches used to handle and investigate the liquid specimen each method has its own constraints regarding temperature range and accuracy. Depending on the material to be investigated and particular measuring requirements the individual method's strengths and weaknesses have to be taken into account to choose the appropriate investigation method.

This chapter is intended to provide an overview of commonly used methods to determine density and their functionality, and should be understood as literature compilation to give the reader an outline of the techniques employed in this area of research.

2.1 Archimedean method

A detailed description of the Archimedean method can be found in [1–4].

The Archimedean method is based on the density-dependence of hydrostatic buoyancy force, exerted on an submerged body by the ambient fluid. There are two versions:

- The direct type:
A suitable inert solid of known volume is submerged in the liquid metal under investigation.

- The indirect type:
The liquid metal specimen is contained in a crucible that is submerged in a suitable, inert liquid of known density.

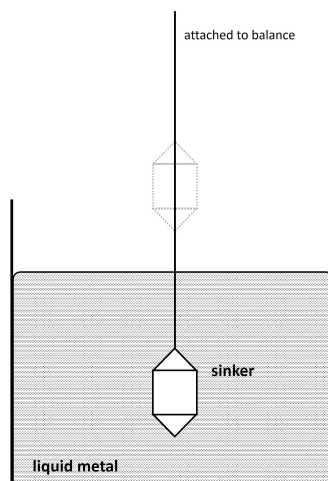


Figure 2.1: Schematic depiction of the direct type version of Archimedeian method.

By weighing the solid before and during submersion with a balance, density can be determined using the known principles of buoyancy. Figure 2.1 depicts schematically the direct type version of the Archimedeian method. The sinker is usually made of silica, graphite, metal or ceramic depending on the liquid under investigation. For lifting and lowering the sinker, with simultaneous weight measurement, the sinker is attached by a wire to the arm of the balance. As the direct type is much more straightforward in experimental handling, this approach is the usual implementation of the Archimedeian method.

To achieve high accuracy, the volume of the immersed part of the holding wire has to be known and thermal expansions of the wire and sinker have to be taken into account. Additionally force caused by surface tension with respect to the immersing holding wire has to be considered.

The following expression for determining density D can be derived in case of a direct type setting:

$$D = \frac{W_1 - W_2 + \sigma}{V + V_W} \quad (2.1)$$

with

- W_1 ... weight of the sinker before immersion
- W_2 ... weight measured when the sinker is submerged
- V ... volume of the sinker
- V_W ... volume of the wire part immersed in the liquid
- σ ... force caused by surface tension acting against the immersion of the wire. $\sigma = 2\pi r\gamma\cos\theta$, with radius of the wire r , surface tension of the fluid γ , contact angle between wire and fluid θ .

The lack of reliable surface tension data for liquid metals is a limiting factor for this calculation. Various experimental solutions have been developed to find a correction for the surface tension effects, from using a holding wire with varying diameter, using sinkers of different volumes or using two sinkers simultaneously. The Archimedean method enables density determinations over a wide temperature range. Especially for investigating less reactive fluids at low temperatures data with high accuracy can be obtained. In case of metals at high temperatures interactions between sinker and wire material with the liquid metal specimen are hardly to prevent and the difficulty to ensure uncontaminated surfaces on a metallic liquid hamper surface tension effect corrections.

2.2 Pycnometric method

A detailed description of the pycnometric method can be found in [1, 2, 4].

The principle of this method is to measure the mass of a metal specimen by filling a capacity of fixed volume. Pycnometers used in the high temperature range are made of refractory materials such as graphite, ceramics, boron nitride. For density determination the solid specimen is melted and filled in the holding capacity of the pycnometer. After solidification the mass of the specimen material is measured and the density is determined. This method is based on a precise knowledge of the volume of the holding capacity requiring a careful choice of

material and precise manufacturing of the capacity. The volume of the capacity is usually calibrated at room temperature using liquids of well known density and thermal expansion is considered using precise data of expansion coefficients. Care has to be taken to ensure a complete filling of the capacity with the liquid specimen material.

Disadvantage of this method is that no continuous temperature dependent density determination can be performed. For each temperature point a separate filling and weighing of the specimen material is necessary.

2.3 Push-rod dilatometer method

A detailed description of the dilatometric method can be found in [2, 4–6].

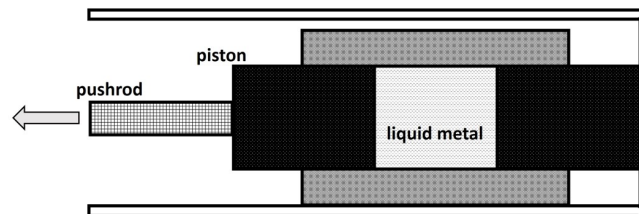


Figure 2.2: Schematic depiction of the push-rod dilatometer functionality.

The principle of dilatometers is to measure volume and volume changes of a specimen of known mass. Push-rod dilatometers are frequently used to determine the linear thermal expansion of solid materials. By using crucibles containing of piston cylinders the measuring abilities have been extended to handling liquid phases. The liquid specimen is placed in a cylindrical container of a material of known thermal expansion properties between a plate and a moveable piston. Figure 2.2 depicts the principle functionality schematically. The thermal expansion of the liquid specimen is determined by measuring the movement of the piston. The sample holders are made of refractory materials such as graphite, sapphire or polycrystalline alumina depending on the specimen material under investigation. For calibrating the dilatometer system commonly sapphire standards are

measured under the same conditions used for the specimen measurement. Single and dual push-rod dilatometers are available. The former determines the absolute volume change of a material; the second compares the length change compared to a reference material. The measured thermal expansion of the liquid specimen contains of the volumetric expansion of the specimen material and the radial expansion of the container, requiring a correction of the data. The temperature range attainable is determined by the furnace and specimen holder material. Dilatometers with a temperature range up to 2000 K are commercially available.

2.4 Maximum bubble pressure method

A detailed description of the maximum bubble pressure method can be found in [2–4, 7].

In this method density is determined by measuring the hydrostatic pressure. The liquid metal is placed in a container. A capillary tube, made of refractory materials, is immersed in the liquid and by sending gas through the tube a small spherical bubble is formed at the end of the nozzle. Figure 2.3 depicts the setting schematically. The maximum pressure to produce the bubble can be described by summation of the hydrostatic pressure of the liquid and the pressure caused by the surface tension of the bubble:

$$p = Dgh + \frac{2\gamma}{r} \tag{2.2}$$

with

- D ... density of the liquid metal
- h ... immersion depth of the capillary tube
- γ ... surface tension of the liquid metal
- r ... radius of the formed spherical bubble

The unknown surface tension γ can be eliminated by performing measurements at different immersion depths and density can be obtained by:

$$D = \frac{p_1 - p_2}{g(h_1 - h_2)} \quad (2.3)$$

with

p_1, p_2 ... pressures to produce the bubble at different immersion depths

h_1, h_2 ... different immersion depths

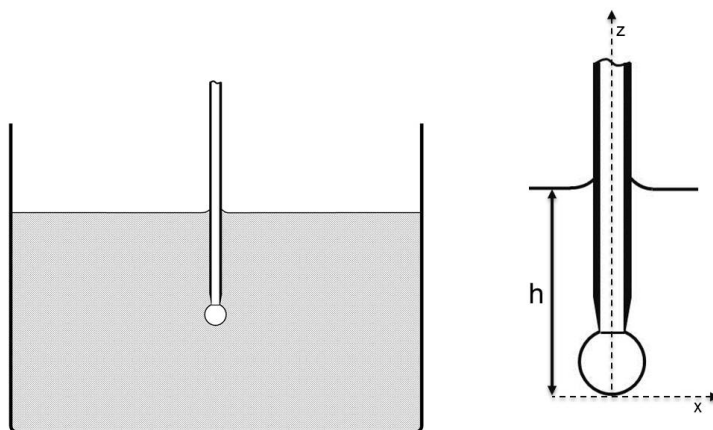


Figure 2.3: Schematic illustration of the maximum bubble pressure method.

It is assumed that surface tension and radius of the bubble are independent of immersion depth, requiring a homogeneous temperature of the liquid. Corrections have to be made to take into account the thermal expansion of the capillary tube increasing the length of the tube below the liquid surface and therefore on the one hand changing the immersion length and on the other hand displacing liquid. Additionally the thermal expansion of the container has to be considered. Care has to be taken in using a reliable gas-purification assembly to avoid oxide films arising on the metal surface.

Advantage of this method is that by producing a new bubble a new surface is generated, reducing contaminations and allowing the investigation of reactive metals. Additionally this method can be used for surface tension determinations as well. Disadvantage is the requirement of a relatively large amount of liquid metal.

2.5 Sessile drop method

A detailed description of the sessile drop method can be found in [2, 4, 8–10].

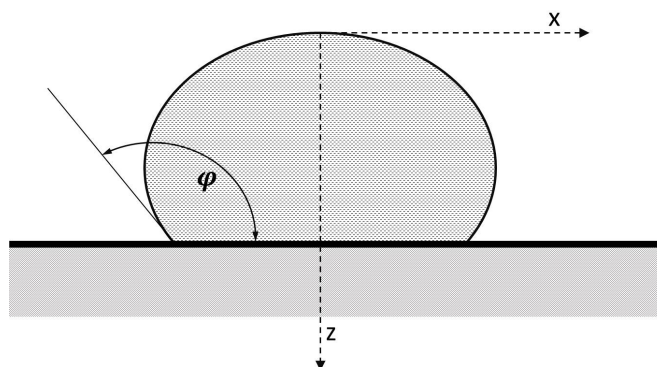


Figure 2.4: Schematic depiction of a sessile drop profile.

This method is based on determining the volume of a sessile drop of known mass by optical techniques. Especially metallic liquids with high surface tension that form a spherical droplet on a substrate are well suited for this method (contact angle should be larger than 90°). Particular attention has to be paid to the choice of substrate material to avoid reactions with the liquid metal. The substrate should be inert and nonwet. Commonly used substrate materials are graphite, ZrO_2 , Al_2O_3 . For volume determination the geometry (schematically depicted in Figure 2.4) of the droplet is recorded using digital camera settings. The contour of the drop is identified and volume is calculated by sectoral integration. Difficulties to handle this approach are variations of the symmetry of the droplet and the assignment of real dimensions to the magnified image recordings. A calibration using reference samples of known geometry is necessary to provide accurate volume determination.

A modified variation of the sessile drop method is the constrained drop method, schematically depicted in 2.5. This method can be considered as combination of Pycnometric Method and Sessile Drop Method. By filling a cup-shaped container with the liquid specimen material a drop is formed on the top by excess metal. The cup made of refractory material is usually of cylindrical shape provided with a sharp ridge to impose a symmetric shape of the drop surmounting the container edge. For volume determination the volume of the container and the volume of

the drop are summarized.

The drop techniques are suitable to investigate liquid metals at high temperatures and beside offer the possibility to determine the quantity of surface tension simultaneously.

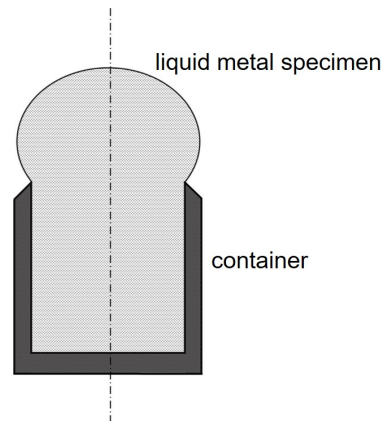


Figure 2.5: Schematic depiction of a constraint drop.

2.6 Levitation methods

Levitation methods are based on avoiding interactions of the liquid specimen material with its environment by evading the utilisation of a container. The specimen is levitated by an external force and heated and investigated by contactless means to maintain non-contact conditions. When heated up in its liquid phase a levitated specimen assumes a spherical shape minimizing the free surface energy. Depending on the force applied for hovering the specimen, methods categorized in aerodynamic, acoustic, electrostatic and electromagnetic levitation have been developed.

For density determination the volume of the levitated liquid droplet is determined by recording photographic images and evaluating the silhouette of the droplet. With the known mass of the specimen, density can be calculated. Temperature is usually determined using a pyrometer.

Particular advantage of this method is the possibility to investigate reactive metals at high temperatures. Also no corrections concerning surface tension effects have to be made to determine density. But problems concerning evaporation

can arise and constitute a limiting factor for levitation methods. The optical temperature determination constitutes an additional error source increasing the uncertainty of the measurement. In the recent past methods of electrostatic levitation and electromagnetic levitation have become popular.

Electrostatic levitation

A detailed description of the electrostatic levitation technique can be found in [11–14]

The Coulomb force acting between a positively charged specimen and a pair of parallel electrodes is used to overcome gravity and levitate the specimen. The specimen is charged photoelectric employing ultraviolet irradiation and heated employing a laser assembly. In the higher temperature regime the charge is perpetuated by thermionic emission. For controlling the horizontal position a set of spherical electrodes are distributed around the bottom electrode. To hold the specimen in fixed position a computer controlled feedback positioning system is required, measuring the present position of the specimen and regulating the electrode voltages. For density determination the volume of the specimen, with a diameter of typically 2 *mm*, is calculated by evaluating photographic recordings. The electrostatic levitation method is suitable to investigate density of reactive metals at high temperatures but is rather complex in its experimental implementation as a fast feedback positioning system is requisite to provide a stable levitation of the specimen.

Electromagnetic levitation

A detailed description of electromagnetic levitation can be found in [14–18].

Electrically conducting specimen are levitated by a high frequency electromagnetic field generated with a conical formed coil. Eddy currents induced in the specimen interact with the external field and the specimen is lifted by Lorentz force to a position of lower field strength. The specimen is heated up due to ohmic losses of the induced currents demanding a cooling of the specimen, usu-

ally by an adjusted gas flow of helium to the sample through a cooling nozzle. The experiments are usually performed under inert gas atmosphere. Again, density is determined by recording the silhouette of the specimen by a photographic image recording system. Advantage of the electromagnetic levitation is that the levitating is self-stabilizing as there is a restoring force for deviations from the equilibrium position, simplifying the experimental effort, compared with electrostatic levitation.

2.7 Gamma radiation attenuation method

A detailed description of the gamma radiation attenuation method can be found in [2, 19, 20].

This method is based on the attenuation of a gamma ray beam passing through a sample. The interaction of gamma ray photons and sample atoms lead to an attenuation of the incident beam according to:

$$I = I_0 \exp(-\mu\rho x) \quad (2.4)$$

with

- I_0 ... intensity of the incident beam
- I ... intensity of the emergent beam
- μ ... mass absorption coefficient of the sample material
- ρ ... density of the medium
- x ... thickness of the sample

The experimental setup usually consists of a sample crucible positioned in a furnace, a gamma source (such as Co-60 or Cs-137) housed in a lead container for radiological shielding and a radiation counter for measuring the ray beam intensities. A small orifice in the lead housing provides the emission of the incident beam which is then collimated and impinges through a tunnel in the furnace wall on the sample crucible. The radiation counter is positioned on the opposite site

of the furnace to determine the intensity of the attenuated beam. For density determination the exact diameter of the sample crucible, described as x in the equation above, has to be known. Accordingly the thermal expansion of the crucible has to be considered in the calculation.

Combining measurements at different temperatures, the temperature behaviour of density can be determined without taking account of the absolute value of the crucible diameter. Density can be described by:

$$D_1 = D_2 \left[\frac{1 + \alpha(T_2 - T_{\text{RT}})}{1 + \alpha(T_1 - T_{\text{RT}})} \right] \left[\frac{\ln(I_1/I_{01})}{\ln(I_2/I_{02})} \right] \quad (2.5)$$

with

D_1	...	density at temperature T_1
D_2	...	density at temperature T_2
T_{RT}	...	room temperature
α	...	coefficient of expansion of the crucible material
I_1, I_2	...	intensities of the emergent beams
I_{01}, I_{02}	...	unabsorbed ray beam intensities

Advantage of this method is that liquid surfaces are not directly involved in the measurement avoiding complications concerning wetting or surface tension corrections. The method is especially suitable for investigating high-density metals causing distinct attenuation.

In summary, choosing a method to determine the density of a metallic liquid phase depends largely on the properties of the liquid metal or alloy to be investigated. Criteria to be taken into account are, for example, the temperature range of the liquid phase to be studied, chemical interactions between specimen material and containment material, vapour pressure of the specimen material or the amount of specimen material available.

Containerless-Methods have the advantage that chemical reactions contaminating the material under investigation can be considered as negligible, but in turn the diagnostics have to be contactless as well, which impeded precise diagnostics, such as

the difficulties associated with pyrometric temperature measurement. As there is no ideal method to investigate the liquid phase of metals, the employment of different methods and comparing of respective results is a reasonable way of assessing the quantity of interest.

3 Fast Resistive Pulse-Heating Method

The fast resistive pulse-heating method is the practical implementation of the idea to overcome the various difficulties in handling metallic liquids at high temperatures, such as intense reactivity, loss of mechanical strength, evaporation or problems concerning heat transfer, by drastically reducing the investigation time. The specimen is heated due to its ohmic resistance by applying a high electrical current pulse and is investigated contemporaneous. Pulse-heating settings operating at experimental durations in the millisecond, microsecond and even nanosecond time regimes were developed [16]. It turned out that with regard to afford thermodynamic equilibrium of the specimen material, for investigating the solid state millisecond experimentation is suitable, whereas for investigating the liquid state experimental durations in the microsecond regime are applicable.

The pulse-heating system at TU Graz was developed with the objective to investigate the liquid phase of high melting metals. A wire-shaped specimen is positioned vertically aligned in the center of a discharge chamber as part of an electrical discharge circuit (descriptions can be found in [21, 22]). In the experiment the specimen material is heated up by the passage of an electrical current of about 10000 A, leading to heating rates up to $10^8 \text{ K} \cdot \text{s}^{-1}$. The rapid heating process reduces the experimental duration to about $50 \mu\text{s}$. Within this time the specimen is heated from room temperature up in the liquid phase, where the specimen wire can be considered as a vertically aligned liquid column, maintaining its cylindrical shape and position as consequence of the fast ongoing short-time process. The material is heated up further until the boiling point is reached and the specimen explodes as result of the intense volume increase. As ambient at-

mosphere usually argon or nitrogen with a pressure of 2.3 bar is used. Primary interest was the determination of specific enthalpy, isobaric heat capacity and electrical resistivity of the liquid phase, especially of high melting metals. For considering the thermal expansion of the liquid samples in the electrical resistivity results, an adapted CCD camera system was added monitoring the radial thermal expansion of the cylindrical formed specimens. Cagran and Hüpf performed a multitude of measurements determining the volume-corrected electrical resistivity.

3.1 Exerimental setup

A picture of the experimental setting is given in Figure 3.1. In the center the discharge chamber is placed, where the specimen holder is inserted for the experiment. The chamber is equipped with three windows allowing an optical monitoring of the specimen during pulse-heating. On the lower left in the picture the pyrometer for temperature determination can be seen. Perpendicularly the setting to measure the thermal expansion is arranged, consisting of a photoflash to backlit the wire specimen from behind and a CCD-monitoring-system positioned on the opposite.

Figure 3.2 depicts the circuit diagram of the pulse-heating setup. The discharge circuit utilizes a capacitor bank ($500 \mu\text{F}$) as energy storage, which can be charged by a high voltage generator up to 10 kV (minimum charging voltage is 3 kV). The experimental procedure is controlled by two fast electric switches (high voltage mercury vapour ignitron tubes) activated by settings consisting of krytrons and capacitors (detailed description can be found in [23–26]). By switching the first ignitron the capacitor bank is discharged over the specimen wire and the heating process is started. The experiment is stopped by switching the second ignitron, which short-circuits the capacitor bank, usually shortly after reaching the material's boiling point.

For protection against electromagnetic disturbances, caused by the rapid variation of current, the computer system for data acquisition is placed in a shielded room

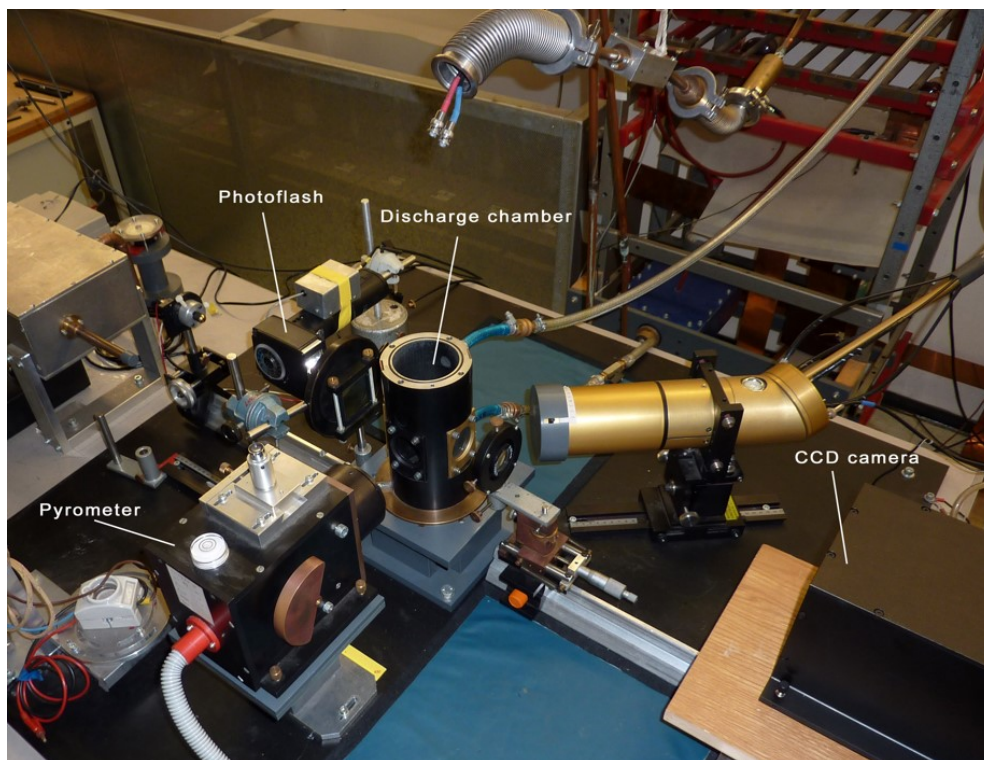


Figure 3.1: Picture of the experimental setup of the pulse-heating system.

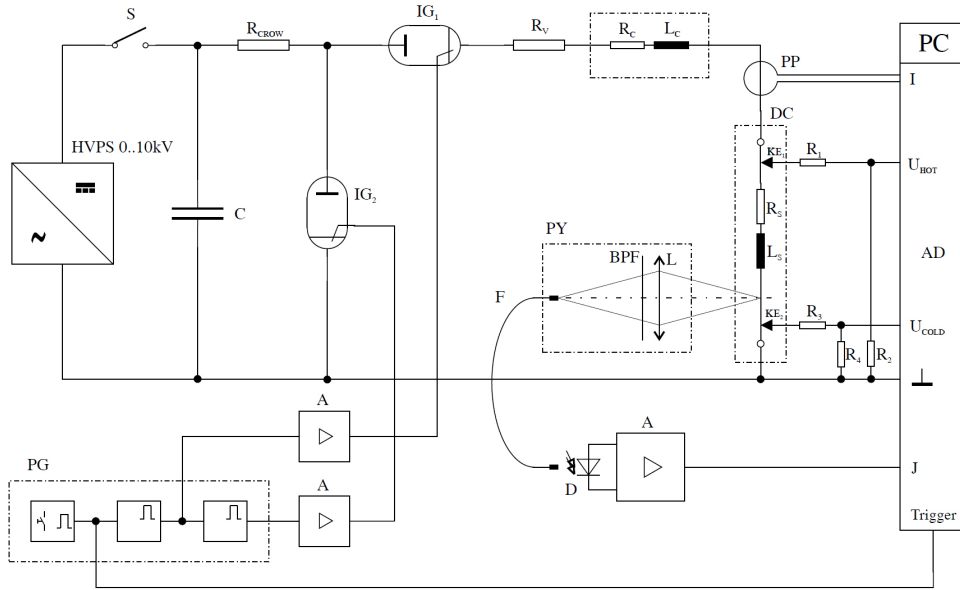


Figure 3.2: Circuit diagram of the pulse-heating setup. Taken from [23] (p. 5).
 HVPS: high voltage generator; C: capacitor bank; S: switch; R_{CROW} : short circuit resistor; IG_1 : start-ignitron; IG_2 : stop-ignitron; R_V : dropping resistor; R_C, L_C : ohmic and inductive load resistor; PP: inductive current measurement (Pearson-Probe); PY: pyrometer; BPF: interferenzfilter; L: lense; $R_{1,2,3,4}$: voltage divider resistors; R_S, L_S : ohmic and inductive specimen resistances; PG: puls generator; A: amplifier; F: optical waveguide; D: detector (photocathode); I: current; U_{HOT}, U_{COLD} : voltage drop measurement with respect to common potential; J: pyrometersignal.

(Faraday-room) and each measuring line is encased by a copper pipe connected to the shielded room's walls. Controlling signals are conducted by optical fibers and electronic devices are cased in aluminium housings.

3.2 Measured quantities

For investigating the specimen usually four quantities are measured directly during the heating process. The electrical current through the specimen, the voltage drop along the specimen, the thermal radiance emitted from the heated specimen surface and the radial thermal expanding of the wire specimen. All four directly determined quantities are recorded as function of experimental time and are related to temperature afterwards when the radiance signal had been evaluated.

3.2.1 Electrical quantities

Electrical current is measured by an induction coil (manufacturer: *Pearson Electronics, Inc*) with included real-time integration element. The resulting voltage signal, proportional to the current, is transferred to the measuring board of a computer system.

For measuring the voltage drop along the specimen two knife-edge probes are placed on the wire, with a distance metered before starting the experiment. The position of the knife-edges is measured using a cathetometer (scale graduation of $\frac{2}{100}$ mm), the diameter of the specimen wire is determined utilizing a laser-micrometer (precision $\pm 5 \mu\text{m}$, LS-7010, Keyence Corporation). Figure 3.3 shows the vertically positioned wire. The picture shows two metal foil contacts (made of molybdenum), the so-called knife-edges, connected to the wire surface by a support construction. Both voltages are measured with respect to a known common potential to cancel out contact resistances between specimen surface and measuring contacts in the voltage drop calculation, when subtracting both voltage signals. The voltage signals are adapted by two ohmic voltage dividers and transferred to the computer system.



Figure 3.3: Picture of the wire specimen positioned vertically aligned in the sample holder. Two metal foil contacts (knife edge probes) are connected horizontal to the wire surface for voltage drop measurements.

3.2.2 Thermal radiance

To be able to describe the determined thermophysical properties as function of temperature the surface radiance emitted by the specimen during pulse-heating is detected using a pyrometer. Depending on radiance intensity and temperature range of interest pyrometers working at different wavelength ranges are used. The pyrometer assembly is depicted schematically in Figure 3.4. For the investigations described in this thesis following pyrometers were employed:

Table 3.1: Pyrometers used for temperature determination in the experiments described in this thesis.

λ_0 ... center wavelength

$\Delta\lambda$... bandwidth

No.	λ_0 (nm)	$\Delta\lambda$ (nm)	Temperature range (K)	Diode material
1	1570	85	$\approx 1050 - 2600$	InGaAs
2	2320	300	$\approx 600 - 2000$	InGaAs

Pyrometer No. 1 working at 1570 nm is suited to determine liquid phase tem-

peratures up to temperatures of approximately 2600 K, which covers the liquidus temperatures of most higher-melting metals of practical interest. The pyrometer consists essentially of a lens system (effective focal length of 60 mm) for optical imaging, an interference filter as wavelength selective element, an image field stop and a photodiode for detection (described in [27]). Due to the cylindrical specimen shape the field stop was constructed rectangular (9.8 mm height, 0.17 mm width). This corresponds to the specimen area imaged, since the optics have a magnification of 1. To ensure that thermal expanding of the investigated specimen has no influence on the radiance detection, specimens investigated in the course of this thesis were chosen to have diameters much larger than the width of the imaged area. The detection system consisting of photodiode and electronic amplifier unit is separated in a shielded box for protection against electrical interferences. The collected light is transmitted to the detection unit by a multiple glass fiber bundle, featuring a rectangular shaped entry for linkage to the rectangular shaped field stop and a circular shaped tail end for conjunction to the photodiode. To be able to align the pyrometer on the specimen the setting is equipped with a hinged mirror and a measuring microscope. Turning the mirror in the optical path projects the image of the specimen surface in the object plane of the microscope and allows a reproducible adjusting of the pyrometer.

To render possible investigations below 1000 K, in course of a diploma thesis [28] (by M. Kurz) pyrometer No. 2 was built. Differences to increase sensitivity are a cooling of the photodiode by Peltier effect and usage of an interference filter of larger spectral bandwidth. The photodiode assembled is a special model from company Hamamatsu featuring high detectivity ($5.8 \cdot 10^{11} \text{ cm} \cdot \text{Hz}^{1/2} \cdot \text{W}^{-1}$). The diode is two-stage Peltier-cooled to -20°C reducing dark current and temperature noise which enables a higher amplification of the signal.

The resulting amplified voltage signals are, by reason of shielding, transmitted by coaxial cables led in copper pipes to the data acquisition system in the Faraday-room. Data are recorded by a 4-channel transient recorder (14-bit analog digital converter) with a sampling rate of 10 MS/s. Data points are captured in time intervals of 100 ns.

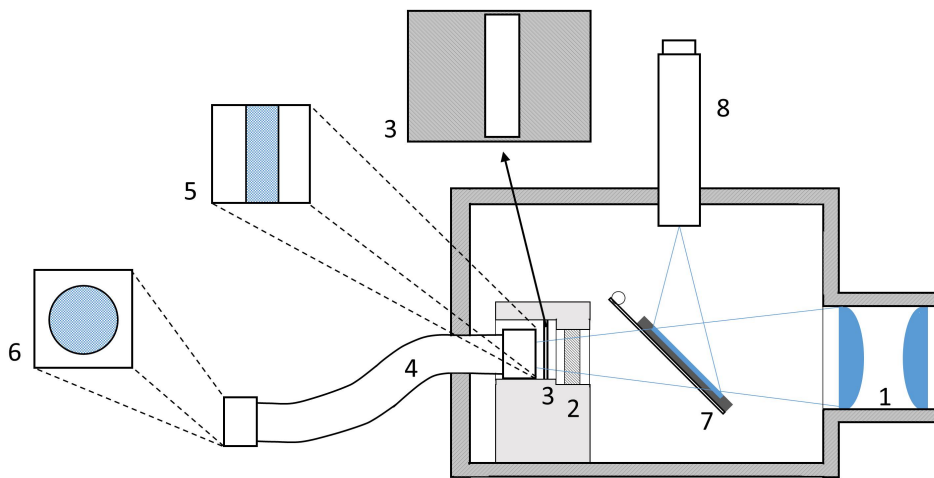


Figure 3.4: Schematic cross section of the pyrometer. 1: lens system consisting of a pair of achromatic lenses, 2: interference filter, 3: image field stop (rectangular shaped), 4: multiple glass fiber bundle, 5: rectangular shaped entry of the glass fiber bundle for linkage to the field stop, 6: circular shaped tail end of the glass fiber bundle for conjunction to the photodiode, 7: hinged mirror and 8: measuring microscope for adjusting.

3.2.3 Thermal radial expanding

Thermal expanding of the specimen during pulse-heating is monitored by shadowgraph imaging. The cylindrical formed liquid specimen column is backlit by a photoflash and the silhouette is pictured and recorded. To monitor the radial thermal expansion of the specimen an adapted CCD camera setting, capable to record several images during the short experimental duration of less than 50 μs , is necessary. This requires a fast successive image recording within time-intervals of just a few μs , which is accomplished by modifying the CCD array controlling and storage management to avoid long read-out times. Additionally an image intensifier arrangement is required to amplify the, as consequence of the short exposure time strongly reduced, background illumination intensity.

Image intensifier arrangement

The image intensifier arrangement (manufactured by Hamamatsu Photonics) consists of a photocathode (GaAsP) that converts incident light into photoelectrons, a micro-channel-plate (MCP) for electron multiplication, and a phosphor screen (P46) for electron reconversion into light. The arrangement is schematically depicted in Figure 3.5. The number of electrons emitted from the photocathode is proportional to the input light intensity. The electrons are accelerated by a voltage between photocathode and MCP and then are multiplied by producing secondary electrons in the channels of the MCP when impacting the channel walls. The resulting electrons are further accelerated and impinge on the phosphor screen, reconverting the electrons into light (decay time about 2 μs). This arrangement intensifies optical images with an amplification factor of about 10000. The phosphor screen is connected to an optical fiber plate (consisting of parallel aligned glass fibers with a diameter of 6 μm) generating the output image. Electronic controlling of the arrangement was integrated by PCO AG corporation.

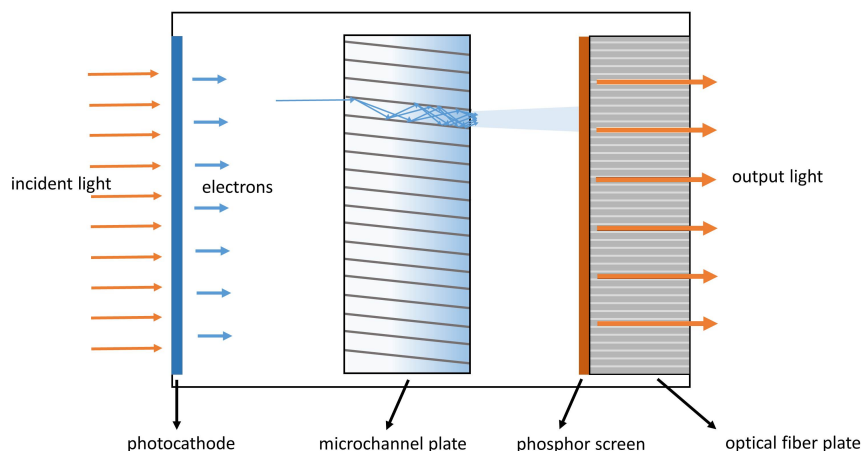


Figure 3.5: Schematic depiction of the image intensifier arrangement. A photocathode converts the incident light into photoelectrons. The microchannel-plate amplifies the signals by secondary electron multiplication. The resulting electrons are reconverted to light by a phosphor screen. The output image is generated by an optical fiber plate connected to the screen.

CCD system

A fast image recording is enabled by utilizing the CCD array (384 pixels horizontal x 576 pixels vertical) as recording unit and as storage unit contemporaneously. The CCD array is partitioned into an exposure area and an area used for storing the monitored images. The first 16 pixel-lines of the array can be exposed, the remaining pixel-lines serve as fast writable storage to puffer the recorded images information. The recording procedure is depicted schematically in Figure 3.6. In the experiment the wire specimen is backlit by a photoflash to provide shadowgraph records with pronounced contrast. A magnified shadowgraph image of a segment of the wire specimen is projected on the monitoring system and recorded by the exposure area (the exposure time is set by the channel plate) of the CCD array. The recorded image information is shifted to the storage area of the chip and the exposure area can be reused for recording. A fast succession of exposing and image data buffering enables an image recording in time-intervals of about $5 \mu\text{s}$, which corresponds to a frame rate of 200000 s^{-1} .



Figure 3.6: Schematic illustration of the image recording procedure to enable fast picture acquisition. 16 pixel-lines of the CCD array are used to record an image, the remaining pixel-lines serve as fast writeable storage to cache the recorded images. After exposing the 16 pixel-lines area the recorded image information is shifted to the storage area. The 16 pixel-lines are cleared and can be reused for exposure.

The time-consuming readout of the CCD array is done after the experiment. Figure 3.7 depicts an illustration of the storage area of the CCD array used for evaluation. The observable streaks represent the recorded images, each consisting of 16 pixel x 384 pixel, as preset by the size of the exposure area. The increasing widths of the sequentially shadowgraph images describe the radial thermal expansion of the specimen during the heating process.

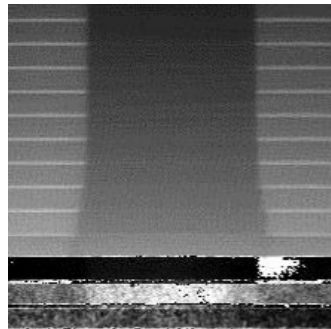


Figure 3.7: Illustration of the storage area of the CCD array, representing an imaging sequence recorded during a pulse-heating experiment.

Time schedule

The time schedule of the experimental process used for the investigations described in this thesis is depicted in Figure 3.8. The actual pulse-heating was started after a lead time, since the photoflash takes some time to reach the maximum of its emission characteristic. 180 μs after triggering the flash, the light emission reaches a constant maximum intensity for a time frame of about 150 μs . Hence the heating experiment has to be timed to run during this time slot to gain shadowgraph images with constant background illumination and high in contrast. To be sure to catch the time frame a safety gap of additional 50 μs was added and the pulse-heating was started at time stamp 230 μs . Contemporaneous with heating the image monitoring was started as well. Images are taken in time intervals of about 5 μs , yielding about 10 single images per experiment. To reach a more homogeneous image distribution with respect to the temperature course, a time gap between start of pulse-heating and start of image recording was added, alternating with a value between 1 μs and 5 μs .

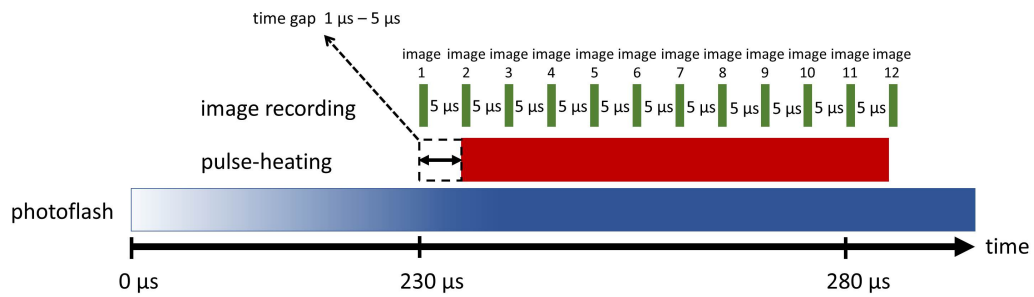


Figure 3.8: Schematic illustration of the experimental time schedule. Pulse-heating starts after $230 \mu\text{s}$, since the photoflash takes a lead time of $180 \mu\text{s}$ to reach maximum lighting intensity. Pulse-heating starts after $230 \mu\text{s}$ plus a time gap of $1 \mu\text{s} - 5 \mu\text{s}$ to reach a more uniform image distribution with respect to temperature, as images are recorded in time intervals of $5 \mu\text{s}$.

3.3 Data evaluation and determination of thermophysical properties

Based on the four directly measured quantities a variety of thermophysical properties can be calculated and derived. The relationships between measured quantities and deduced properties are illustrated in Figure 3.9. The relations directly affecting the thermal expansion measurement are accentuated in blue, the prospected density link in red.

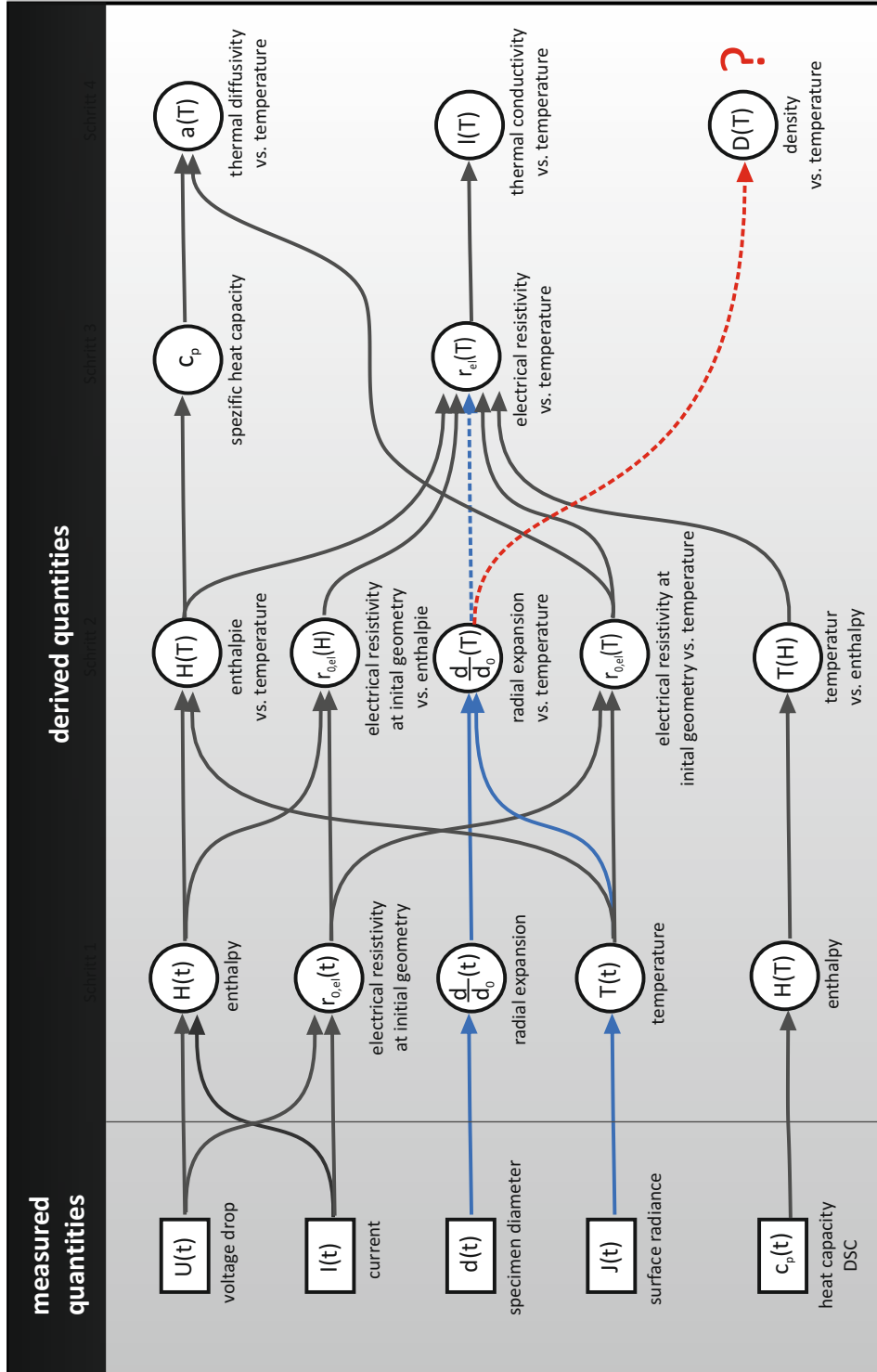


Figure 3.9: Flow diagram illustrating the relationship between measured quantities and deduced properties in course of the pulse-heating evaluation procedure.

3.3.1 Enthalpy and isobaric heat capacity

At pulse-heating supplied electrical energy is converted into heat by reason of the electrical resistivity of the specimen. Since heat losses can be considered negligible due to the short-time experimentation, supplied specific heat Q_s can be described by integrating the electrical power:

$$Q_s(t) = \frac{1}{m} \cdot \int_0^t U(t') \cdot I(t') dt' \quad (3.1)$$

with

- $H_s(t)$... specific enthalpy at time t
- m ... mass of the specimen, obtained from geometry and density at room temperature
- $U(t')$... voltage drop along the specimen at time t'
- $I(t')$... current through the specimen at time t'

Mass m is calculated using the measured parameters specimen diameter d_{RT} and knife-edge distance l_{RT} , and the literature value of density D_{RT} at room temperature (298 K).

$$m = D_{RT} \cdot l_{RT} \cdot \frac{d_{RT}^2 \cdot \pi}{4} \quad (3.2)$$

According to the definition of thermodynamic enthalpy $H = U + p \cdot V$ (with enthalpy H , pressure p , volume V , heat Q), the differential form follows to:

$$dH = dU + p \cdot dV + V \cdot dp = dQ + V \cdot dp \quad (3.3)$$

Pulse-heating can be considered as isobaric process ($p = const.$), so the change of enthalpy with respect to enthalpy at room temperature and ambient pressure correlates to the supplied heat. Assuming a enthalpy at room temperature of zero, specific enthalpy H_s results to:

$$H_s(t) = Q_s(t) \quad (3.4)$$

Examining the enthalpy-temperature curve enables the determination of heat of fusion corresponding to the jump of the enthalpy curve at melting, and by determining the slope of the enthalpy-temperature function, the quantity of isobaric heat capacity can be determined.

$$c_p = \left(\frac{\partial H}{\partial T} \right)_p \quad (3.5)$$

3.3.2 Electrical resistivity

Electric resistance of a conductor material is described by the geometry-independent quantity of electrical resistivity and is calculated from the voltage drop along the investigated specimen segment $U(t)$, the current through the specimen material $I(t)$ and the geometry of the specimen (wire diameter $d(t)$, specimen cross-section area $A(t)$, length of the specimen segment under consideration $l(t)$):

$$\rho(t) = R(t) \cdot \frac{A(t)}{l(t)} = \frac{U(t)}{I(t)} \cdot \frac{d(t)^2 \cdot \pi}{4 \cdot l(t)} \quad (3.6)$$

The determination of time- and temperature dependency of the specimen geometry by CCD-camera monitoring takes a separate evaluation procedure. Therefore the determination of specific electrical resistivity is done in two steps.

Using the specimen parameters of specimen diameter and specimen-segment length, measured prior the pulse-heating process, electrical resistivity with initial specimen geometry ρ_{IG} (without consideration of thermal expansion) is calculated by:

$$\rho_{IG}(t) = \frac{U(t)}{I(t)} \cdot \frac{d_{RT}^2 \cdot \pi}{4 \cdot l_{RT}} \quad (3.7)$$

with

ρ_{IG} ... specific electrical resistivity without considering

thermal expansion
 d_{RT} ... specimen diameter at room temperature
 l_{RT} ... length of the examined specimen segment at room
temperature

Then, by taking into account the results evaluating the radial thermal expansion monitoring, electrical resistivity can be determined. It is assumed that due to the rapid heating and clamping of the wire, only little longitudinal expanding occurs and the major proportion of thermal expansion appears in radial direction, as described in section 3.3.4. Therefore electrical resistivity can be stated by:

$$\rho(t) = \rho_{IG} \cdot \left(\frac{d(t)}{d_{RT}} \right)^2 \quad (3.8)$$

with

$\rho(t)$... specific electrical resistivity considering thermal expansion
 $d(t)$... specimen diameter at time t
 d_{RT} ... specimen diameter at room temperature

It should be mentioned that ρ_{IG} is not only an interim result in the determination of electrical resistivity, as it is used as input parameter in the calculation of thermal diffusivity, which is independent of thermal expansion as well.

3.3.3 Temperature

Temperature is determined evaluating the voltage output of the pyrometer employed for measuring the radiance emitted from the specimen surface. Spectral radiance emitted from a heated body can be described deploying Planck's law in consideration of the specimen's emissivity. Planck's law explains the spectral radiance emitted by an idealized thermal emitter with maximum emissivity (black body):

$$L_{\lambda,B}(\lambda, T) = \frac{c_1}{\pi \cdot \lambda^5} \cdot \frac{1}{e^{\frac{c_2}{\lambda T}} - 1} \quad (3.9)$$

with

- $L_{\lambda,B}(\lambda, T)$... radiance emitted by a black body at a certain wavelength λ and temperature T
- c_1, c_2 ... the two radiation constants with $c_1 = 2\pi \cdot h \cdot c^2$ and $c_2 = \frac{h \cdot c}{k_B}$ ($h =$ Planck's constant, $c =$ speed of light, $k_B =$ Boltzmann constant)

The real body's deviation in emitting is described by considering emissivity $\epsilon(\lambda, T)$, describing the ratio of radiance emitted by the real body $L_\lambda(\lambda, T)$ to the radiance emitted by a black body $L_{\lambda,B}(\lambda, T)$ at same wavelength and temperature:

$$L_\lambda(\lambda, T) = \epsilon(\lambda, T) \cdot L_{\lambda,B}(\lambda, T) \quad (3.10)$$

Besides the emitted radiance, the voltage signal generated by the pyrometer depends on measuring geometry, transmission of the optical measuring arrangement, width of the detectable spectral range and detector sensitivity. The pyrometer's voltage signal U_{Pyro} can be described as:

$$U_{\text{Pyro}}(T) = G \cdot L_{\lambda,B}(\lambda_c, T) \cdot \epsilon(\lambda_c, T) \cdot \tau \cdot E(\lambda_c) \cdot \Delta\lambda \quad (3.11)$$

with

- G ... geometry factor (considering the measuring geometry)
- τ ... transmissionfactor of the optical arrangement
- E ... sensitivity of the photodiode
- λ_c ... central wavelength of interference filter
- $\Delta\lambda$... width of the detectable spectral range

By summarizing all nearly temperature-independent quantities in one constant C , the pyrometer signal can be stated as:

$$U_{\text{Pyro}}(T) = C \cdot \epsilon \cdot (e^{\frac{c_2}{\lambda \cdot T}} - 1)^{-1} \quad (3.12)$$

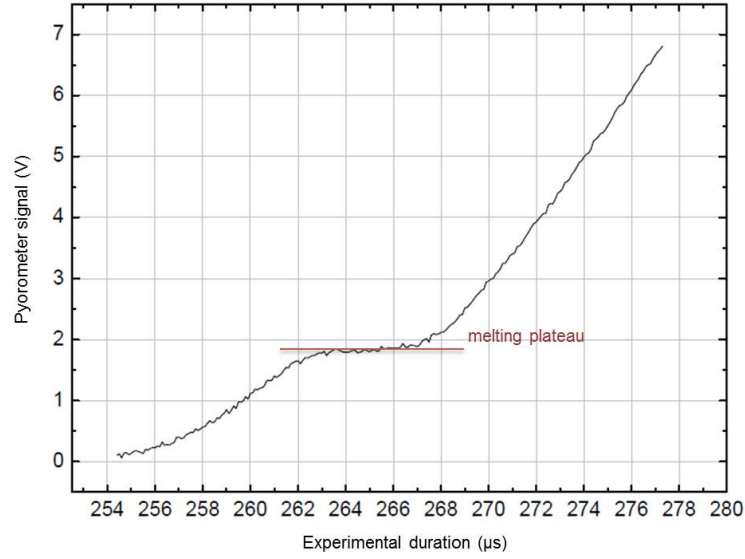


Figure 3.10: Typical pyrometersignal as function of experimental duration. Melting of the specimen is observable as pronounced plateau in the recorded surface radiance signal and can be used to scale the curve on the known temperature of melting. The actual pulse-heating was started after a lead time of $230 \mu\text{s}$, corresponding to the time period the photoflash intensity takes to reach its maximum.

For temperature evaluation in this work, the voltage signal is referenced to a point of known temperature, the liquidus temperature of the specimen material, which can be assigned to the pronounced melting plateau observable in the voltage-time function of the pyrometer output signal, depicted in Figure 3.10. The liquidus temperature was either adopted from literature or determined by DTA (differential thermal analysis) employing a STA 449 C Jupiter (Netzsch). Using the assumption of a constant normal spectral emissivity in the entire liquid phase (discussed in [29]) the temperature can be described with:

$$T = \frac{c_2}{\lambda \cdot \ln \left(\frac{U_{\text{Pyro}}(T_{\text{liqu}})}{U_{\text{Pyro}}(T)} \cdot (e^{\frac{c_2}{\lambda \cdot T_{\text{liqu}}}} - 1) + 1 \right)} \quad (3.13)$$

3.3.4 Thermal conductivity and thermal diffusivity

Thermal conductivity denotes the heat flow through a body as consequence of a temperature gradient ΔT . The heat flow density \vec{q} flowing against the temperature gradient is described by the proportional factor thermal conductivity λ with:

$$\vec{q} = -\lambda \cdot \nabla T \quad (3.14)$$

Heat flow density is based on two mechanisms, the coupling of atomic lattice vibrations (phonon interactions) and the energy transport through freely moving valence electrons. In pure metals thermal conductivity is dominated by the contribution of the free electrons and can be described by the electrical conductivity $\sigma = \frac{1}{\rho}$. Thermal conductivity λ can be estimated applying the Wiedemann-Franz law stating, based on the free electron model (Drude model), that the ratio of thermal conductivity and electrical conductivity of a metal is proportional to temperature. Thermal conductivity can be calculated by:

$$\lambda(T) = \frac{L \cdot T}{\rho(T)} \quad (3.15)$$

with

- $\lambda(T)$... thermal conductivity as function of temperature T
- L ... Lorenz-number, theoretical value of $2.45 \cdot 10^{-8} \text{ V}^2 \cdot \text{K}^{-2}$
(Lorenz-number varies for different metals and alloys [30])
- $\rho(T)$... electrical resistivity

Thermal diffusivity a can be estimated using electrical resistivity at initial geometry and density at room temperature:

$$a = \frac{L \cdot T}{\rho_{\text{IG}} \cdot c_p \cdot D_{\text{RT}}} \quad (3.16)$$

with

- $a(T)$... thermal diffusivity as function of temperature T

- ρ_{IG} ... electrical resistivity without considering thermal expansion
- c_P ... specific isobaric heat capacity
- D_{RT} ... density at room temperature

3.3.5 Thermal radial expansion and density determination

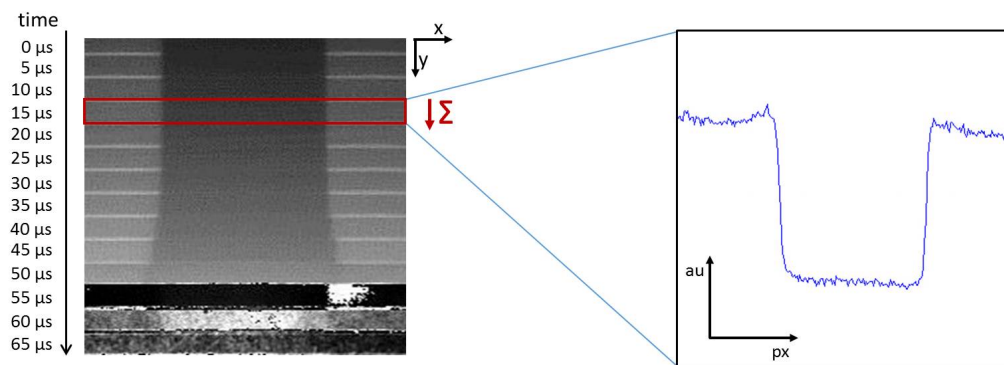


Figure 3.11: Each streak in the shadowgraph image sequence recorded during a pulse-heating experiment represents one single image (16 pixels vertical, 384 pixels horizontal) at a distinct time-stamp. By summing up vertically the grey scale values of the pixel-lines an intensity profile is generated describing the diameter of the specimen at the corresponding time-stamp.

For evaluating the monitored shadowgraph image sequences, the grey scale values of each single image (consisting of 16 pixel x 384 pixel) are depicted. By summing up vertically the pixel-line grey scale values an intensity profile consisting of 384 intensity values is calculated.

$$I_x = \sum_{y=1}^{16} gv(P_{x,y}), \quad (x = 1, \dots, 384) \quad (3.17)$$

with

I_x ... intensity at horizontal position x

$gv(P_{x,y})$... grey scale value of pixel element $P_{x,y}$
 $P_{x,y}$... pixel element at horizontal position x
 and vertical position y

The intensity profile is displayed graphically to provide a visual analysis (depicted in Figure 3.11). The width of the intensity profile describes the diameter of the specimen at the corresponding time-stamp of the recorded single image.

The width of the profile is determined by locating full width at half maximum (FWHM), as described in Figure 3.12. Maximum and minimum of the profile are located visually and assigned by two horizontal lines. At half distance between these lines a third line was drawn (red line in Figure 3.12), whose points of intersection with the profile curve represents the width of the profile curve and the diameter of the specimen, respectively. This procedure is performed with each single image and delivers the increasing diameter of a specimen in pixel units.

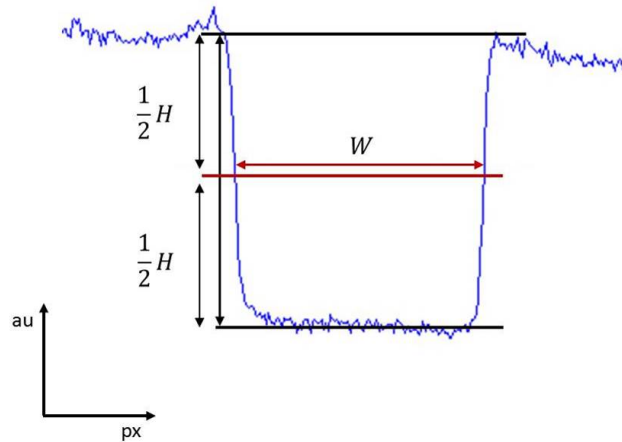


Figure 3.12: Full width at half maximum evaluation (FWHM) of the intensity profile. The black lines assign maximum and minimum of the profile. At half distance between the lines a third line in red is drawn. The points of intersection of this line with the profile curve represent the diameter of the specimen in pixel units.

Thermal radial expansion is obtained by relating the obtained intensity profile widths of the image sequences recorded during pulse-heating $W(T)$ to intensity profile widths of image sequences recorded prior starting the heating process W_{RT} .

Prior each pulse-heating experiment an image sequence at room temperature is recorded to be able to scale the sequence recorded during heating.

$$\frac{d(T)}{d_{RT}} = \frac{W(T)}{W_{RT}} \quad (3.18)$$

with

$W_{RT}; W(T)$... width of intensity profile at room temperature; width of the intensity profile as function of temperature T
 $d_{RT}; d(T)$... diameter of the specimen at room temperature; diameter as function of temperature T

Since this setting performs a fast monitoring of a segment of the specimen wire, only the radial expansion of the wire is determined.

Experimental series in the past [31] indicate that in the setup at TU Graz, no longitudinal expansion of the vertically clamped wire occurs provided that the heating rate used for the experiment is high enough. Employing a camera capable to monitor the entire wire, but with the limitation that only one picture during one experiment could be recorded, Cagran [31] investigated specimens while performing pulse-heating experiments with different heating rates. Depending on the heating rate different expansion behaviours could be observed, presented in Figure 3.13. If the heating rate was not high enough longitudinal expansion and bending of the wire could be observed, depicted in Figure 3.13(a), but above a sufficiently rapid heating no longitudinal expansion could be noticed any more, as displayed in Figure 3.13(b).

Hüpf [32] supposed that the absent longitudinal expansion is compensated by an increased radial expansion of the specimen, allowing the determination of the specimen's volume expansion on basis of the radial expansion measurement. This on the one hand enables the determination of electrical resistivity in consideration of thermal expansion of the specimen, and on the other hand offers the possibility to determine the density of the specimen material as function of temperature. Density as function of temperature $D(T)$ can be calculated from density at room

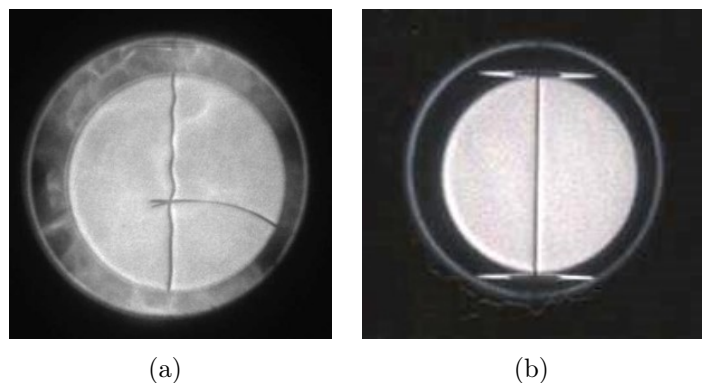


Figure 3.13: Pictures recorded during pulse-heating, illustrating the different expansion behaviours of wire specimens when using different heating rates (pictures recorded by Claus Cagran). This figure is reprinted with permission from Thermal Conductivity 30/Thermal Conductivity 18, 2010. Lancaster, PA: DEStech Publications, Inc [31]. Picture (a) displays the expansion behaviour when using a too small heating rate, leading to longitudinal expansion and bending of the wire specimen (the nearly horizontal aligned contact viewable in the picture, is a knife-edge used for voltage-drop measurements). Picture (b) depicts the expansion behaviour at high heating rates. The wire maintains its shape and exhibits no longitudinal expanding.

temperature by considering thermal radial expansion. Density of a cylindrical shaped specimen with length l can be described with:

$$D_{RT} = m \cdot \frac{1}{l \cdot \pi \cdot \frac{d_{RT}^2}{4}} \quad (3.19)$$

$$D(T) = m \cdot \frac{1}{l \cdot \pi \cdot \frac{d(T)^2}{4}} \quad (3.20)$$

with

$D_{RT}; D(T)$... density at room temperature; density as function of temperature T

$d_{RT}; d(T)$... diameter of the specimen at room temperature; diameter as function of temperature T

Assuming a constant length of the specimen, density can be calculated from the

ratio of the specimen diameters:

$$D(T) = D_{\text{RT}} \cdot \left(\frac{d_{\text{RT}}}{d(T)} \right)^2 = D_{\text{RT}} \cdot \left(\frac{W_{\text{RT}}}{W(T)} \right)^2 \quad (3.21)$$

The thermal volume expansion measurement and accordingly density determination of the pulse-heating setup is based on preventing longitudinal expansion of the wire specimen under investigation. The increased radial expansion compensating the absent longitudinal expansion was monitored and used to determine the thermal volume expansion of the specimen. Figure 3.14 illustrates schematically the conception of the wire expansion behaviour assumed to permit determination of density.

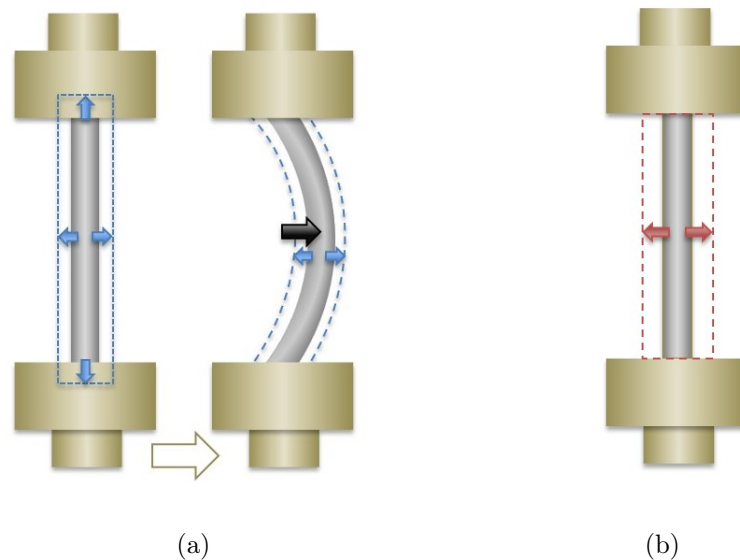


Figure 3.14: The illustration shows the vertically aligned specimen wires mounted in the brass jaws of the specimen holder. Depiction (a) describes the thermal expanding of the specimen during a typical pulse-heating experiment at TU Graz. The specimen exhibits expansion in radial and longitudinal direction. The longitudinal expansion leads to bending of the specimen. (b) depicts the expansion behaviour necessary to permit the determination of thermal volume expansion and density. Longitudinal expansion is prevented and compensated by an increased radial expansion of the specimen.

Experiments in the past showed that especially when investigating materials with

pronounced mechanical strength and high electrical resistivity, longitudinal expansion and bending of the clamped wire specimen could be reduced by simply increasing the heating rate. But in case of materials with lower mechanical strength and high electrical conductivity (for example Cu), increasing the heating rate was not sufficient to prevent bending of the specimen. Additionally, an immoderate increase of the heating rate leads to unnecessary short experimental durations degrading the quality of the measuring results.

Hüpf also performed pulse-heating experiments at high pressures (about 1000 bar) using water as ambient medium. The thermal expansion measurements delivered results showing an increased thermal expansion in comparison with experiments performed in nitrogen atmosphere at 2.3 bar. There couldn't be found an explanation for these results.

This work concerns with thermal expansion determination at 2.3 bar in argon atmosphere. Maybe a future step could be using the optimized thermal expansion measurement setting to determine thermal expansion at high pressures again.

For optimizing the density determination the following issues were considered to avoid longitudinal expansion respectively bending, deforming or movement of the wire specimen during pulse-heating. On the one hand the experimental boundary conditions were changed in order to minimize disturbances affecting the vertical aligned liquid metal column during the pulse-heating. On the other hand the shadowgraph monitoring was enhanced by adapting the optical setting and adjusting the monitoring, to provide sensitive image recording at higher heating rates.

A multitude of experiments were performed to find a compromise between specimen and measurement parameters used and longest possible experimental duration. As indicator showing bending and movement of the wire specimen the CCD camera system was used depicting variations in position of the wire as lateral swerving of the shadowgraphs in the recorded picture series, depicted in Figure 3.15.

Experimental conditions that turned out to be suitable to determine density were:

- The thermal expansion determination and voltage drop measurement should not be performed simultaneously. The two knife-edges used for voltage mea-

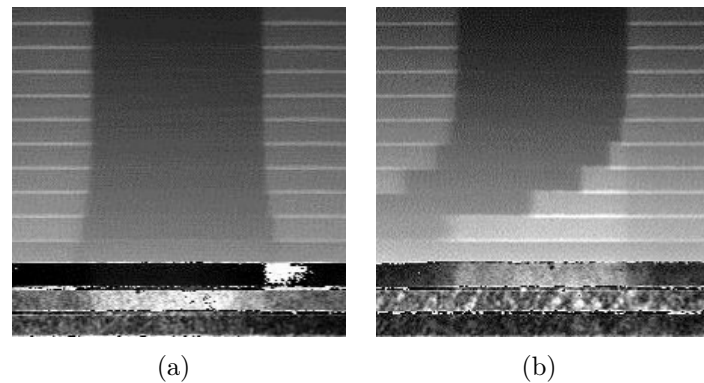


Figure 3.15: Recordings of image series during pulse-heating experiments with different experimental conditions. Picture (a) illustrates the specimen behaviour when performing measurements with the optimized setting under suitable conditions. Picture (b) displays an image series where bending of the wire can be seen as lateral swerving of the shadowgraphs.

measurements pressed on the wire surface favour lateral movement of the liquid metal column.

- The wire length was shortened from typical 70 mm to 40 mm (with a wire diameter of 0.5 mm), to improve the stability of the vertical aligned liquid metal column, which virtually is preserved by its own inertia.
- It should be ensured that the two brass jaws used for clamping the wire are positioned vertically aligned with the clamped wire, to avoid lateral forces acting on the wire during the heating up.
- The optical setting (adjusted using a laser) consisted of:
 - Photoflash to backlit the specimen.
 - Collecting lens positioned in the distance of its focal length to generate parallel light rays for the projection.
 - Adjustable orifice for cutting out non parallel light rays.
 - Interference filter to cut out the pyrometer sensitive spectral range of the photoflash illumination spectrum, to avoid disturbances in the

temperature determination. Although the thermal expansion monitoring is arranged perpendicularly to the surface radiance measurement, disturbances through scatterings and reflections can occur and are observable in the surface radiance signal. By improving the accuracy of the temperature determination, the quality of the density determination is enhanced indirectly.

- Discharge chamber equipped with windows to enable observing of the specimen.
- Collection lens projecting a segment of the specimen on the CCD monitoring system.
- The image recording and optical setting parameters were adjusted in order to generate symmetric intensity profiles that are as sharp-edged as possible. This means that the cup shaped profiles corresponding to a single exposure should exhibit edge gradients as steep as possible. Figure 3.11 depicts the intensity profile of a shadowgraph image recorded during a pulse-heating experiment. While in the past, objective was to obtain profiles featuring high intensities, the approach to optimize symmetry and edge-gradients also at the expense of intensity, simplifies the FWHM (full width at half maximum) evaluation. Depending on the material and pulse-heating parameters, exposure times between 550 ns and 700 ns have been used for recording the image series.

To verify that optical setting and background illumination with parallelized light rays provide an imaging behaviour featuring a linear relation between specimen expansion and monitored specimen expansion, wire samples of different diameters, ranging from 0.25 mm to 0.75 mm, were monitored. The intensity profiles (15 images for each specimen diameter) were evaluated and the received values averaged. The relationship between monitored image-widths in pixel and metered specimen diameters in mm were plotted and confirmed to be linear, described in Figure 3.16.

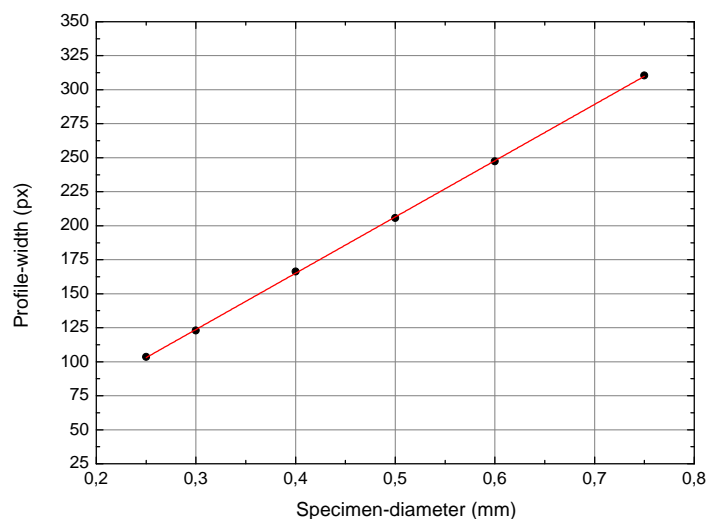


Figure 3.16: Linear relationship between specimen diameters and widths of the corresponding monitored images. Wire specimen diameters ranging from 0.25 mm to 0.75 mm were considered.

In course of optimizing the pulse-heating system the voltage divider's ratios were remeasured to: 1030.6 ± 1.7 and 310.7 ± 0.2 . The calibration factors were determined by measuring the resulting partial voltages with the measuring board when applying different input voltages. To avoid corruptions due to warming of the resistors, input voltages < 3 V were used. In order to modernize the data processing unit a second data recording system (new measuring boards and software system) was built-up in the context of the diploma-thesis by Thomas Macher. The voltage divider's ratios of the second system were determined to: 1045.1 ± 4.2 and 310.6 ± 1.3 , described in [33].

The measured quantities were evaluated using the software *Hotwire*, which was originally created by Sachsenhofer [23] and has been modified to preserve compatibility with other software such as *MAPHS*, which enables the automatized uncertainty determination of the gained thermophysical properties on the basis of GUM ('guide to the expression of uncertainty in measurement') and was created by Macher [33] (2014). The software *Wiredia*, originally created by Schützenhöfer and modified by the time, was used to evaluate the recorded images by depict-

ing them as intensity profiles. Additionally the software *Origin* (manufacturer: *OriginLab*) was applied to create *LabTalk*-scripts for evaluating the thermal expansion measurements and determine density.

4 Electromagnetic Levitation

Method

The electromagnetic levitation method is based on minimizing interactions with the environment by evading containment. In contrast to pulse-heating, which establishes 'quasi-containerless' investigation conditions by extremely reducing the investigation time, electromagnetic levitation actually enables containerless handling by hovering the specimen electromagnetically. The possibility to investigate specimen material under complete contact-free conditions makes this method ideally suited for the investigation of highly reactive materials.

An electromagnetic levitation apparatus usually consists of a conical formed metallic coil generating an inhomogeneous high-frequency electromagnetic field to heat and levitate the specimen. Above, a second coil wound in opposite direction is positioned, generating an opposing field. The specimen is caged between the two coils in the region of low magnetic induction. The levitated liquid specimen takes a drop-like shape performing surface oscillations around its equilibrium shape. To sustain contact-free conditions, the specimen has to be investigated applying non-contact diagnostics.

In order to expand the investigation capabilities of the work group at TU Graz and to provide the opportunity to appraise the density results obtained by the pulse-heating setup, an electromagnetic levitation apparatus was build up as cooperation project between Kirmanj Aziz and the author of this work. Aim was the determination of density and surface tension applying this apparatus.

(Experiments and results concerning the determination of surface tension can be found in the thesis of Aziz [34] and in [35–37]).

The electromagnetic levitation method is an established technique to investigate

liquid metals. It was first proposed by Muck (1920) [38]. The Westinghouse group received first experimental results (1952). In the 1960s the theoretical background was described and experiments started aiming the determination of thermophysical properties [39, 40]. Fromm and Jehn [41] discussed suitable levitation coil designs. Experiments investigating surface oscillations (necessary for surface tension determination) of the levitated specimen followed. The theoretical description explicating the oscillation frequencies were given in the 1980s [42, 43], experimentally implemented by [44]. In the 1990s DLR (German Aerospace Center) developed an electromagnetic levitation system for microgravity conditions (TEMPUS) [45], tested on parabolic flights.

Concerning density determination first descriptions were given by Shiraishi and Ward [40]. Photographic images of the oscillating specimen were taken from side view and from top view simultaneously and only those featuring no deformation of the specimen were used for evaluation. Density was determined by calculating volume from the side-view images assuming rotational symmetry. This approach was applied by several groups, such as [46, 47]. To avoid the disadvantage of temperature dependent image-contrasts Brillo and Egry [48] described the procedure to record shadowgraph-images of the specimen by illuminating the specimen from behind by an expanded parallel laser beam and remove self-radiation of the specimen utilizing a band-pass filter. Using this shadowgraph technique precise density determinations of a multitude of liquid metallic phases could be determined.

This listing is not intended to exhaustively describe all steps in the development of the electromagnetic levitation method nor are all groups mentioned doing research by employing this method. It merely seeks to provide a brief overview of the evolution of this technique. A detailed description can be found in [49].

4.1 Electromagnetic levitation

An inhomogeneous high-frequency electromagnetic field is generated by conical formed coils. This field induces eddy currents in the specimen material (according to Lenz's law), interacting with the external field and lifting the specimen by Lorentz force in direction of lower field strength against gravity, depicted

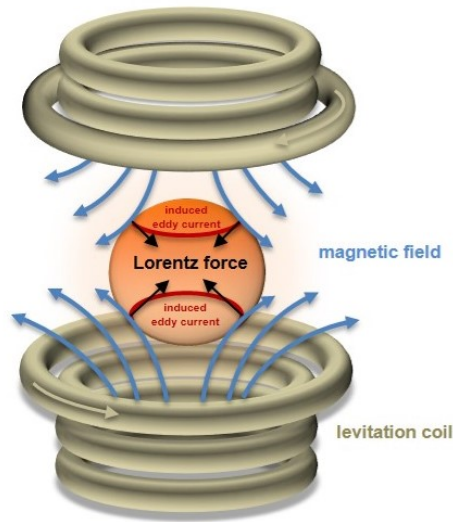


Figure 4.1: Illustration depicting electromagnetic levitating.

schematically in Figure 4.1. It was described [41] that by using an arrangement of two coaxial coils (generating opposing fields) a radial restoring force could be realized, stabilizing the specimen in lateral direction as well. The Lorentz force acting on the specimen was described by [39] as:

$$F \propto \nabla B^2 \quad (4.1)$$

with

$$\begin{aligned} F & \dots \text{Lorentz force acting on the specimen} \\ B & \dots \text{magnetic field strength} \end{aligned}$$

Additionally, the induced eddy currents heat the sample due to its ohmic resistance. The power losses were described as: [39]

$$P \propto B^2 \quad (4.2)$$

with

$$P \dots \text{resistive power losses heating the sample}$$

B ... magnetic field strength

The gravitational force and levitation force acting on the liquid specimen lead to a deformation of the specimen geometry in a drop-like shape. The electromagnetic fields induce turbulent fluid flows inside the liquid specimen causing oscillations and rotating of the shape of the droplet [50]. The oscillations are determined by the surface tension of the liquid specimen material, as it's the restoring force minimizing the free surface energy. Based on this relation it is possible to determine the surface tension of the specimen material by monitoring the oscillations and evaluating the oscillation frequencies, described in [51]. Since levitating and heating are linked with each other, the implementation of a cooling system is necessary, to be able to control the temperature of the specimen under investigation.

4.2 Experimental setup

The experimental setup was constructed with the intention to provide an investigation of the levitated specimen by high-speed cameras and pyrometer. A monitoring of the liquid drop should be possible from side view for density determination and from top view for surface tension determination. As density determination is based on shadowgraph imaging, an illumination device to backlit the specimen is necessary and a photographic imaging system on the opposite to record the specimen shape.

The levitation setup built-up (depicted schematically in Figure 4.2), consisted of:

- vacuum chamber with three optical windows for monitoring
- radio frequency current generator (Trumpf Huettinger GmbH+Co. KG, Freiburg, Germany). Output power: 6 kW. Operated with a frequency of 400 kHz and generating an alternating current of $I_{rms} = 350$ A flowing through the levitation coil.
- vacuum pump system consisting of:

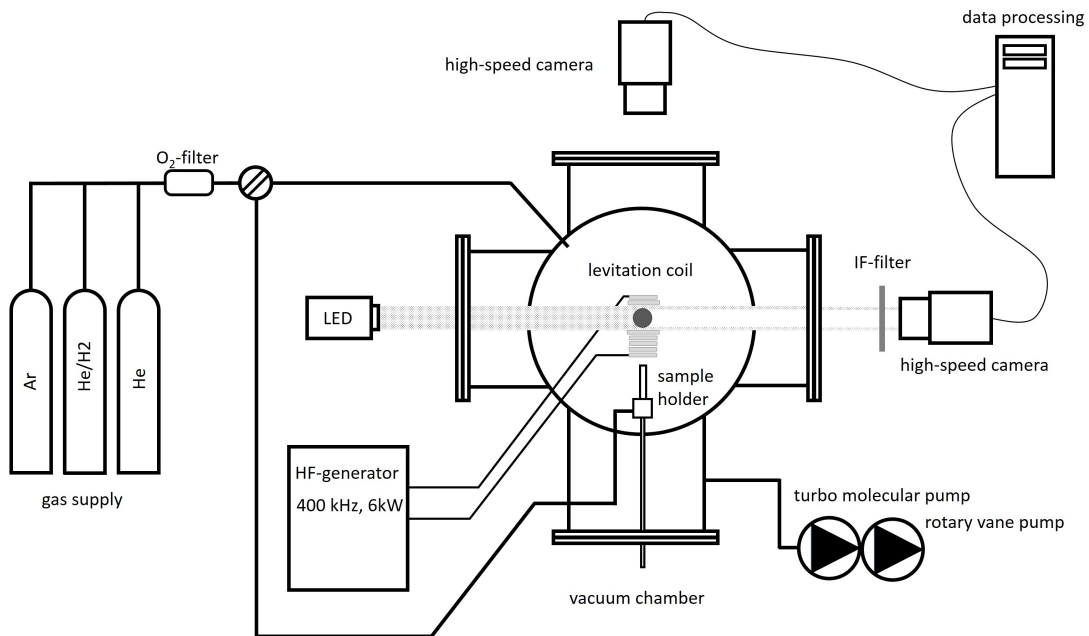


Figure 4.2: Schematic depiction of the levitation apparatus. In the center the vacuum chamber is placed with the levitation coil positioned in it. From the left the specimen is backlit by a LED panel to monitor shadow-graph images by a high speed camera positioned on the opposite.

- rotary vane pump (Pfeiffer Balzers Duo 0016B, Pfeiffer Vacuum GmbH, Germany), pressures down to 10^{-2} mbar
- turbo molecular pump (Pfeiffer Balzers TPU 330, Pfeiffer Vacuum GmbH, Germany), pressures down to 10^{-6} mbar
- pressure gauges:
 - pressure range $< 10^{-4}$ mbar:
Penning cold cathode vacuum gauge (Balzers IKR-020, Pfeiffer Vacuum GmbH, Asslar, Germany)
 - pressure range 10^{-4} mbar - 1 mbar:
Pirani gauge (Balzers TPR-016, Pfeiffer Vacuum GmbH, Asslar, Germany)

- pressure range 1 mbar - 2000 mbar:
Leybold DI 2000 from Oerlikon Leybold Vacuum GmbH, Cologne, Germany
- cooling system: Kühlmobil 141 from Van der Heijden-Labortechnik GmbH, Dörentrup, Germany
- gas supply (including O₂-filter (Air Liquide Alphagaz-Purifier) to ensure a oxygen reduced atmosphere)
- pyrometer (IMPAC IGA 6 ADVANCED, LumaSense Technologies GmbH, Frankfurt/Main, Germany) with a spectral range of 1.45 μm -1.8 μm
- image acquisition system consisting of high speed camera, macro lens, frame grabber and image processing unit
- LED panel with 100 W at about 520 nm, provided with a diffuser to obtain a homogeneous background illumination

Figure 4.3 shows a picture of the electromagnetic levitation setup built-up at TU Graz. The vacuum chamber was provided with large windows to enable a monitoring of the specimen without optical restrictions. A multitude of vacuum flanges allows the attachment of vacuum pumps, pressure gauges, gas supplies, electrical connections and a linear motion feedthrough for the sample holder.

For heat dissipation two cooling circuits were arranged. The electronics of the radio frequency generator were cooled to about 20°C by a closed-loop cooling circuit (Kühlmobil 141 from Van der Heijden-Labortechnik GmbH) using distilled water as cooling medium. The second cooling circuit was necessary to cool the levitation coil to prevent the coil material from melting. As cooling medium tap water with a flow rate of 0.8 l · min⁻¹ was used.

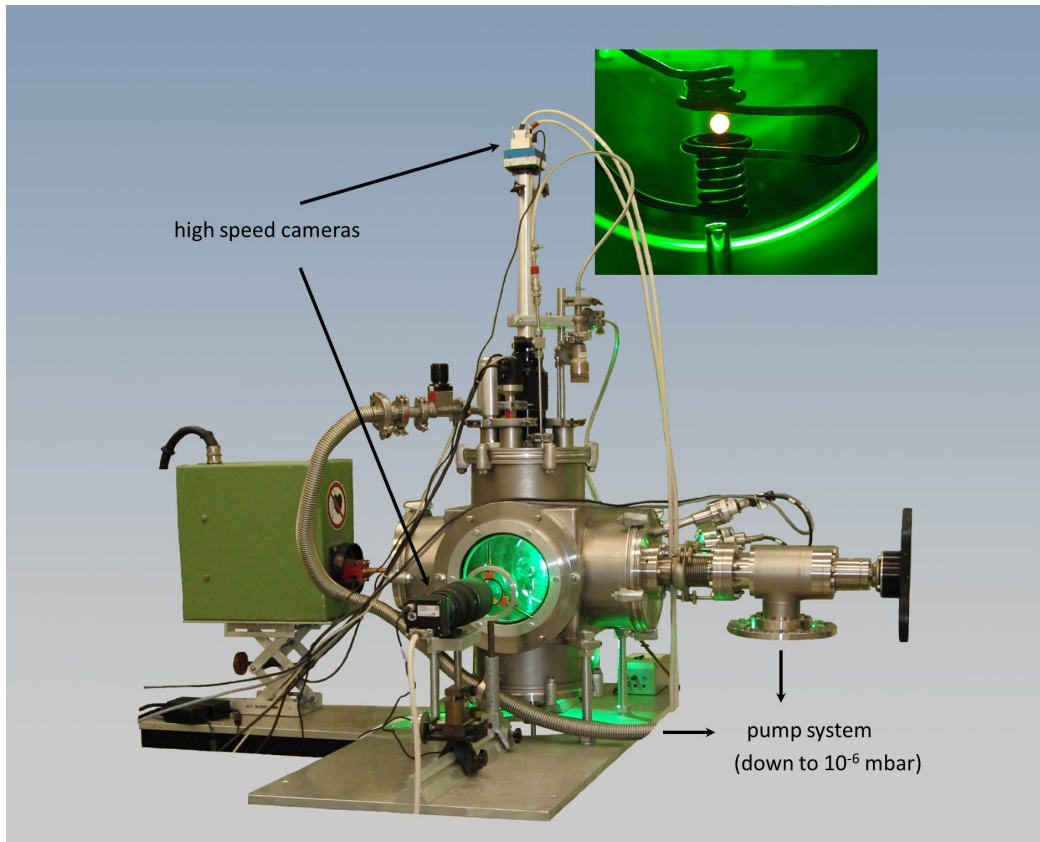


Figure 4.3: Picture of the built-up levitation apparatus. In the center the vacuum chamber equipped with three windows for optical monitoring (front, back and top view) can be seen. From the left the levitation coil is inserted into the chamber; vacuum pumps are connected from the right. The green light visible in the chamber stems from the LED panel used as background illumination.

The levitation coils used were formed of copper tubes to provide a cooling by flowing water through them during the experiment. Figure 4.4 shows a picture of a typical levitation coil used to heat, hover and position the specimen. The coil consists of two oppositely wound zones to cage the specimen between them. The lower zone features a higher number of windings to compensate the gravitational force acting on the specimen. The effective coil design has to be adjusted on the specimen material to accomplish a stable levitating.

The vacuum chamber was equipped with a moveable sample holder to be able to position the specimen between the two coaxial coils before the levitating starts.

As result of the continuous energy input in the specimen material during the levitation procedure, the specimen has to be cooled to set a constant temperature. The sample holder was constructed hollowly to enable a cooling with an adjusted gas flow of helium to the specimen through the sample holder.

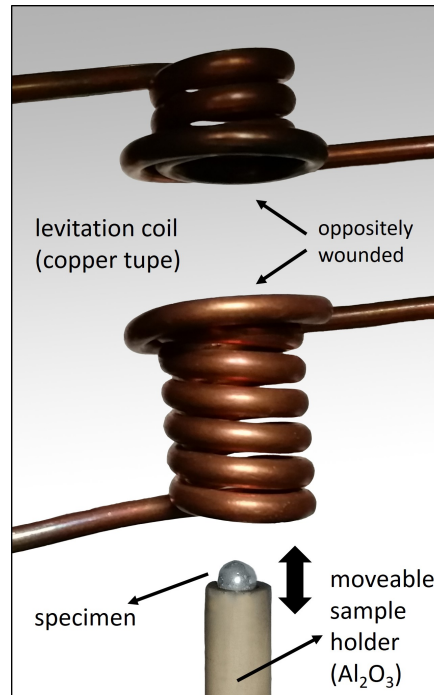


Figure 4.4: Picture of a typical levitation coil to heat and position the specimen. Below the coil the hollowly constructed sample holder can be seen.

4.2.1 Experiment atmosphere

The experiments were performed under inert gas atmosphere with a pressure of about 750 mbar to prevent problems concerning evaporation and to enable a cooling of the specimen by gas flow. Before starting levitation, the vacuum chamber was evacuated to about 10^{-6} mbar and then subsequently filled with a mixture of argon, helium, and a small amount of hydrogen (less than 4 vol%) to establish an oxygen reduced environment. Gases (by Air Liquid corporation) used to establish a defined atmosphere were Helium N60 (purity ≥ 99.9999 vol%), Argon N50 (purity ≥ 99.999 vol%), ARCAL 10 (Ar+2.4 vol.% H_2) and a custom made gas mixture (He+4 vol.% H_2). During the experiment pressure was kept

on a constant level regulated by a solenoid valve connection between vacuum chamber and rotary vane pump.

4.2.2 Temperature

Temperature of the levitating liquid droplet again was determined contactless by utilizing a pyrometer. The surface radiance emitted from the liquid specimen surface was measured in the spectral range of $1.45\ \mu\text{m}$ - $1.8\ \mu\text{m}$. The pyrometer used (IMPAC IGA 6 ADVANCED, LumaSense Technologies GmbH, Frankfurt/Main, Germany) is suitable to be employed in a temperature range between about 250°C and 2500°C . Specifications are given in Table 4.1.

Table 4.1: Specification description of the pyrometer utilized for temperature determination of the levitated specimen.

Spectral range	$1.45\ \mu\text{m}$ - $1.8\ \mu\text{m}$
Response time	$120\ \mu\text{s}$
Resolution	0.1°C
Measurement uncertainty	$< 1500^\circ\text{C} : 0.3\% + 2^\circ\text{C}$ $> 1500^\circ\text{C} : 0.6\%$
Temperature range	$\approx 250^\circ\text{C} - 2500^\circ\text{C}$

For pyrometer controlling and signal recording the software *InfraWin 5.0.1.52* (provided by LumaSense Technologies GmbH) was used.

The spectral radiance emitted during performing an investigation cycle was measured to be evaluated afterwards. Measuring distance was 250 mm. The measurement spot size on the levitated droplet surface had a diameter of about 0.8 mm (specimen diameter was about 6 mm). For temperature evaluation again the melting plateau was used as reference point (by assigning the liquidus temperature of the specimen to the melting plateau in the pyrometer signal) according to the principle described in chapter 3.3.3. Temperature then was calculated with the assumption of a constant normal spectral emissivity in the entire liquid phase. The liquidus temperature of the specimen material was either adopted

from literature or determined by DTA (differential thermal analysis) employing a STA 449 C Jupiter (Netzsch corporation).

4.2.3 Levitation coil construction

The levitation coil was self-constructed using a copper tube with an outer diameter of 3 mm and an inner diameter of 1.5 mm. For creating the coil with two oppositely wound zones a steel rod with a diameter of 10 mm was used to turn the tube around, as depicted in Figure 4.5. A design with 7 loops in the lower zone and 4 loops in the upper turned out to be well-suited to establish stable levitating at the apparatus at TU Graz. Depending on the specimen material investigated the coil design has to be adapted, which particularly means to adjust the gap g between the two winding zones and the spacings between the individual windings. A smaller gap leads to stronger heating of the specimen material, but also increases the electromagnetic pressure exerted by the surrounding electromagnetic cage, which could cause more pronounced deformations of the specimen shape and interfering a stable levitating. The effective design has to be adjusted on the material to be investigated, its mass and its size to achieve a stably levitating specimen featuring little deformations of its shape.

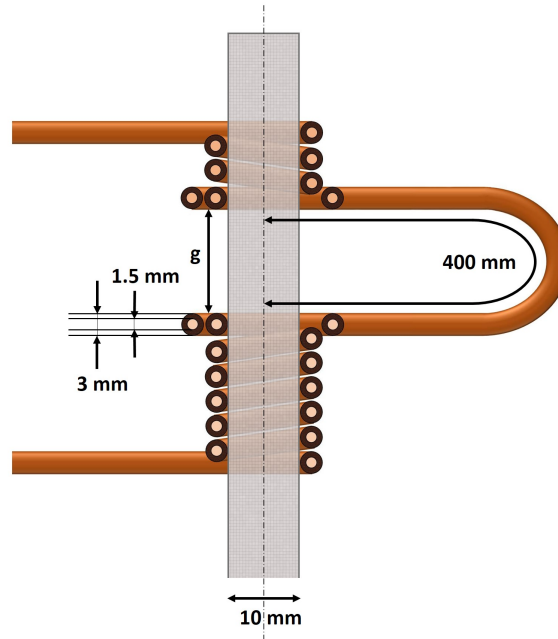


Figure 4.5: Schematic illustration of the levitation coil self-constructed by winding a copper tube (outer diameter of 3 mm and an inner diameter of 1.5 mm) around a steel rod (diameter of 10 mm). The effective design parameters have to be adjusted on the investigated material.

4.2.4 Image acquisition system

As density determination is based on image averaging, for monitoring the levitating specimen a high-speed recording system was build-up, consisting of: a high-speed camera (EoSens CL, Mikrotron GmbH, Unterschleissheim, Germany); a macro objective lens (AF Micro-Nikkor ED 200 mm f/4 D IF, Nikon Corporation); a frame grabber (Matrox Radiant eCL, Matrox Electronic Systems Ltd.) and a PC as image processing unit.

The high-speed camera working with a frame rate of 120 s^{-1} records images with a spatial resolution of 1024 pixel x 1024 pixel (grey-value dynamics of 8 bit). The macro lens was used as objective and enables a picturing with magnification 1. The frame grabber is connected by a Full-Camera-Link configuration with the high-speed camera, and interconnected by an x8-PCIe interface with the processing unit. This affords the required data transfer rate for handling the data stream of 120 monitored images per second. The images are buffered in the RAM of the

processing unit and afterwards when the recording sequence is finished stored to a solid-state drive for further processing.

4.3 Density determination

For density determination the approach of shadowgraph imaging was used to ensure image recordings rich in contrast and independent of the brightness of the incandescent specimen. The setting (depicted schematically in Figure 4.6) consisted of a LED panel (100 W at about 520 nm) equipped with a diffuser (to obtain a homogeneous background illumination) for backlighting, and positioned oppositely, a high-speed CCD camera, recording the shape of the levitating specimen with a frame rate of 120 fps. An interference filter, placed in front of the camera system, prevented influences due to the thermal self radiation of the specimen and provided pronounced contrast of the recorded images. Figure 4.7 shows pictures of a levitated liquid sample recorded with the monitoring system.

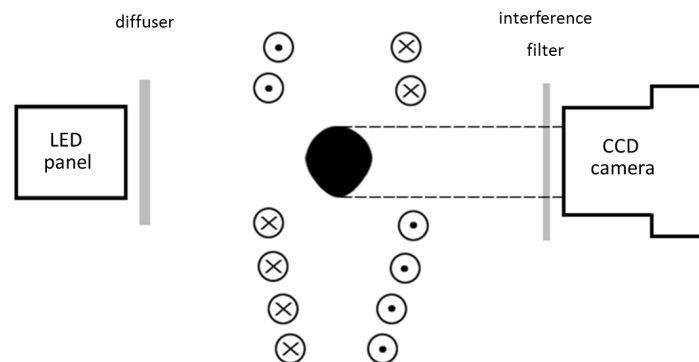


Figure 4.6: Schematic depiction of the thermal expansion measurement setting.

Basic prerequisite for the image recording is an unobstructed line of vision on the sample from the horizontal side. This has to be provided by an appropriate design of the levitation coil adjusted on the investigated material and its mass, to ensure that the specimen is not masked by any part of the coil-windings. (It turned out that at the TU Graz setting specimen diameters between 4 mm and 6 mm were well suited for sideview-recording).

As the specimen's shape performs oscillations, each recorded image shows a

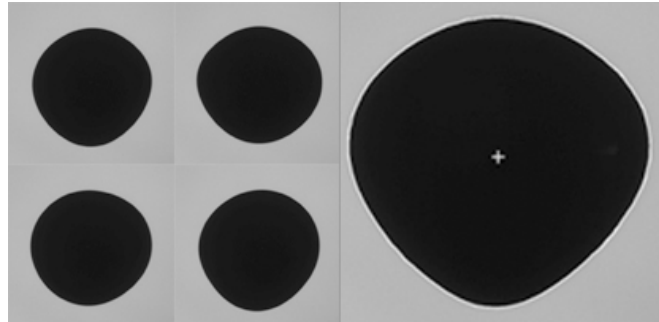


Figure 4.7: Images of a levitated liquid sample recorded with the monitoring system. The image on the right was evaluated and the center of mass and edge curve of the shadowgraph were determined.

droplet slightly deformed. If the deviations from the specimen's equilibrium shape are small compared to the sample's diameter, the equilibrium shape can be calculated by averaging several hundred recorded images. The volume of the specimen can be calculated based on the assumption of an axially symmetric equilibrium shape with respect to the vertical axis [48].

4.3.1 Experimental procedure

Before starting the investigation procedure preliminary experiments have to be performed adjusting coil design (winding's diameter, spacings between the windings, gap between upper and lower coil) and investigated material (mainly specimen size) with the objective to obtain an unobstructed view on the specimen from the side and concurrently establish a preferably motionless levitating of the specimen in the liquid phase.

Before the specimen was inserted into the experimental chamber for investigation it was abraded and cleaned with acetone by an ultrasonic bath, and weighted using a precision balance (AB104-S-A, Mettler-Toledo GmbH, Germany). Then the specimen was positioned on the specimen holder. The experimental chamber was evacuated to about 10^{-6} mbar and subsequently filled with a mixture of argon, helium and a small amount of hydrogen to about 750 mbar. Then the levitation process was started and the specimen heated up into its liquid phase. Temperature was controlled by adjusting the helium gas flow through the hollowly sample

holder. The specimen temperature was regulated to a desired temperature point and the high-speed shadowgraph recording started. 2500 images at each temperature point were recorded. For finishing the experiment the liquid droplet was cooled down in the solid phase by increasing the helium gas flow to the specimen and, when reached low temperatures caught with the specimen holder. To consider mass losses due to evaporation in the evaluation, the specimen material was weighed before and after the experiment.

In case of materials that tend to form a pronounced oxide layer on their surface (as for example aluminium) it turned out to be advantageous to heat the material up to high temperatures to get rid of the oxide layer through vaporization, and afterwards perform the specimen investigation in the line of a stepwise cooling down process. Areas with oxide-compounds are distinctly visible on the droplet surface due to their differing (usually large) emissivities and can be observed as bright specks moving along the droplet surface.

4.3.2 Evaluation procedure

The density determination was based on the calculation of:

$$D(T) = \frac{m(T)}{V(T)} \quad (4.3)$$

with

$m(T)$... the mass of the specimen at temperature point T

$V(T)$... volume of the specimen at temperature point T

The mass of the sample at a distinct temperature point was determined by weighing the sample before and after the levitating process and assuming a linear decrease of mass with experimental time. For volume determination the recorded image series (2500 images at each temperature point) were evaluated. Each individual image was analysed using the following procedure:

Step 1 - Finding the shadowgraph object:

Each recorded image consisted of an array of 1024 pixels horizontal and 1024 pixels vertical with a grey-value depth of 8 bit. To find the shadowgraph object the pixel array was screened and filtered using a predefined grey value threshold. The grey value of every pixel P_i was compared with the set threshold value TH . If the pixel's grey value was higher than the threshold value the pixel was considered to be part of the shadowgraph object.

$$PO = \{P_i \mid gv(P_i) > TH\} \quad (4.4)$$

with

- PO ... set of all pixel elements that are part of the shadowgraph object
- P_i ... the pixel element with the number i (according Figure 4.8)
- $gv(P_i)$... grey value of the pixel element P_i
- TH ... threshold value

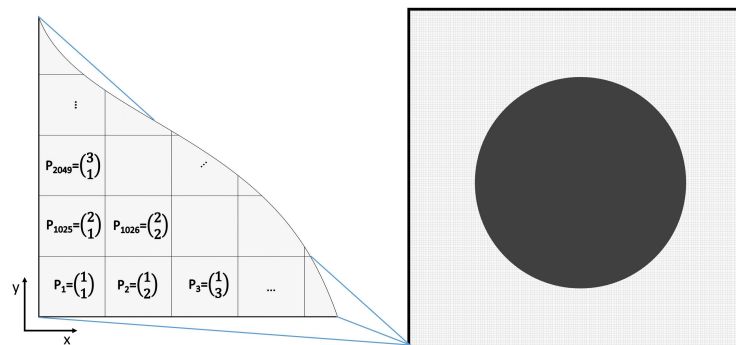


Figure 4.8: Schematic illustration of the indication of the individual pixels of the CCD array in order to determine the shadowgraph object.

Step 2 - Calculating the center of mass of the shadowgraph object:

The pixel elements of the set PO , identified in step 1, were used to determine the center of mass (actually the center of area) of the shadowgraph object, depicted in Figure 4.9. The pixel positions are averaged vectorially and the coordinate of center of mass is calculated:

$$\overrightarrow{CM} = \begin{pmatrix} \bar{x} \\ \bar{y} \end{pmatrix} = \frac{1}{n} \sum_{i=1}^n \overrightarrow{PO}_i = \frac{1}{n} \sum_{i=1}^n \begin{pmatrix} x_i \\ y_i \end{pmatrix} \quad (4.5)$$

with

- \overrightarrow{CM} ... vector to the center of mass of the shadowgraph object
- \bar{x}, \bar{y} ... x and y coordinate of center of mass
- \bar{y} ... y coordinate of the center of mass vector
- \overrightarrow{PO}_i ... vector indicating the pixel element PO_i
- x_i, y_i ... x and y coordinate of pixel element PO_i
- n ... number of pixel elements in the set PO

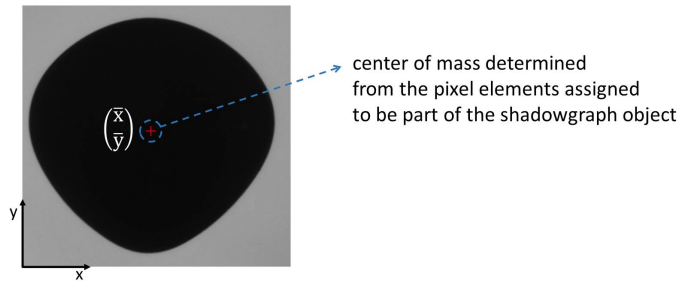


Figure 4.9: Center of mass determination of the shadowgraph object. Pixels that are part of the shadowgraph object are averaged vectorially to calculate the center of mass coordinate.

Step 3 - Locating the edge curve of the shadowgraph object:

For locating the edge curve of the shadowgraph object the radial brightness distributions were depicted in one degree steps in polar coordinates. The radial

brightness curve $I_\phi(r)$ at angle ϕ was determined by selecting the pixels lying along the line starting at center of mass and leading radially outwards at angle ϕ , as illustrated in Figure 4.10. The corresponding grey scale values are plotted for evaluation.

$$I_\phi(r) = gv(P_{\vec{R}}) \quad , \quad \text{with} \quad \vec{R} = \begin{pmatrix} \bar{x} \\ \bar{y} \end{pmatrix} + r \cdot \begin{pmatrix} \cos(\phi) \\ \sin(\phi) \end{pmatrix} \quad (4.6)$$

with

$I_\phi(r)$...	radial brightness curve at angle ϕ
$gv(P_{\vec{R}})$...	grey scale value of pixel $P_{\vec{R}}$
$P_{\vec{R}}$...	pixel at position \vec{R}
r	...	distance to center of mass
ϕ	...	polar angle

The resulting curves showed a steep slope of intensity from 10 to 160 grey scale values within 25 pixels. Each resulting profile curve was fitted polynomial (third-degree) and the point of inflection was calculated. The points of inflection are considered as representation of the edge of the shadowgraph object.

The edge curve of each recorded image was determined executing step 1 - step 3.

Determining the equilibrium shape

In order to eliminate the influence of the shape oscillations, the equilibrium shape was obtained by averaging all 2500 frames belonging to one temperature point and fitting of the resulting curve by Legendre polynomials up to sixth order. Then the volume of the resulting equilibrium shape was calculated with the assumption of an axially symmetric shape, with respect to the vertical axis. With determined volume as function of temperature, and mass as function of temperature, density was calculated. Figure 4.11 depicts as example the calculated equilibrium shape (of a copper specimen) obtained by averaging the evaluated images. The equilibrium shape's deviation from a circular form was considered as indication for the axis symmetry of the investigated liquid droplet and was used as quality criteria

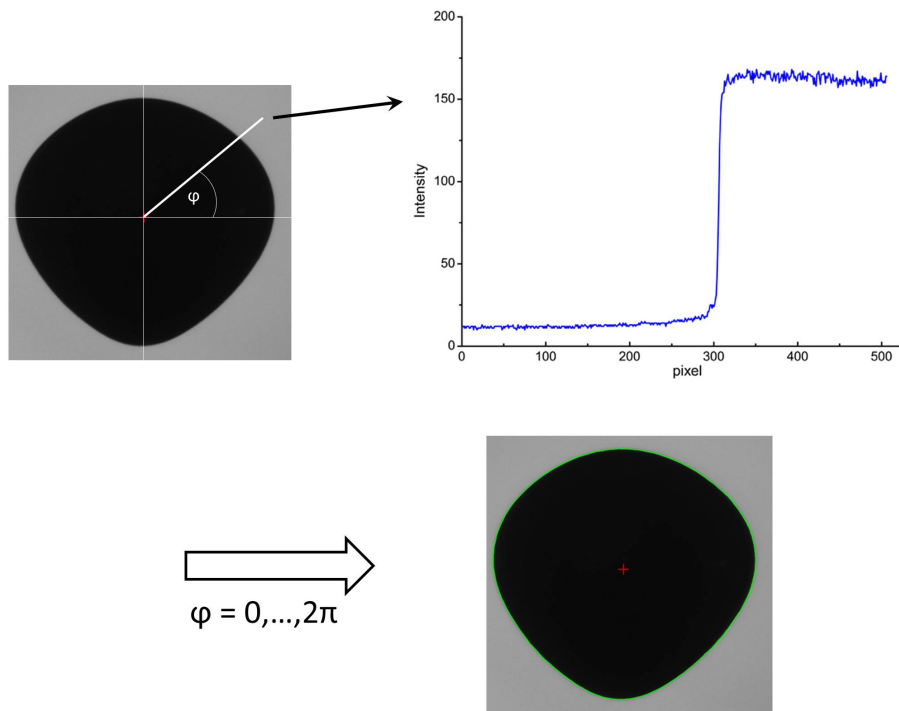
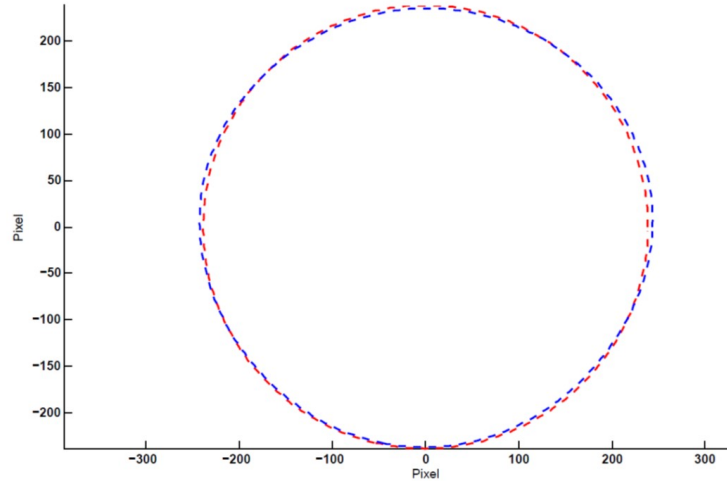


Figure 4.10: Illustration of the edge curve evaluation. The radial brightness distribution was depicted in one degree steps in polar coordinates, indicated by the white line. To locate the edge curve the resulting profile curve, depicted on the right, was fitted polynomial and the point of inflection was calculated.

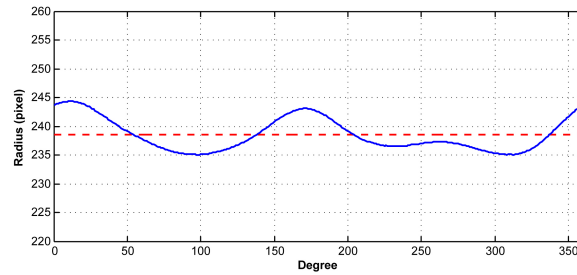
describing the adjustment between levitation coil and specimen material. (Evaluated image sequences exhibiting deviations greater than 6 % were considered inapplicable for evaluation, as the respective results often showed large variations and discrepancies. The 6 % constraint was arbitrarily set, since it turned out to be practicable for the setting at TU Graz, and should not be considered as generally reasonable).

Calibration measurements

The image series recorded for the volume measurement were monitored employing a CCD device working in pixel units. To be able to scale the evaluated droplet shapes, calibration measurements using bearing balls with defined di-



(a)



(b)

Figure 4.11: Depiction of the calculated equilibrium shape by averaging 2500 recorded images. The curve in blue represents the equilibrium shape of the specimen. To illustrate the spherical form of the determined equilibrium shape, in (a) a circle calculated with the mean equilibrium shape radius was depicted in red for comparison. (b) illustrates the deviation (in this case below 2 %) of the determined equilibrium shape from a circular form. The deviation was used as indicator for the axis symmetry of the specimen and was used as quality criteria describing the adjustment between levitation coil and specimen material.

ameters (ranging from 5 mm to 8 mm) were performed prior each levitation experiment. Figure 4.12 depicts the relationship between evaluated volume in pixel units and monitored specimen volume in mm units. The bearing balls were placed on the sample holder in the vacuum chamber and hovered by a gas flow streaming through the hollowly sample holder. Image series of the different sized bearing balls were evaluated and conversion factors determined and interpolated to scale the recorded droplet shapes on.

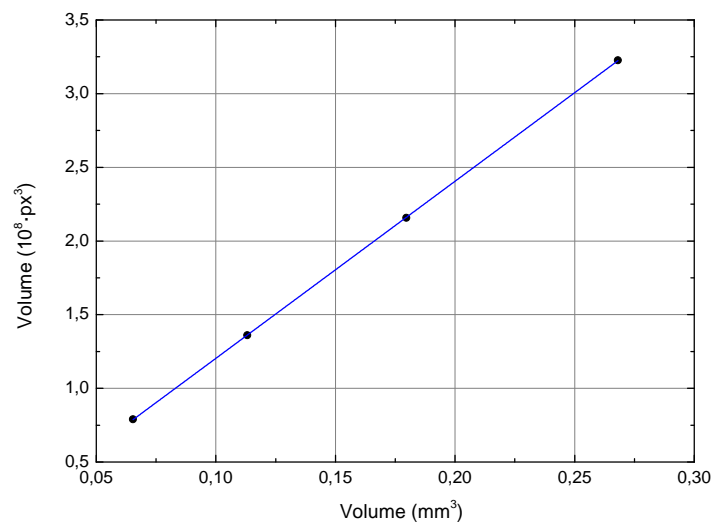


Figure 4.12: Relationship between evaluated volume in pixel units and monitored specimen volume in mm units, obtained by calibration measurements monitoring bearing balls with defined diameters.

This approach of volume evaluation was based on the assumption of an axially symmetric shape of the determined two-dimensional equilibrium representation. In case of pronounced oscillating liquid specimen shapes, deviations from the equilibrium shape can not be canceled out completely by averaging, resulting in large scattering of the determined density data or overestimation of the determined volume values. In order to avoid pronounced specimen oscillations it was of considerably importance to ensure a good adjustment between levitation coil and specimen material in the line of the preliminary experiments prior starting the respective investigation procedures. Experiments were performed meeting considerations concerning affecting and suppressing specimen oscillations by positioning magnets (made of neodymium in this case) laterally beside the coil. A

reproducible effect of purposeful influencing the specimen's oscillations couldn't be found, so all the material investigations described in chapter 5 of this work were performed with the classical setting explicated above.

5 Measuring Results

After modifying the pulse-heating expansion measurement setting and building up the electromagnetic levitation system, first density determination experiments were performed using pure metals as specimen material. Nickel and copper were chosen, since on the one hand they differ considerably in their thermophysical properties and on the other hand for both of them reliable literature data of their temperature-dependent liquid phase densities are available for comparison. Additionally, experiments in the past showed nickel to be a material well suited to be investigated with the pulse-heating setup as relatively little specimen movement could be observed in image series recorded during pulse-heating. In contrast, pure copper showed pronounced bending and was meant to be an appropriate material to test the consequences of the implemented modifications in the pulse-heating density setting on the monitored shadowgraph series and determined density values. The results achieved were in good agreement with literature and verified the functionality of the two measurement setups.

Next material of interest was aluminium, as in the past investigations using the pulse-heating method were limited to materials featuring a melting point above 1100 K. This restriction was caused by the pyrometers sensitivity range, starting at this temperature and allowing a temperature assignment only for temperatures above. To overcome this restraint, in the course of a diploma thesis (by Dipl.-Ing. Markus Kurz) a peltier cooled pyrometer capable of resolving radiances of lower melting metals during the short time of pulse-heating was constructed.

Utilizing this new pyrometer pulse-heating experiments with aluminium as specimen material could be carried out and the liquid phase density of aluminium was determined and compared with the results obtained from the levitation system. As the investigations of pure metals yield satisfying results, consequently the next step was the investigation of alloys. The industrial relevant alloy Manganin

(Cu86Mn12Ni2) was investigated and since thermophysical properties of the liquid phase of this material were generally scarcely available, besides density, additionally, properties of specific enthalpy, electrical resistivity, thermal conductivity and thermal diffusivity were determined.

Another alloy of interest was TiAl6V4, as despite its frequent usage literature data of the liquid phase density were rarely available. TiAl6V4 was investigated with both methods and liquid phase densities determined and compared to each other. While this alloy could be investigated by the pulse-heating setup without complications, the high temperature of the liquid phase (liquidus temperature of at 1923 K) posed a problem for investigations with the electromagnetic levitation system. Amidst great difficulty, some data points above the melting point could be determined, but featured large deviation from the results obtained by the pulse-heating setting.

All pulse-heating experiments were performed under argon atmosphere (2.3 bar) applying the setting described in chapter 3. For temperature determination the pyrometer working at 1570 nm (bandwidth of approx. 85 nm) was used, except for the investigation of aluminium where a pyrometer working at 2320 nm (bandwidth of approx. 300 nm) was utilized. The electromagnetic levitation experiments were performed in an environment consisting of a mixture of argon and helium with a small amount of hydrogen. The composition varied during a single experiment depending on the material and temperature, since the atmosphere and helium gas-flow were used to cool the levitating specimen and to set the desired specimen temperature.

5.1 Nickel

Investigations of nickel applying the pulse-heating setting and the electromagnetic levitation setup were performed. Experiments in the past showed nickel to be well suited to be examined in the framework of pulse-heating as its pronounced mechanical strength on the one hand facilitates a relatively reproducible handling during specimen preparation and assembly of the specimen wire in the specimen holder, and on the other hand leads combined with its moderate electrical con-

ductivity to little specimen movement and bending of the clamped wire during the heating process.

Specimen materials used were Ni-wires with 99.98 wt% (purchased from Advent, No: Ni535315) and Ni-slugs with 99.995 wt% (purchased from Alfa Aesar, LOT: L29X008). For temperature determination as reference point to calibrate the pyrometer signals, a melting temperature of $T_m = 1728$ K was adopted from [52].

Following measuring parameters were found to be suitable to avoid specimen movement and enable thermal expansion recordings of pronounced contrast exhibiting symmetric intensity profiles.

- wire diameter: 0.5 mm
- wire length: 50 mm
- load voltage: 4830 V
- dropping resistor: 0.5 Ω
- exposure time: 700 ns
- MCP voltage: 233 V
- process time: 55 μ s

The recorded image series were depicted as intensity profiles and evaluated by locating FWHM (full width at half maximum) as described in chapter 3. Thermal radial expansion was obtained by relating the image sequence recorded during the pulse-heating to an image sequence recorded prior starting the heating process. Density was calculated and depicted as function of temperature, presented in Figure 5.1. Data obtained by the new approach, depicted as open circles with dedicated linear least square fit, are compared with results obtained in the past, depicted as dashed line in green.

The general density-temperature behaviour has not changed, but the results show that the new approach yields density data lying below the former results. This is comprehensibly explainable as the the total avoidance of the longitudinal ex-

pansion of the wire led to an increased radial expansion representing the volume expansion and density respectively in a much better fashion.

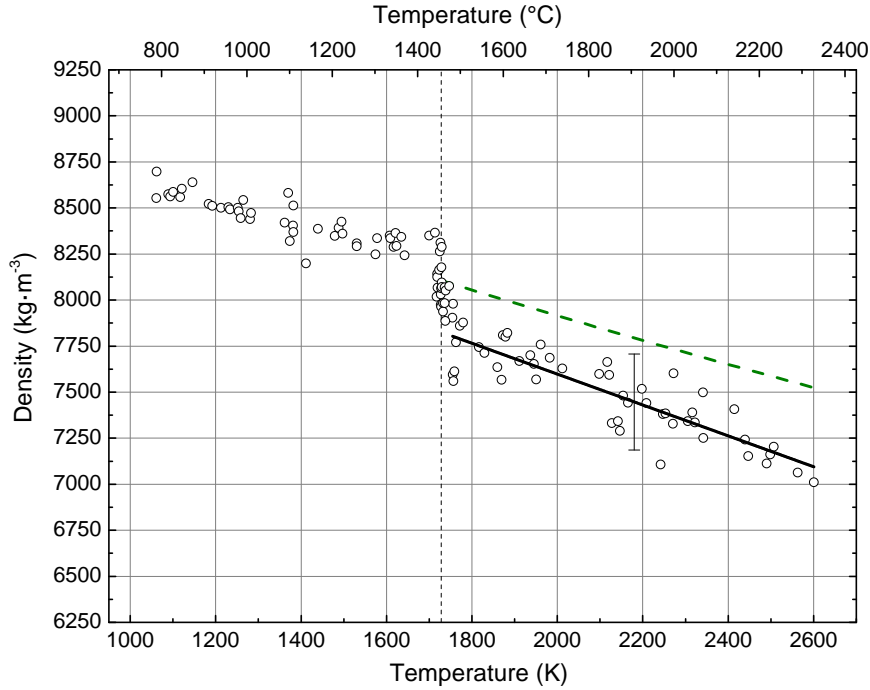


Figure 5.1: Density of nickel as function of temperature obtained by pulse-heating. Open circles with dedicated solid line in black: results for density with linear least square fit by using the new approach. Dashed line in green: results obtained in the past [53]. Vertical dashed line: temperature of phase transition, 1728 K.

The linear least square fit of the pulse-heating density results ensues to:

$$D_{\text{puls}}(T) = 9274 - 0.838 \cdot T \quad (1755 \text{ K} \leq T \leq 2600 \text{ K}) \quad (5.1)$$

For the investigations of nickel with the electromagnetic levitation setup sample sizes were adjusted attaining spherical droplets featuring diameters of about 5 mm in the liquid phase. Temperatures up to 1940 K could be reached until arising vaporization impedes the measurement. 2500 images per temperature point were recorded and evaluated. The calculated density as a function of temperature is depicted in Figure 5.2 as blue colored full triangles. The respective linear least

square fit results to:

$$D_{\text{levi}}(T) = 10157 - 1.325 \cdot T \quad (1705 \text{ K} \leq T \leq 1940 \text{ K}) \quad (5.2)$$

For comparison Figure 5.2 presents the data obtained by pulse-heating and the data obtained by levitation. Additionally, as literature reference, data of Assael et. al. [54] are depicted, merging density results of several different measuring methods. The results were published in [55]. Uncertainties were estimated (using a coverage factor $k = 2$) to $D_{\text{pulse}} : 3.5 \%$ and $D_{\text{levi}} : 1.6 \%$. Literature data of Assael et al. [54] were given with an uncertainty of 1.7% . Deviations due to a possible change of normal spectral emissivity during the liquid phase were not considered.

The results show a good concordance between the results obtained by the pulse-heating setting and the electromagnetic levitation technique, and the literature reference data as well.

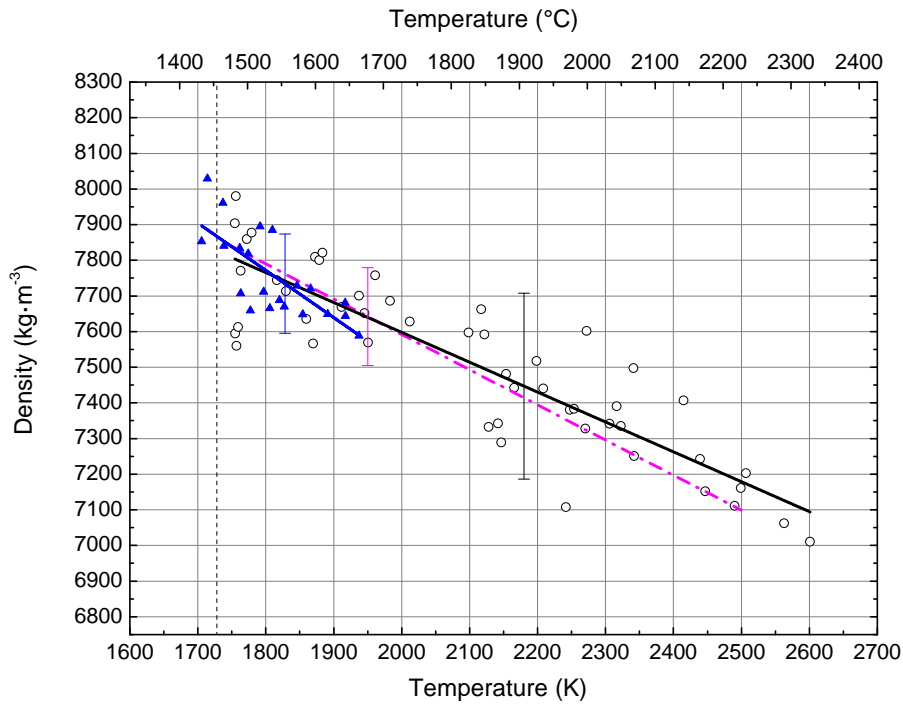


Figure 5.2: Density of liquid nickel as function of temperature. Open circles with dedicated line in black: results for density with linear least square fit obtained by pulse-heating. Full triangles with dedicated solid line in blue: results for density with dedicated linear least square fit determined by the levitation method. Dash-dotted line in pink: literature reference data for comparison [54]. Vertical dashed line: temperature of phase transition, 1728 K.

Table 5.1: Density results of liquid nickel determined with the pulse-heating setting (D_{puls}) and the levitation technique (D_{levi}).

Temperature (K)	D_{puls} ($kg \cdot m^{-3}$)	D_{levi} ($kg \cdot m^{-3}$)
1705		7898
1750	7808	7838
1800	7766	7772
1850	7724	7706
1900	7682	7640
1950	7640	7573
2000	7598	
2050	7556	
2100	7514	
2150	7472	
2200	7430	
2250	7389	
2300	7347	
2350	7305	
2400	7263	
2450	7221	
2500	7179	
2550	7137	
2600	7095	

5.2 Copper

Copper was investigated employing the pulse-heating setting and the levitation setup for comparison. Pulse-heating experiments examining copper in the past exhibited this material to be delicate in regard to thermal expansion determinations, since the material's high electrical conductivity and low mechanical strength leads to pronounced bending of the clamped wire sample frustrating the approach to assume a completely suppressed longitudinal thermal expansion of the specimen.

Copper samples investigated were Cu-wires with 99.996 wt% (purchased from Advent, No: Cu510815) and Cu-slugs with 99.9999 wt% (purchased from Alfa Aesar, LOT: E15Y023). For temperature determination as reference point to calibrate the pyrometer signals a melting temperature of $T_m = 1358$ K was adopted

from [56].

Following measuring parameters were found to be suitable to avoid specimen movement and enable thermal expansion recordings of pronounced contrast exhibiting symmetric intensity profiles.

- wire diameter: 0.5 mm
- wire length: 40 mm
- load voltage: 7176 V
- dropping resistor: 0.25 Ω
- exposure time: 567 ns
- MCP voltage: 233 V
- process time: 45 μ s

The wire length was drastically shortened from typically 70 mm to about 40 mm to improve the stability of the vertical aligned liquid metal column. Image series were recorded with reduced exposure times to react on the short process times and high heating rates. The recorded image series were depicted as intensity profiles and evaluated according the procedure described in chapter 3. Thermal radial expansion was obtained by relating the image sequence recorded during the pulse-heating to an image sequence recorded prior starting the heating process. Density was calculated and depicted as function of temperature, presented in Figure 5.3. Data obtained by the optimized setting, depicted as open circles with respective linear least square fit, are compared with results obtained in the past, depicted as dashed line in green.

The new approach delivers density data lying below the former results, which is comprehensible since the suppressed longitudinal expanding of the clamped wire was compensated by the increased radial expansion representing better the thermal volume expansion of the sample and density respectively. The difference in slope between the density-temperature curves can be explained by the increased instability of the liquid metal column at high temperatures, resulting

in movement and deformations of the specimens in the past experiments. The higher the temperature the more pronounced were lateral movement and longitudinal expansion of the specimen and the worse was the thermal volume expansion representation of the determined radial thermal expansion.

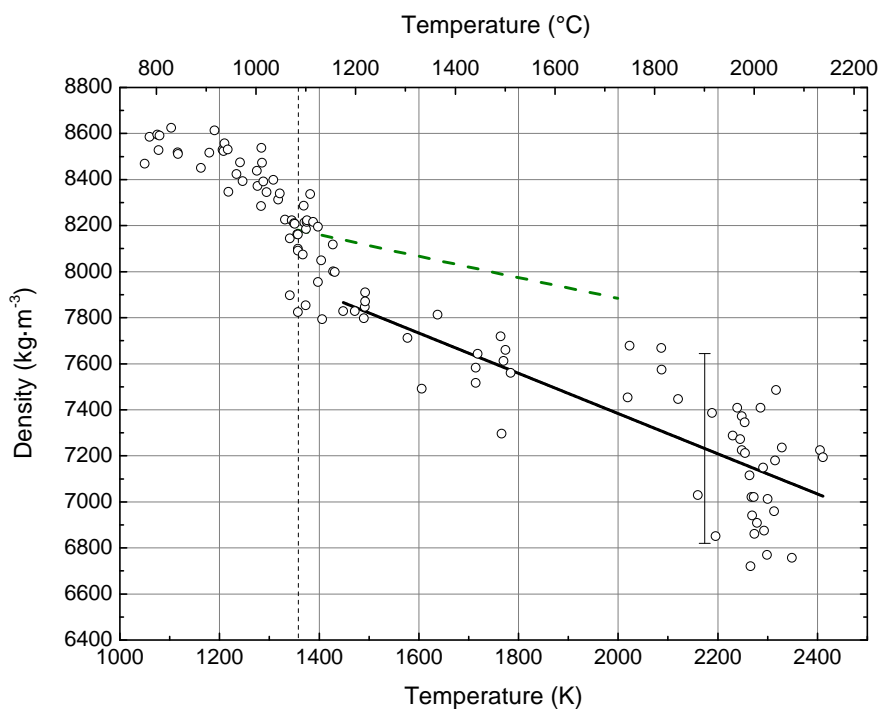


Figure 5.3: Density of copper as function of temperature obtained by pulse-heating. Open circles with dedicated solid line in black: results for density with linear least square fit by using the new approach. Dashed line in green: results obtained in the past [57]. Vertical dashed line: temperature of phase transition, 1358 K.

The linear least square fit of the pulse-heating density results ensues to:

$$D_{\text{puls}}(T) = 9132 - 0.874 \cdot T \quad (1450 \text{ K} \leq T \leq 2400 \text{ K}) \quad (5.3)$$

For the copper investigations employing the electromagnetic levitation setup, sample sizes were adjusted attaining spherical droplets featuring diameters of about 6 mm in the liquid phase. Temperatures up to 1710 K could be reached until arising vaporization impedes the measurement. 2500 images per tempera-

ture point were recorded and evaluated. The calculated density as function of temperature is depicted in Figure 5.4 as blue colored full triangles. The respective linear least square fit results to:

$$D_{\text{levi}}(T) = 8903 - 0.790 \cdot T \quad (1355 \text{ K} \leq T \leq 1710 \text{ K}) \quad (5.4)$$

For comparison Figure 5.4 presents the data obtained by pulse-heating and the data obtained by levitation. Additionally, as literature reference, data of Assael et. al. [58] are depicted, merging density results of several different measuring methods. The results were published in [55].

Uncertainties were estimated (using a coverage factor $k = 2$) to $D_{\text{pulse}} : 5.2 \%$ and $D_{\text{levi}} : 1.5 \%$. Literature data of Assael et al. [58] were given with an uncertainty of 1.3% . Deviations due to a possible change of normal spectral emissivity during the liquid phase were not considered.

The results show a good concordance between the results obtained by the pulse-heating setting and the electromagnetic levitation technique, and the literature reference data as well.

The density results determined with the pulse-heating setting and the levitation technique are given in Table 5.3.

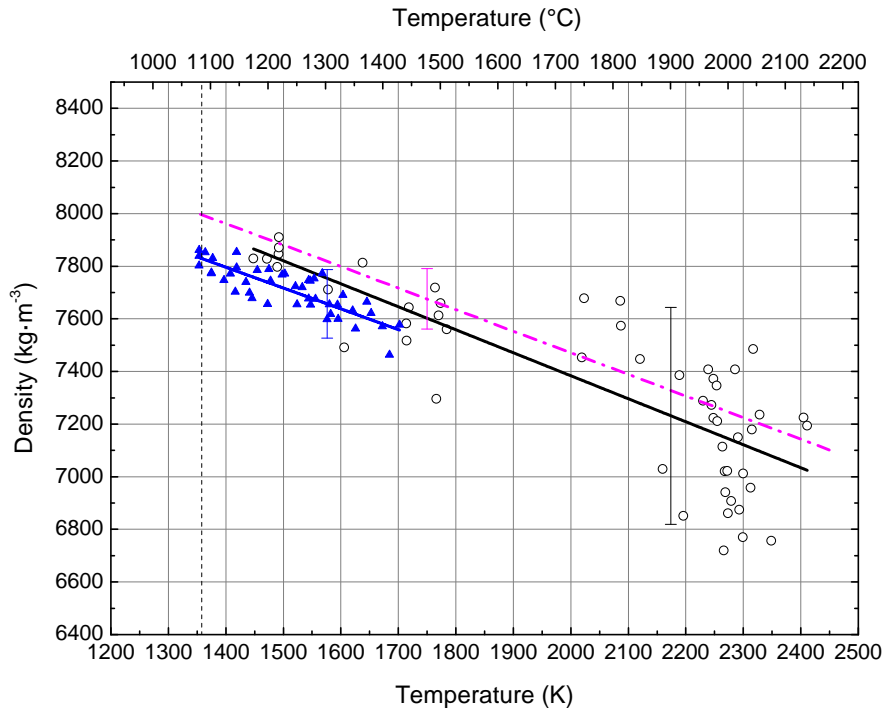


Figure 5.4: Density of liquid copper as function of temperature. Open circles with dedicated line in black: results for density with linear least square fit obtained by pulse-heating. Full triangles with dedicated solid line in blue: results for density with dedicated linear least square fit determined by the levitation method. Dash-dotted line in pink: literature reference data for comparison [58]. Vertical dashed line: temperature of phase transition, 1358 K.

Table 5.2: Density results of liquid copper determined with the pulse-heating setting (D_{puls}) and the levitation technique (D_{levi}).

Temperature (K)	D_{puls} ($kg \cdot m^{-3}$)	D_{levi} ($kg \cdot m^{-3}$)
1355		7833
1400		7797
1450	7865	7758
1500	7821	7718
1550	7777	7679
1600	7734	7639
1650	7690	7600
1700	7646	7560
1750	7603	
1800	7559	
1850	7515	
1900	7471	
1950	7428	
2000	7384	
2050	7340	
2100	7297	
2150	7253	
2200	7209	
2250	7166	
2300	7122	
2350	7078	
2400	7034	

5.3 Aluminium

Investigations of aluminium were performed employing the pulse-heating setting and the levitation setup for comparison. In the past only metals and alloys featuring a liquidus temperature above 1100 K were investigated by pulse-heating since the available pyrometers were not sensitive to determine temperature below. To overcome this restraint, in the course of a diploma thesis (by Dipl.-Ing. Markus Kurz) a peltier cooled pyrometer capable of resolving radiances of lower melting metals during the short pulse-heating process was constructed and utilized to determine thermophysical properties of aluminium. Kurz performed thermal ex-

pansion determinations in the classical approach, making this results well suited to serve as comparison data for the results obtained with the new setting and showing the consequences of the new approach on low melting metals.

Specimen material investigated were Al-wires with 99.999 wt% (purchased from Advent, No: AL501115) and Al-slugs with 99.999 wt% (purchased from Advent, No: AL501909). For temperature determination as reference point to calibrate the pyrometer signals a melting temperature of $T_m = 933$ K was adopted from [56].

Following measuring parameters were found to be suitable to avoid specimen movement and enable thermal expansion recordings of pronounced contrast exhibiting symmetric intensity profiles.

- wire diameter: 0.5 mm
- wire length: 40 mm
- load voltage: 6900 V
- dropping resistor: 0.25 Ω
- exposure time: 600 ns
- MCP voltage: 233 V
- process time: 40 μs

The material's high electrical conductivity and low mechanical strength necessitated high loading voltages and short process times. The wire length was drastically shortened to about 40 mm to improve the stability of the vertical aligned liquid metal column. Image series were recorded with reduced exposure times to react on the short process times. The recorded image series were depicted as intensity profiles and evaluated according the procedure described in chapter 3. Thermal radial expansion was obtained by relating the image sequence recorded during the pulse-heating to an image sequence recorded prior starting the heating process. Density was calculated and depicted as function of temperature, pre-

sented in Figure 5.5. Data obtained by the optimized setting, depicted as open circles with respective linear least square fit, are compared with results obtained during the diploma thesis by Markus Kurz [28], depicted as dashed line in green. The new approach delivers density data showing a density-temperature behaviour different compared to the former approach. The difference in slope can be explained by the increased instability of the liquid metal column at higher temperatures, resulting in deformations of the specimen in the former experiments, frustrating the assumption of a completely suppressed longitudinal thermal expansion of the specimen.

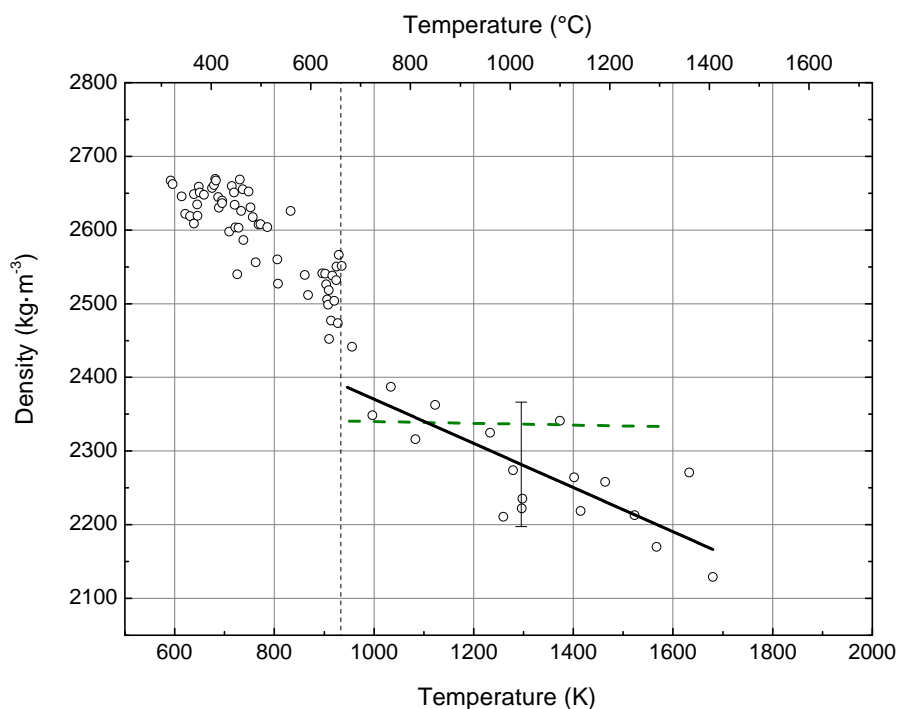


Figure 5.5: Density of aluminium as function of temperature obtained by pulse-heating. Open circles with dedicated solid line in black: results for density with linear least square fit by using the new approach. Dashed line in green: results obtained in the past [28]. Vertical dashed line: temperature of phase transition, 933 K.

The linear least square fit of the pulse-heating density results ensues to:

$$D_{\text{puls}}(T) = 2670 - 0.299 \cdot T \quad (956 \text{ K} \leq T \leq 1680 \text{ K}) \quad (5.5)$$

For the aluminium investigations employing the electromagnetic levitation setup, sample sizes were adjusted attaining spherical droplets featuring diameters of about 6 mm in the liquid phase. Temperatures up to 1370 K could be reached until arising vaporization impedes the measurement. 2500 images per temperature point were recorded and evaluated. The calculated density as function of temperature is depicted in Figure 5.6 as blue colored full triangles. The respective linear least square fit results to:

$$D_{\text{levi}}(T) = 2569 - 0.255 \cdot T \quad (1000 \text{ K} \leq T \leq 1370 \text{ K}) \quad (5.6)$$

For comparison Figure 5.6 presents the data obtained by pulse-heating and the data obtained by levitation. Additionally, as literature reference, data of Assael et. al. [59] are depicted, merging density results of several different measuring methods.

Uncertainties were estimated (using a coverage factor $k = 2$) to $D_{\text{pulse}} : 3.7 \%$ and $D_{\text{levi}} : 1.5 \%$. Literature data of Assael et al. [59] were given with an uncertainty of 0.65 %. Deviations due to a possible change of normal spectral emissivity during the liquid phase were not considered.

The density results determined with the pulse-heating setting and the levitation technique are given in Table 5.3.

Basically, the results show a good concordance between the results obtained by the pulse-heating setting and the electromagnetic levitation technique, and the literature reference data as well. Data obtained by levitation are a little lower than the given reference. Data obtained by pulse-heating can be considered to correspond with the other results as consequence of the pronounced scattering of the pulse-heating data. The overall density-temperature behaviours of the results correspond to each other.

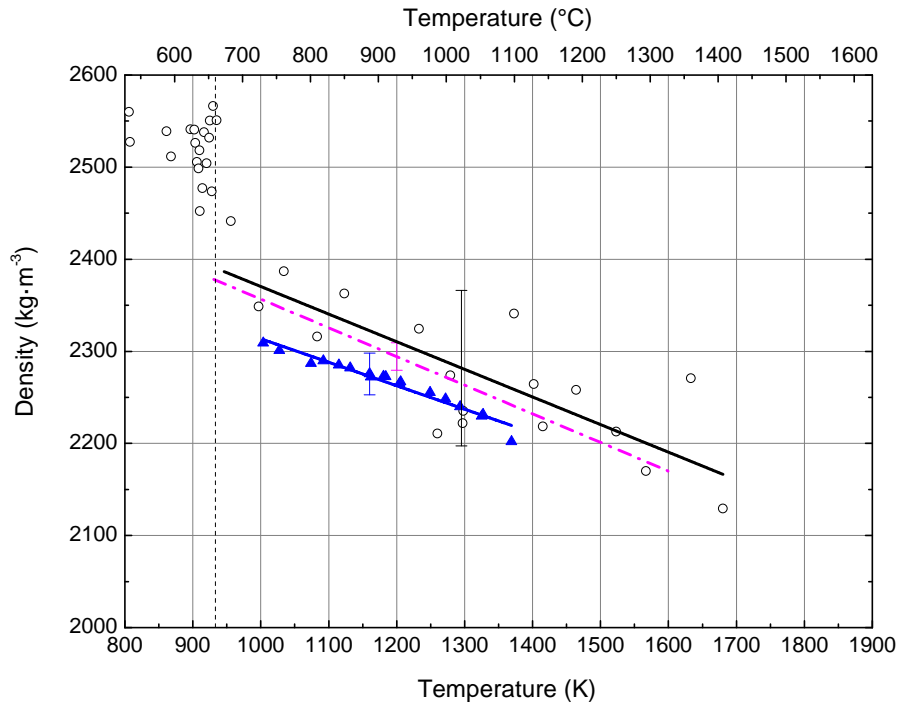


Figure 5.6: Density of liquid aluminium as function of temperature. Open circles with dedicated line in black: results for density with linear least square fit obtained by pulse-heating. Full triangles with dedicated solid line in blue: results for density with dedicated linear least square fit determined by the levitation method. Dash-dotted line in pink: literature reference data for comparison [59]. Vertical dashed line: temperature of phase transition, 933 K.

Table 5.3: Density results of liquid aluminium determined with the pulse-heating setting (D_{puls}) and the levitation technique (D_{levi}).

Temperature (K)	D_{puls} ($kg \cdot m^{-3}$)	D_{levi} ($kg \cdot m^{-3}$)
956	2384	2325
1000	2371	2314
1050	2356	2301
1100	2341	2289
1150	2326	2276
1200	2311	2263
1250	2296	2250
1300	2281	2238
1350	2266	2225
1370	2260	2220
1400	2251	2212
1450	2236	2199
1500	2222	2187
1550	2207	2174
1600	2192	2161
1650	2177	2148
1680	2168	2141

5.4 Manganin - Cu86Mn12Ni2

Cu86Mn12Ni2 is a resistance alloy known for its virtually temperature-independent electrical resistivity in the temperature range between 0°C and 100°C. It's marketed under the trademark name Manganin (trademark proprietor 'Isabellenhütte Heusler GmbH & Co. KG'.) and is a commonly used material for manufacturing ammeter shunts and measuring lines. Since literature data are scarce particularly at higher temperatures, a set of thermophysical data of this alloy was determined including specific enthalpy, electrical resistivity, isobaric heat capacity and density as function of temperature, applying the pulse-heating system. Additionally electrical resistivity and density in the solid state were determined employing a four-point probe setup and a two-beam laser dilatometer, respectively. Solidus and liquidus temperatures were determined by differential thermal analysis (DTA) using a heating rate of $10 \text{ K} \cdot \text{min}^{-1}$ to $T_{\text{sol}} = 1177 \text{ K}$ and $T_{\text{liq}} = 1269 \text{ K}$.

A detailed description of the examination setups used and results obtained can be found in the manuscript of the respective publication [60] on p. 118. Investigated Manganin samples were manufactured by Isabellenhütte Heusler GmbH & Co. KG, No: 569780.

Concerning density determination with the pulse-heating setting following measuring parameters were found to be suitable to avoid specimen movement and enable thermal expansion recordings of pronounced contrast exhibiting symmetric intensity profiles:

- wire diameter: 0.5 mm
- wire length: 45 mm
- load voltage: 5244 V
- dropping resistor: 0.5 Ω
- exposure time: 663 ns
- MCP voltage: 233 V
- process time: 50 μs

The recorded image series were depicted as intensity profiles and evaluated according the procedure described in chapter 3. Thermal radial expansion was obtained by relating the image sequence recorded during the pulse-heating to an image sequence recorded prior starting the heating process. Density was calculated and depicted as function of temperature, presented in Figure 5.7. Data obtained by pulse-heating are depicted as open circles with respective linear least square fit in the liquid.

The linear least square fit of the pulse-heating density results ensues to:

$$D_{\text{puls}}(T) = 8466 - 0.849 \cdot T \quad (1290 \text{ K} \leq T \leq 1860 \text{ K}) \quad (5.7)$$

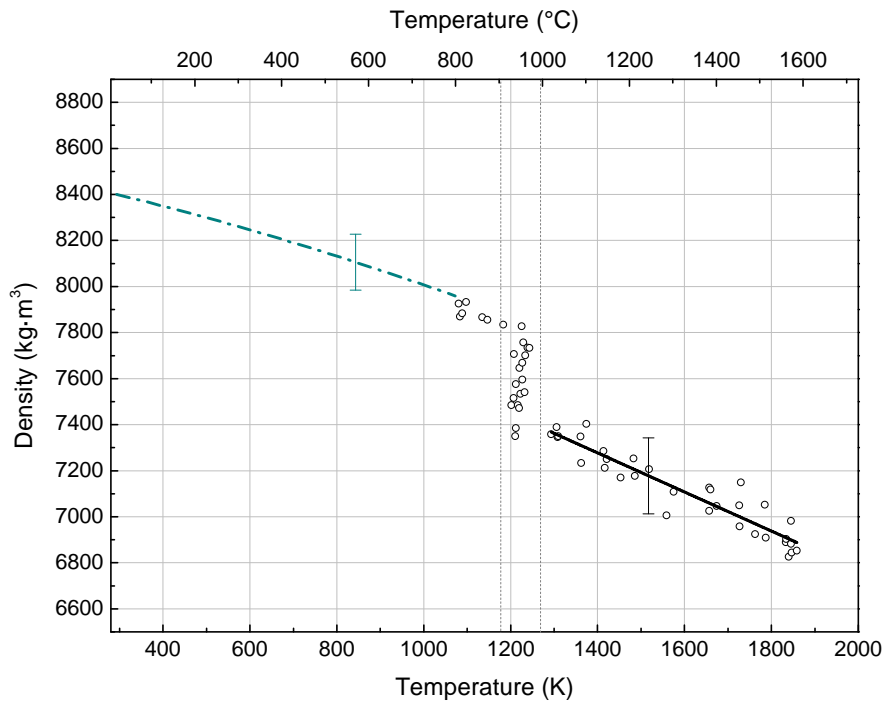


Figure 5.7: Density of Manganin as function of temperature. Open circles with dedicated solid line in black: results for density with linear least square fit by obtained by pulse-heating. Dash-dotted line in turquoise: results obtained by laser dilatometer measurements in the solid (performed by M. Luckabauer). Vertical dashed lines: temperatures of phase transition, $T_{\text{sol}} = 1177$ K and $T_{\text{liq}} = 1269$ K.

Investigations employing the electromagnetic levitation system were impeded by reason of intense vaporizing of the specimen material when reaching the liquid phase. Since no literature data regarding the density of Manganin at high temperatures could be found, only the density data obtained by laser dilatometer measurements in the solid (performed by M. Luckabauer) are plotted in Figure 5.7 for comparison. The laser dilatometer curve depicted as dash-dotted line in green matches well with the pulse-heating data at the end of the solid phase at their point of encounter. Certainly the pulse-heating data in the solid has to be considered as rough estimate since the assumption of a constant normal emissivity is reasonable only for the liquid phase. But the good agreement of the results of the two measuring techniques allows a certain appraisal of the pulse-heating data. Corresponding density values of both techniques are given in Table 5.4.

Table 5.4: Density results of Manganin determined with the pulse-heating setting (D_{puls}) in the liquid and the laser dilatometer (D_{dil}) in the solid.

Temperature (K)	D_{puls} ($\text{kg} \cdot \text{m}^{-3}$)	D_{dil} ($\text{kg} \cdot \text{m}^{-3}$)
300		8397
350		8374
400		8350
450		8325
500		8299
550		8273
600		8246
650		8219
700		8190
750		8162
800		8132
850		8102
900		8071
950		8039
1000		8007
1050		7974
1070		7961
1290	7371	
1300	7362	
1350	7320	
1400	7277	
1450	7235	
1500	7193	
1550	7150	
1600	7108	
1650	7065	
1700	7023	
1750	6980	
1800	6938	
1850	6895	
1860	6887	

5.5 TiAl6V4

TiAl6V4 is a material frequently used in industrial applications such as aerospace and medical engineering due to its pronounced strength and resistance behaviour. Nevertheless thermophysical data, as density, at high temperatures are scarcely available.

TiAl6V4 was investigated employing the pulse-heating setting and the levitation setup for comparison.

Samples investigated were Ti90Al6V4-wires (purchased from GoodFellow, No: TI015260/1). For temperature determination as reference point to calibrate the pyrometer signals a liquidus temperature of $T_{\text{liq}} = 1923$ K was adopted from [61].

Pulse-heating measuring parameters found to be suitable to avoid specimen movement and enable thermal expansion recordings of pronounced contrast exhibiting symmetric intensity profiles were:

- wire diameter: 0.5 mm
- wire length: 55 mm
- load voltage: 4775 V
- dropping resistor: 0.5 Ω
- exposure time: 633 ns
- MCP voltage: 233 V
- process time: 55 μs

The material's pronounced mechanical strength eased the handling regarding specimen preparation and assembling of the specimen in the pulse-heating setting and led to a straightforward operating when performing the pulse-heating experiments. The stability of the vertical aligned liquid metal column could be facilitated without difficulties. Image series were recorded with relatively long exposure times leading to images of pronounced contrast. The recorded image

series were depicted as intensity profiles and evaluated according the procedure described in chapter 3. Thermal radial expansion was obtained by relating the image sequence recorded during the pulse-heating to an image sequence recorded prior starting the heating process. Density was calculated and depicted as function of temperature, presented in Figure 5.8. Data obtained by the pulse-heating setting are depicted as open circles with respective linear least square fit of the liquid phase.

The linear least square fit of the pulse-heating density results ensues to:

$$D_{\text{puls}}(T) = 4955 - 0.452 \cdot T \quad (2046 \text{ K} \leq T \leq 2592 \text{ K}) \quad (5.8)$$

For comparison literature data of Li et al. [62] are plotted as dash-dotted line in pink. There is a good agreement of the pulse-heating results with the literature data. Uncertainties were estimated (using a coverage factor $k = 2$) to $D_{\text{pulse}} : 3 \%$. Literature data of Li et al. [62] were given with an uncertainty of 1 %. Deviations due to a possible change of normal spectral emissivity during the liquid phase were not considered.

For investigations employing the electromagnetic levitation setup, sample sizes were adjusted attaining spherical droplets featuring diameters of about 6 mm in the liquid phase. It appeared to be very difficult to melt the specimen with the levitation setup. Experiments were performed under argon atmosphere with reduced pressures (of about 350 mbar) and narrow coil distances. This measures in turn led to pronounced movement and distinct oscillations of the specimen. 2500 images per temperature point were recorded and evaluated. The calculated density as function of temperature is depicted in Figure 5.8 as blue colored full triangles. The respective linear least square fit results to:

$$D_{\text{levi}}(T) = 4490 - 0.271 \cdot T \quad (1869 \text{ K} \leq T \leq 1977 \text{ K}) \quad (5.9)$$

Corresponding density values of both techniques are given in Table 5.5.

The levitation results obtained lie far below the results obtained by pulse-heating and literature as well. This can be explained by the large oscillations the specimen

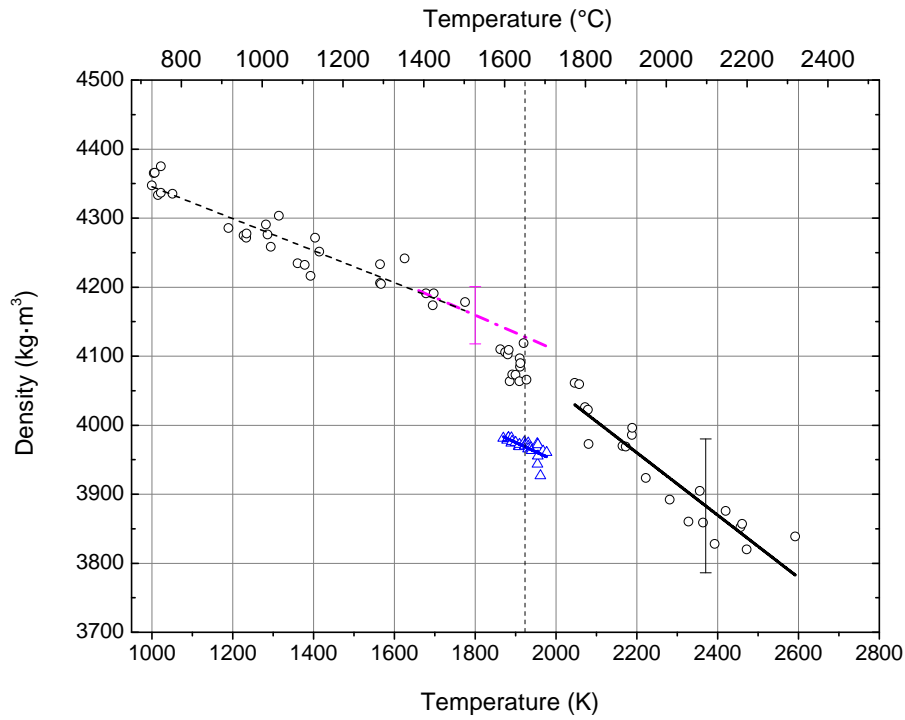


Figure 5.8: Density of TiAl6V4 as function of temperature. Open circles with dedicated line in black: results for density with linear least square fit obtained by pulse-heating. Full triangles with dedicated solid line in blue: results for density with dedicated linear least square fit determined by the levitation method. Dash-dotted line in pink: literature data for comparison [62]. Vertical dashed line: liquidus temperature of $T_{\text{liqu}} = 1923$ K.

Table 5.5: Density results of liquid TiAl6V4 determined with the pulse-heating setting (D_{puls}) and the levitation technique (D_{levi}).

Temperature (K)	D_{puls} ($kg \cdot m^{-3}$)	D_{levi} ($kg \cdot m^{-3}$)
1869		3984
1900		3975
1950		3962
1977		3954
2046	4030	
2050	4028	
2100	4006	
2150	3983	
2200	3961	
2250	3938	
2300	3915	
2350	3893	
2400	3870	
2450	3848	
2500	3825	
2550	3802	
2592	3783	

was performing during the measurement, which frustrated the assumption of an axially symmetric equilibrium shape of the levitating liquid droplet. The investigation of this material pointed the upper temperature limit of the levitation apparatus at TU Graz.

6 Uncertainties

This chapter gives an overview of the uncertainty estimation used to determine the uncertainties given in chapter 5.

Uncertainties were estimated by combining the standard uncertainties Δx_i of the input quantities x_i to calculate the standard uncertainty Δy of the estimate y , on the basis of a measurement model $y = f(x_1, \dots, x_N)$ relating the output quantity y to the input quantities.

$$\Delta y = \sqrt{\sum_{i=1}^N (c_i \cdot \Delta x_i)^2} \quad (6.1)$$

$$c_i = \frac{\partial f}{\partial x_i}$$

The uncertainties of the input quantities contribute to the uncertainty of the output quantity (in uncorrelated case) according to GUM with $c_i \cdot \Delta x_i$. The sensitivity coefficients c_i describe the dependence of the output quantity on small changes of the input quantities, and correspond to the partial derivative of the measurement model with respect to x_i .

To give an interval about the output estimate wherein the value of the measurand should confidently lie, the expanded uncertainty is used. It's denoted as product of combined standard uncertainty with a coverage factor k . Uncertainties in the course of this thesis are given with a coverage factor $k = 2$ (which corresponds for a normal distribution to a level of confidence of approximately 95 %).

6.1 Pulse-heating

Uncertainty of temperature

For the determination of uncertainty in temperature the software *MAPHS* (created in the course of a master thesis by Macher [33] (2014) based on the work of [63]) was used to combine the uncertainties impacting the pyrometrical temperature measurement at pulse-heating at TU Graz.

Main influencing parameters are (using a coverage factor $k = 2$) the uncertainty arising from the measuring board (depending on the used display range) ($\pm 4\%$), the uncertainty due to the temperature dependence of the pyrometer calibration constant ($\pm 8\%$), the uncertainty arising from the pyrometer adjustment ($\pm 3\text{ K}$) and the uncertainty of the liquidus temperature used for referencing the radiance signal ($\pm 10\text{ K}$).

An additional factor that has to be considered is the skin-effect occurring at pulse-heating. It describes the unequal distribution of current density over the cross section of a conductor in case of alternating currents. The current density is largest near the surface of the conductor and decreases with depths. Therefore at pulse-heating the near-surface area of the wire specimen is heated stronger than the center. This leads to an uncertainty in the specimen temperature determination since the pyrometrically measured radiance corresponds to the surface temperature of the specimen. According to [64, 65] the temperature difference between specimen surface and specimen center caused by the skin effect during pulse-heating can be rough estimated with:

$$\Delta T_{Skin} \approx \frac{0.25 \cdot \mu_0 \cdot I^2}{D \cdot c_p \cdot \pi^2 \cdot r^2} \quad (6.2)$$

with

- μ_0 ... vacuum permeability, $\mu_0 = 4 \cdot \pi \cdot 10^{-7}$
- I ... maximum current during the pulse-heating experiment
- D ... density of the specimen material
- c_p ... isobaric heat capacity of the specimen material
- r ... specimen radius

The occurring temperature difference is material dependent. In case of nickel the temperature gradient in the specimen material is rather low and calculates to about 7 K. In case of copper the gradient is substantially larger and results to about 21 K.

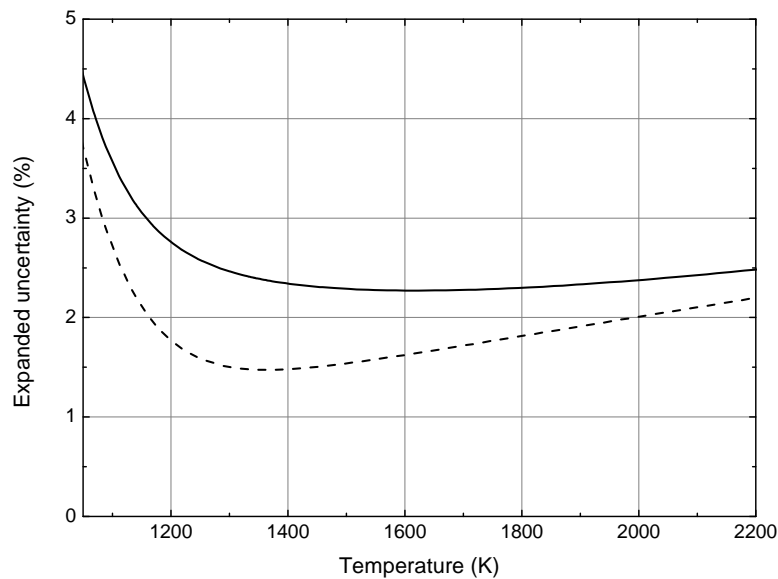


Figure 6.1: Estimated expanded uncertainty of temperature for copper. The solid line describes the uncertainty behaviour with considering skin-effect. The dashed line without considering the impact of skin effect.

To illustrate the consequences on the uncertainty calculation Figure 6.1 depicts the estimated expanded uncertainty of temperature for copper with and without considering the impact of the skin-effect caused temperature gradient.

The comparison shows a difference up to 1 % at lower temperatures. The expanded uncertainty results to about $\Delta T = 2.5$ %. Figure 6.2 depicts the corresponding uncertainty contributions of the influencing parameters. The uncertainty of temperature is dominated by the uncertainty contributions of skin-effect and pyrometer constant. Uncertainty contributions arising from the measuring board play a minor role especially at higher temperatures.

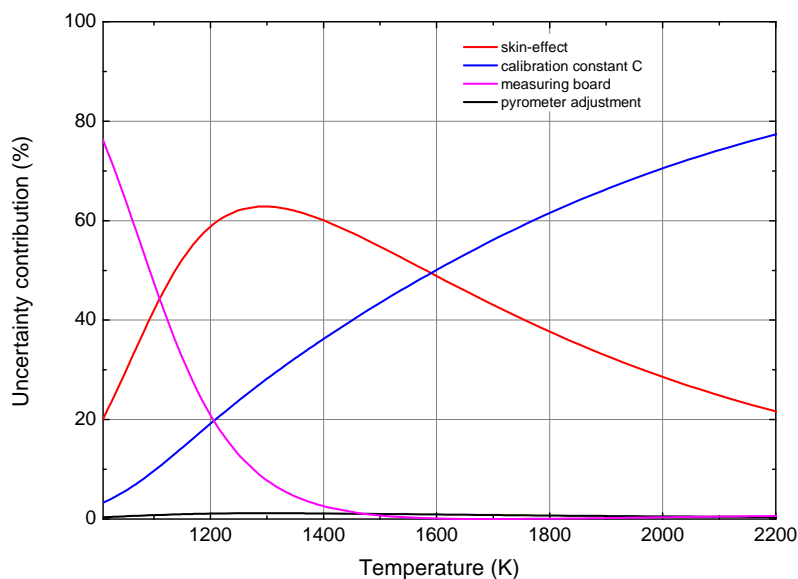


Figure 6.2: Illustration of the uncertainty contributions to the temperature uncertainty estimation for copper.

Rough estimated, the uncertainty of temperature at pulse-heating at TU Graz results to about 3 %. Uncertainties due to a possible change of normal spectral emissivity during the liquid phase are not considered.

Uncertainty of Density

In the pulse-heating density determination the essential measuring quantity is the diameter d of the specimen. The uncertainty Δd of the diameter results from the imaging of the wire cross section by the CCD system and the corresponding evaluation procedure. Important is not the absolute value of d , but the ratio between d_{RT} (diameter at room temperature) and d , as density follows from $\frac{d_{RT}^2}{d^2}$. In the experiment the diameter $d(t_{exp})$ is determined as function of time t_{exp} . Δt_{exp} doesn't describe a variation, but represents the lack of knowledge of the time the recorded image is assigned to, as the image is created during an expended exposure time. The uncertainty in time Δt_{exp} leads to an uncertainty in the

corresponding temperature $\Delta T_{t_{\text{exp}}}$, depending on the slope of the temperature-time curve.

$$\Delta T_{t_{\text{exp}}} = \Delta t_{\text{exp}} \cdot \frac{\partial}{\partial t} T \quad (6.3)$$

A small thermal expansion of the specimen leads to a low uncertainty contribution $\Delta \left(\frac{d_{\text{RT}}^2}{d^2} \right)_T$ due to the uncertainty of temperature ΔT .

$$\Delta \left(\frac{d_{\text{RT}}^2}{d^2} \right)_T = \frac{1}{k} \cdot \Delta T \cdot \frac{\partial}{\partial T} \left(\frac{d_{\text{RT}}^2}{d^2} \right) \quad (6.4)$$

$$\Delta \left(\frac{d_{\text{RT}}^2}{d^2} \right)_{t_{\text{exp}}} = \Delta T_{t_{\text{exp}}} \frac{\partial}{\partial T} \left(\frac{d_{\text{RT}}^2}{d^2} \right) \quad (6.5)$$

As density is calculated with:

$$D(T) = D_{\text{RT}} \cdot \frac{d_{\text{RT}}^2}{d^2}, \quad (6.6)$$

the combined uncertainty can be estimated by:

$$\Delta D = \sqrt{(S_1 \cdot \Delta D_{\text{RT}})^2 + (S_2 \cdot \Delta d)^2 + (S_3 \cdot \Delta d_{\text{RT}})^2 + (S_4 \cdot \Delta T)^2 + (S_5 \cdot \Delta t_{\text{exp}})^2 + (S_6 \cdot \Delta \frac{\partial}{\partial t} T)^2 + (S_7 \cdot \Delta \frac{\partial}{\partial T} (D_{\text{RT}} \cdot \frac{d_{\text{RT}}^2}{d^2}))^2} \quad (6.7)$$

$$S_1 = \frac{d_{\text{RT}}^2}{d^2} \quad S_2 = D_{\text{RT}} \cdot \frac{2d_{\text{RT}}^2}{d^3} \quad S_3 = D_{\text{RT}} \cdot \frac{2d_{\text{RT}}}{d^2}$$

$$S_4 = \frac{1}{2} \frac{\partial}{\partial T} \left(D_{\text{RT}} \cdot \frac{d_{\text{RT}}^2}{d^2} \right) \quad S_5 = \frac{\partial}{\partial t} (T) \cdot \frac{\partial}{\partial T} \left(D_{\text{RT}} \cdot \frac{d_{\text{RT}}^2}{d^2} \right)$$

$$S_6 = \frac{\partial}{\partial T} \left(D_{\text{RT}} \cdot \frac{d_{\text{RT}}^2}{d^2} \right) \quad S_7 = \frac{\partial}{\partial t} (T)$$

Repeated evaluating of d_{RT} and Δd results to standard deviations of 0.2. A rough estimation with 0.5 results an expanded uncertainty of 2 % (taking as example

nickel). Assuming that the recorded profiles deteriorate during the experiment, the evaluation with $\Delta d = 1$ results to an expanded uncertainty of 3 %.

The uncertainty of density is dominated by the uncertainty of the diameter determination. Uncertainties contribute relatively with about: d : 60 %, d_{RT} : 20 %, t_{exp} : 13 % and T : 5 %.

Therefore, improvements of the pulse-heating density determination concerning precision should concentrate on enhancing the sensitivity or resolution of the monitoring system.

6.2 Electromagnetic levitation

Considering the measurement uncertainty of the pyrometer (according specification description) and the inaccuracy of the liquidus temperature used for referencing the pyrometer signal, the uncertainty of temperature at electromagnetic levitation was estimated to about $\Delta T = 10$ K. This corresponds to an uncertainty in density (depending on the density-temperature curve) of about 0.2 %. At present development status the variations of the determined density values are mainly caused by the occurring surface oscillations of the levitated liquid droplets and deviations from the assumption of axis symmetry of the specimen shape. Therefore the uncertainty of density was estimated using the empirical standard deviation of the density data scattering. The uncertainty of density estimates to about 2 %.

Current measures aims to reduce the surface oscillations, which seem to be strongly influenced through the cooling of the droplet by gas flow. Additionally a second camera system recording from top, synchronised in time with the side view monitoring is being established in order to enable an estimation of the axis symmetry of the specimen shape and the deviations of it.

7 Discussion

Density determinations by means of the fast resistive pulse-heating setting were based on the assumption that in case of prevented longitudinal expansion of the vertical aligned fixed specimen wire the increased radial expansion occurring instead is a good representation of the thermal volume expansion or density of the specimen material.

The pulse-heating density results of the test materials nickel and copper, depicted in Figure 5.1 and Figure 5.3, substantiate this assumption. Compared to former thermal expansion results, the gained density values are substantially lower, which can be explained by an increased radial expansion due to the impeded longitudinal expansion of the liquid metal column. In case of copper the resulted density-temperature curve showed a difference in slope additionally, explainable by the increased instability of the liquid metal column with temperature, leading to pronounced bending and deformations of the metal column if longitudinal expansion is not prevented. A similar behaviour can be seen in the results of aluminium, depicted in Figure 5.5. The increased tendency to bending and deformation of materials featuring low mechanical strength leads to larger deviations of the density values the higher the temperatures are.

The data obtained for copper show large scattering, compared to the results for nickel. The high electrical conductivity and low mechanical strength of copper necessitated large heating currents and high heating rates to avoid bending of the wire specimen. This led to short process times and less pronounced intensity profiles compared to the data obtained for nickel.

Generally it can be said that materials of low mechanical strength are much more difficult to handle regarding density determination with the pulse-heating setting at TU Graz. Indeed it became apparent that a reproducible experimental working practice was prerequisite to assure the prevention of specimen movement

during the heating process, since the assembly and mounting of the specimen in the sample holder had decisive influence on the stability of the liquid metal column during the heating through the liquid phase.

Nickel and copper were chosen as test materials since reliable literature data of their temperature-dependent liquid phase densities were available. The gained density results show a good agreement with the literature reference, which affirms the applied approach to calculate the thermal volume expansion from the increased radial expansion to be reasonable and practicable.

The investigations of aluminium demonstrated that the pulse-heating technique can be used to determine the density of metals with lower melting points and low mechanical strength as well. The density results of aluminium are in good agreement with literature and the new measuring approach revised the implausible density-temperature behaviour yielded in the past.

Considering the density determinations employing electromagnetic levitation, the results obtained for copper, nickel as well as aluminium show good concordance with the results obtained by pulse-heating and literature reference values as well. The technique using a combination of LED panel a diffuser for backlighting the levitated specimen was demonstrated to be well suited to record images of high contrast. Density determination by electromagnetic levitation is based on the assumption of an axially symmetric shape of the determined two-dimensional equilibrium specimen shape representation. This approach showed to be practicable as long pronounced surface oscillations of the levitating liquid droplet could be prevented. Especially specimen materials of high electrical conductivity such as copper and aluminium appeared to be well suited to be investigated with this setup since stable positioning of the droplet combined with low heating rates led to low interactions through the gas flow cooling. Levitation results for nickel show more spread compared to levitation results for copper because of a nickel's pronounced tendency to exhibit surface oscillations and surface deformations. Central issue to obtain reliable results was to find a good adjustment between levitation coil and specimen material to facilitate a stable levitating with oscillations as small as possible, to permit the assumption of a axial symmetric equilibrium droplet shape.

After investigating pure metals next step was the investigation of alloys. Inten-

tion was to examine the industrial relevant alloys Manganin ($\text{Cu}_{86}\text{Mn}_{12}\text{Ni}_2$) and TiAl_6V_4 employing the pulse-heating setting and perform density determinations by electromagnetic levitation for comparison.

Regarding Manganin a set of thermophysical properties using the pulse-heating setting, a four-point probe setup, a DTA system and a two-beam laser dilatometer was determined, detailed described in [60]. Density determinations using the pulse-heating setting could be performed without particular difficulties after the appropriate experimental parameters were found. Investigating the material using the levitation setup turned out to be problematical since intense vaporization occurred when reaching the melting point frustrating a reasonable measurement. Since no literature data of liquid phase density of Manganin was available, the obtained pulse-heating result was verified by comparing the solid phase density at the end of the liquid phase obtained by pulse-heating as well, with the solid phase density results determined by laser dilatometry (performed by Luckabauer). Even though the pulse-heating data in the solid has to be considered as rough estimate since the assumption of a constant normal emissivity is reasonable only for the liquid phase, the very good concordance of the solid phase data of the two measuring methods allows an assessment of the corresponding liquid phase results.

The investigation of the alloy TiAl_6V_4 employing the pulse-heating setting showed to be straightforwardly since the material's pronounced mechanical strength eased the handling regarding specimen assembly and the stability of the liquid metal column could be facilitated without difficulties. The investigations using the electromagnetic levitation setup turned out to be difficult, since heating the material up to temperatures of its liquid phase could be barely accomplished. Some data points of strong oscillating droplets just above melting could be recorded and delivered density results much lower than the obtained pulse-heating results. The large oscillations of the liquid drop frustrated the assumption of an axially symmetric equilibrium shape and hampered a reasonable data evaluation. The investigation of this material indicated the upper temperature limit of the electromagnetic levitation apparatus at TU Graz.

Comparing the results of the two investigation techniques the different advantages offered by pulse-heating or electromagnetic levitation are apparent. The

pulse-heating setting allows to obtain data in a temperature range unattainable to other techniques, but in the course of this destroys the specimen when reaching the boiling point (specimen explodes to a steam of nanometer-sized particles). The experimental effort is relatively high as a laborious parameter finding process is necessary to find suitable measuring parameters when investigating new materials. The electromagnetic levitation technique in contrast permits the investigation of materials in a restricted temperature range, but due to long experimental durations (compared to pulse-heating) with higher accuracy. Concerning specimen material requirements the levitation technique is relatively unpretentious since specimens of different shapes and sizes can be levitated, given that the prerequisite of electrical conductivity is fulfilled. Pulse-heating requires, besides electrical conductivity, wire-shaped specimens of restricted diameters and lengths, which can not be provided for every specimen material. The experiments demonstrated a crucial advantage of pulse-heating concerning specimen material evaporation. While at pulse-heating material vaporization has only very little influence on the measurements due to the very short experimental durations, investigations with the levitation setup can be frustrated by intense vaporization processes hampering the optical measurement and potentially changing the specimen material composition. This was demonstrated as levitation experiments with CuSn₅Zn₁ as specimen material were performed and almost the entire Zn-portion vanished due to occurring intense evaporating, described in publication [37]. When investigating alloys featuring pronounced evaporation during the levitation investigation, subsequent composition analyses are needed.

Both pulse-heating and electromagnetic levitation are well-suited to investigate reactive materials due to their containerless examination structures. Even though it could be demonstrated that the presented approach applying the pulse-heating setting at TU Graz to determine density is also applicable to low melting metals, the key benefit of the setting is the capability to determine densities in a temperature range above 2000 K (up to about 5500 K). However, its insensitivity to vaporizing effects makes it a valuable method for density comparisons at lower temperatures as well.

It could be shown that if longitudinal expansion of the specimen wire is prevented, the pulse-heating setting at TU Graz can be applied to determine the density of

the liquid phase as function of temperature in an extensive temperature range covering the liquid phase region of most metals and alloys. The accuracies of the density results are dominated by the uncertainties caused by the gained intensity profiles in the course of the evaluation process, where images recorded during the heating process are related to images monitored before starting the heating. The total uncertainty for density was estimated to about 4 % (using a coverage factor $k = 2$). Improvements of the pulse-heating density setting concerning precision should concentrate on enhancing the sensitivity of the monitoring system, which at present is determined by the microchannel plate - phosphor screen combination used as image intensifier system or increasing the resolution of the CCD recording system. A further improvement to enhance the present setting would be to find an illumination device featuring a higher luminous intensity.

Regarding the electromagnetic levitation setup current experiments are aimed to reduce the occurring surface oscillations of the levitated liquid drops. Distinct oscillations lead to overestimations of the specimen volumes and result in too low density values. Disturbing influence seems to be the approach to cool the specimen by gas flow through the hollowly constructed specimen holder to set the specimen temperature. Attempts to regulate the temperature by changing the composition of the surrounding atmosphere appear to be promising to lessen specimen surface oscillations and increase the precision of the measurements. It seems also to be auspicious to use rather specimens of lower diameter to lessen specimen deformations, provided that heating of the specimen is not restricted by this.

Comparisons of pulse-heating density results obtained by the new approach with results from the past show the need to revise some of the former results. Generally, determinations of enthalpy and electrical resistivity have to be performed separately from density determinations, applying the pulse-heating setup at TU Graz. The density results can not be used to consider thermal expansion in course of the electrical resistivity evaluation and vice versa, since the assumption of a total prevention of longitudinal expansion is not complied during the belonging measurement. The radial thermal expansion measurement during enthalpy and electrical resistivity measurements describes the specimen's radial expanding behaviour at the specific boundary conditions of these experiments. A certain level

of longitudinal expansion is usually occurring, leading to a reduced radial expansion compared to the radial expansion determined in the course of the density measurement approach.

8 Outlook

It was shown that the fast resistive pulse-heating setup at TU Graz can be used to determine reliably the density of liquid metals. This offers the possibility to determine density up to temperatures of about 5500 K under conditions of reduced interactivity with the environment and prevented contamination of the sample material.

Focus was on density determination at ambient pressures in argon atmosphere. High pressure pulse-heating experiments at TU Graz in the past, at about 1000 bar with distilled water as pressurized medium, delivered results showing increased radial thermal expansions compared to experiments performed at low pressures. There couldn't be found an explanation for this behaviour. It would be interesting to use the density measurement approach in combination with the high pressure setup to determine thermal expansions in the high pressure range again.

The built-up electromagnetic levitation setup is well suited to determine density of liquid metals at temperatures below 1900 K. Current experiments are aimed to reduce surface oscillations of the levitated liquid droplets by changing the method to regulate the temperature of the specimen, as cooling the specimen through gas flow seems to have disturbing influences on the specimens geometry.

A second camera system recording the levitated liquid droplet from top, synchronised in time with the side view monitoring would help to estimate the axis symmetry of the specimen shape and assess the deviation of a rotational symmetrically form assumed for the evaluation.

9 Publications

Published articles:

- 8.) K. Aziz; A. Schmon; E. Kaschnitz; J. Rattenberger; G. Pottlacher:
Measurement of surface tension of Cu-5Sn by an oscillating drop - levitation technique
International Journal of Thermophysics. 37, p. 1-8, (2016)
DOI: 10.1007/s10765-015-2023-z
- 7.) A. Schmon; K. Aziz; M. Luckabauer; G. Pottlacher:
Thermophysical properties of Manganin (Cu₈₆Mn₁₂Ni₂) in the solid and liquid state
International Journal of Thermophysics. 36, p. 1618-1626, (2015)
DOI: 10.1007/s10765-015-1909-0
- 6.) K. Aziz; A. Schmon; G. Pottlacher:
Measurement of surface tension of liquid nickel by the oscillating drop technique
High Temperatures, High Pressures. 44, p. 475-481, (2015)
- 5.) A. Schmon; K. Aziz; G. Pottlacher:
Density determination of liquid copper and liquid nickel by means of fast resistive pulse heating and electromagnetic levitation
Metallurgical and Materials Transactions / A., 46, p. 2674 - 2679, (2015)
DOI: 10.1007/s11661-015-2844-1
- 4.) K. Aziz; A. Schmon; G. Pottlacher: Measurement of surface tension of liquid copper by means of electromagnetic levitation

High Temperatures, High Pressures. 43, p. 193 - 200, (2014)

- 3.) G. Pottlacher; A. Schmon; K. Aziz:

Investigation of liquid metallic elements and alloys by means of containerless techniques

Journées Annuelles De La SF2M 2012, Matériaux & Techniques. 100, p. 1 - 9, (2012)

- 2.) G. Pottlacher; K. Aziz; A. Schmon:

Thermophysical characteristics of liquid metals and alloys at TU Graz: a status report

High Temperatures, High Pressures. 43, 5, p. 377-394, (2012)

- 1.) A. Schmon; H. Reschab; T. Hüpf; J. Rattenberger; G. Pottlacher:

Thermophysical characteristics of CuMnNi alloys in the temperature range from 1000 K to 1900 K

High Temperatures, High Pressures. 40, 3-4, p. 291-300, (2011)

The publication manuscripts of the two main publications relating to this thesis (publication 5 and 7) are given below:

Publication:

Density Determination of Liquid Copper and Liquid Nickel by Means of Fast Resistive Pulse Heating and Electromagnetic Levitation

A. Schmon, K. Aziz and G. Pottlacher

Metallurgical and Materials Transactions A, 46(6):2674–2679, 2015.

The following manuscript, belonging to this publication, describes the results obtained for the liquid phase densities of copper and nickel by using the pulse-heating setting and the electromagnetic levitation apparatus. The paper was written by the author of this thesis. Experiments regarding density determination using the fast resistive pulse-heating method were performed by the author of this thesis. Investigations applying the electromagnetic levitation apparatus were performed by K. Aziz and the author of this thesis. G. Pottlacher was the supervisor in this project. Together with the author of this thesis K. Aziz and G. Pottlacher were involved in all decisions, especially regarding the review of the final publication manuscript.

**Density determination of liquid copper and liquid nickel
by means of fast resistive pulse-heating and electromagnetic levitation**

A. Schmon, K. Aziz, G. Pottlacher

Institute of Experimental Physics, Graz University of Technology, NAWI Graz, 8010 Graz,
Austria
E-mail: alexander.schmon@tugraz.at

Abstract. Fast resistive pulse-heating techniques and electromagnetic levitation techniques are capable of determining thermophysical properties of metals in the liquid phase. These properties have become increasingly important as input data for modern numerical simulations. Among others density is a very relevant parameter for e.g. casting modelling.

Density determinations of copper and nickel in their liquid states are performed using a fast resistive pulse-heating setup and a recently build up electromagnetic levitation apparatus. Both methods use optical imaging techniques to determine thermal expansion of the specimen under investigation, but are operating at very different experimental durations.

The pulse-heating setup provides a heating of the sample by using it as part of an electrical discharge circuit. Heating-rates of 10^8 K/s lead to experimental durations of about 60 μ s. Temperature is determined by measuring surface radiance emitted from the sample by a pyrometer. The sample's thermal expansion is monitored by an adapted CCD camera system.

The electromagnetic levitation apparatus enables noncontact investigations of samples by levitating and heating them by an induction coil generating inhomogeneous electromagnetic fields. Temperature again is determined by a pyrometer. For thermal expansion determination shadowgraph-images are recorded with a high-speed CCD camera and evaluated with an edge detection algorithm. Thermal expansion then is calculated by averaging several 1000 frames for each temperature point. Investigations of copper and nickel in the liquid state were performed with both techniques and are compared to each other and to literature values.

Introduction

Intense reactivity of liquid metals especially at high temperatures poses a challenge for creating investigation settings preventing interactions of the sample material with its environment. Containerless investigation techniques have been developed to avoid experimental difficulties such as chemical interactions between specimens and the container, heat transfer problems and loss of mechanical strength.

The workgroup of thermophysics and metalphysics at TU Graz has applied pulse-heating experiments on metals at high temperatures in terms of a containerless measuring method for about 35 years and published about 100 papers dealing with the investigation of thermophysical properties of a multitude of metals and alloys (determination of electrical properties of metals described e.g. in [1,2,3]).

1/10

At present one focus is on determining density of liquid metals using the pulse-heating setup for heating the specimens up to the end of their liquid phase and performing thermal expansion measurements simultaneously. In addition an electromagnetic levitation apparatus was built up recently to perform containerless thermal expansion measurements in a much longer time regime.

Both methods use shadowgraph imaging techniques to determine thermal expansion but are different in their approach to reduce and avoid interactions with the environment. Interactions at pulse-heating are minimized by reducing the experimental duration to about 60 μs , requiring an adapted CCD camera system capable of recording several images during this short period. The levitation method, in contrast, creates a contact-free investigation setup by levitating the specimen, allowing experimental durations of several minutes in an inert gas atmosphere.

Copper and nickel were chosen for investigation because literature data of densities in the liquid state up to high temperatures are available for these two metals as reference data compilations [4,5] and allow comparisons with both within this work described techniques.

Experimental

The pulse-heating technique and the levitation technique avoid resistive self-heating of the specimen by generating electrical currents in the material for heating. Thus electrical conductivity of the material under investigation is required.

The pulse-heating discharge circuit mainly consists of a capacitor bank (500 μF) as energy storage, high voltage mercury vapor ignitron tubes as fast electric switches to control the experimental process and a discharge chamber with windows to afford optical monitoring (the setup is described in detail in earlier publications [6,7]). In the experiment a current of approximately 10.000 A is discharged over the vertically aligned wire specimen leading to heating rates of about 10^8 K/s. The specimen is heated from room temperature, 296 K (23°C), to the end of its liquid phase in about 60 μs . During this short time the sample's geometry is preserved allowing investigations of the entire liquid phase of the specimen until boiling point is reached. As ambient atmosphere nitrogen with a pressure of 2.3 bar is used.

For temperature determination the surface radiance of the specimen is detected by a pyrometer (according to ITS-90 [8]) operating at 1570 nm (bandwidth of approx. 85 nm). The melting plateau (characteristic plateau in the voltage signal of the pyrometer indicating the melting transition) is used as reference point and temperature calculated deploying Planck's law and using the assumption of a constant normal spectral emissivity in the entire liquid phase (discussed in [9]). For thermal expansion measurement a combination of multi-channel-plate and CCD array is used [10]. The wire specimen is backlit by a photoflash and magnified shadowgraph images are recorded by the monitoring system. The channel-plate acts as amplifier and sets the exposure time (700 ns). The CCD array records and stores the images. To increase the recording rate the CCD itself is used as buffer memory by restricting the exposure area of the CCD array to 16 pixel lines and using the remaining (576 pixel lines in total) as fast writeable storage (middle picture in Figure 1). Thereby images can be recorded about every 5 μs . The slow readout process can be done after the pulse-heating experiment.

For evaluation every image is displayed as intensity profile (left picture in Figure 1). The width of the profile, determined by FWHM (full width at half maximum), corresponds to the cross section of the wire specimen. Thermal radial expansion is obtained through relating the image series recorded during the heating process to the image series recorded prior starting the pulse heating. As this setting monitors

a section of the wire under investigation, only the radial expansion of the wire is determined. Experiments by Hüpf [11] substantiate that in the setup at TU Graz no longitudinal expansion of the clamped wire occurs provided that the applied heating rate is set high enough. Using a camera able to monitor the entire wire (but only one picture during one experiment) Cagran [12] recorded pictures while performing pulse-heating experiments with different heating rates, depicted in Figure 2. If the heating rate was too small a longitudinal expansion and bending of the wire could be observed. If the heating was rapid enough no longitudinal expanding could be noticed anymore. This behaviour can be seen as well when recording only a section of the wire with the present setting. The bending of the wire specimen can be seen in the image series by depicting the buffer memory of the CCD array (see right picture in Figure 1). In case of no observable longitudinal expansion an increased radial expansion can be monitored instead. Hence in the recent past the thermal radial expansion measurement was used to determine thermal volume expansion.

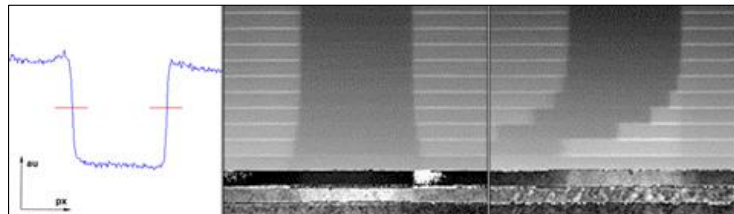


Figure 1: Illustrations of the radial expansion measurements by recording a section of the wire. The left picture depicts the intensity profile dedicated to one single recorded picture monitored by the exposure area restricted to 16 pixel lines. The middle picture shows the image series buffered in the storage area of the CCD array, consisting of pictures recorded in time intervals of about 5 μ s. The right picture shows the image series when using a too low heating rate leading to a bending of the wire specimen.

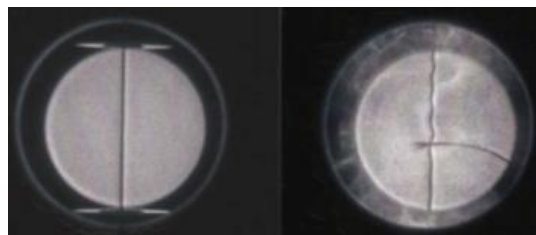


Figure 2: Pictures illustrating the different expansion behaviours of wire specimens during pulse-heating when using different heating rates (pictures recorded by Claus Cagran). This figure is reprinted with permission from *Thermal Conductivity 30/Thermal Conductivity 18*, 2010. Lancaster, PA: DEStech Publications, Inc [11]. The left picture displays a straight wire maintaining its shape and exhibiting no longitudinal expansion. The right picture depicts the expansion behaviour when using a too small heating rate. The wire exhibits longitudinal expansion and bending. (Wire is contacted by knife-edges for voltage-drop measurements, which is the nearly horizontal aligned contact viewable in the right picture).

The electromagnetic levitation setup uses a water-cooled copper coil to heat and levitate the specimen by generating high-frequency inhomogeneous electromagnetic fields (200 kHz). A levitated liquid specimen is depicted in Figure 3 (left picture). Eddy currents induced in the specimen material heat the sample due to its ohmic resistance and electromagnetic forces lift the sample toward regions of lower field strength. The coil (design of the coil according the work of [13, 14]) is positioned in a vacuum chamber equipped with windows for optical diagnostics and provided with a moveable sample holder to position the specimen before levitating is initiated (detailed description in [15]). To achieve an oxygen-reduced environment (750 mbar during the experiment) the chamber is purged with a mixture of argon, helium and a small amount of hydrogen (less than 4 %). As heating and levitating are linked with each other temperature is controlled by cooling the sample with an adjusted gas flow of helium to the sample through a cooling nozzle.

Temperature is determined by measuring the sample's surface radiance by a pyrometer (according to ITS-90 [8]) operating at 1600 nm (bandwidth of approx. 150 nm) using the melting plateau as the reference point and assuming a constant normal spectral emissivity in the liquid phase. For thermal volume expansion determination shadowgraph images of the lifted sample are recorded with a high-speed CCD camera (1024 x 1024 pixels, frame rate of 120 fps). The sample is backlit by a LED-panel (100 W at about 520 nm) provided with a diffuser to obtain a homogenous background illumination. To improve the contrast of the recorded images an interference filter removes contributions due to the thermal self-radiation of the sample.

Each recorded image shows a droplet slightly deformed (see the middle picture in Figure 3). If the deviations from the equilibrium shape are small compared to the sample's diameter, the equilibrium shape can be calculated by averaging several 1000 images. In this case 2500 images for each temperature point are used. The images are evaluated using edge detection algorithms calculating the point of inflection of the radial brightness distribution belonging to each image. The volume is calculated with the assumption of an axially symmetric shape (with respect to the vertical axis) and with the known mass of the sample (measured before and after the experiment) density is determined.

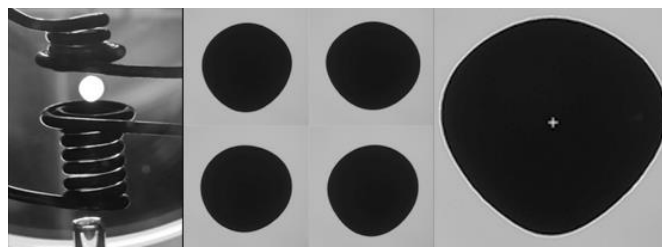


Figure 3: Pictures illustrating the levitation process and density determination by recording shadowgraph images of the levitated specimen. The left picture shows the liquid specimen levitated and heated by electromagnetic fields generated by a water-cooled copper coil. The middle picture depicts 4 out of 2500 shadowgraph images recorded per temperature point to calculate the volume of the spherical specimen. The silhouette is determined using edge detection algorithms depicted in the right picture.

Results

Thermal expansion measurements of copper and nickel were performed applying the two afore described investigation setups. Specimen materials: Cu-slugs: 99.9999 % (purch. from Alfa Aesar, LOT: E15Y023) and Cu-wire: 99.996 % (purch. from Advent, No: Cu510815); Ni-slugs: 99.995 % (purch. from Alfa Aesar, LOT: L29X008) and Ni-wire: 99.98 % (purch. from Advent, No: Ni535315).

As reference points to calibrate the pyrometer signals melting temperature values of $T_m = 1358$ K (1085°C) [8] for copper and of $T_m = 1728$ K (1455°C) [16] for nickel were adopted. For pulse-heating wire shaped specimens with a diameter of 0.5 mm and approx. 50 mm in length were used. Sample sizes for levitating were adjusted attaining spherical droplets with cross sections of about 6 mm in the liquid phase. Thermal expansion measurements obtained by pulse-heating technique are evaluated according the approach described above taking the increased radial expansion as basis to calculate thermal volume expansion and thereof density ($\frac{V}{V_0} = \frac{d^2}{d_0^2}$, with $\frac{V}{V_0}$ the relative volume expansion and $\frac{d}{d_0}$ the relative radial expansion of the wire).

Figure 4 presents the results of the density determinations on copper. Data obtained by the pulse-heating technique and the levitation technique are compared. Additionally literature reference data of Assael et al. [4] merging density results of several different measuring techniques are depicted. The linear least square fit of the pulse-heating results ensues to

$$D_{\text{pulse}}(T) = 9132 - 0.874 \cdot T \quad 1450 \text{ K (1177°C)} < T < 2400 \text{ K (2127°C)} \quad (1)$$

and of the results from the levitation technique to

$$D_{\text{levi}}(T) = 8903 - 0.790 \cdot T \quad 1355 \text{ K (1082°C)} < T < 1710 \text{ K (1437°C)} \quad (2)$$

Corresponding density values of both techniques are given in Table 1.

Uncertainties are estimated (using a coverage factor $k = 2$) to: D_{pulse} : 5.2 %, D_{levi} : 1.5 %. (Reference data of Assael et al. [4] plotted in Figure 4 is given with an uncertainty of 1.3 %). Deviations due to a possible change of normal spectral emissivity during the liquid phase are not considered.

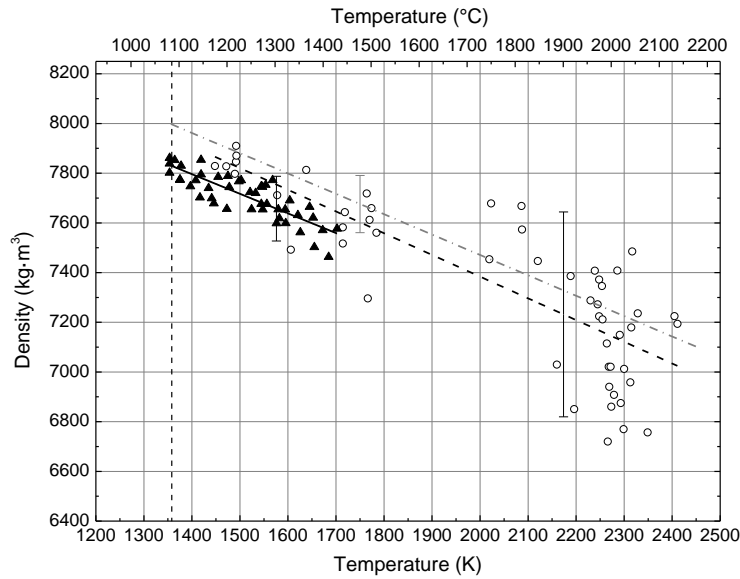


Figure 4: Density of liquid copper as function of temperature. Open circles with respective dashed line: results for density with linear least square fit by using the pulse-heating technique. Full triangles with respective solid line: results for density with dedicated linear least square fit determined by the levitation method. Dash-dotted line in gray: literature data for comparison [4]. Vertical dashed line: temperature of phase transition, 1358 K (1085°C).

Table 1: Density results of liquid copper determined with the pulse-heating technique (D_{pulse}) and the levitation technique (D_{levi}). And literature reference data (D_{ref}) of Assael et al. [4].

Data obtained by pulse-heating and levitating				Reference Data of Assael et al. [4]		
Temperature (K)	Temperature (°C)	D_{pulse} (kg·m ⁻³)	D_{levi} (kg·m ⁻³)	Temperature (K)	Temperature (°C)	D_{ref} (kg·m ⁻³)
1355	1082		7833	1356	1083	7998
1400	1127		7797	1400	1127	7962
1450	1177	7865	7758	1450	1177	7921
1500	1227	7821	7718	1500	1227	7881
1550	1277	7777	7679	1550	1277	7840
1600	1327	7734	7639	1600	1327	7799
1650	1377	7690	7600	1650	1377	7758
1700	1427	7646	7560	1700	1427	7717
1750	1477	7603		1750	1477	7676
1800	1527	7559		1800	1527	7635
1850	1577	7515		1850	1577	7594
1900	1627	7471		1900	1627	7553
1950	1677	7428		1950	1677	7512
2000	1727	7384		2000	1727	7471
2050	1777	7340		2050	1777	7430
2100	1827	7297		2100	1827	7389
2150	1877	7253		2150	1877	7348

2200	1927	7209	2200	1927	7307
2250	1977	7166	2250	1977	7266
2300	2027	7122	2300	2027	7225
2350	2077	7078	2350	2077	7184
2400	2127	7034	2400	2127	7143

Figure 5 presents the density determinations on nickel. Results obtained by the pulse-heating technique and the levitation technique are plotted for comparison, and literature reference data of Assael et al. [5] are depicted. The linear least square fit of the pulse-heating data results to

$$D_{\text{pulse}}(T) = 9274 - 0.838 \cdot T \quad 1755 \text{ K } (1482^\circ\text{C}) < T < 2600 \text{ K } (2327^\circ\text{C}) \quad (3)$$

and of the levitation technique to

$$D_{\text{levi}}(T) = 10157 - 1.325 \cdot T \quad 1705 \text{ K } (1432^\circ\text{C}) < T < 1940 \text{ K } (1667^\circ\text{C}) \quad (4)$$

Corresponding density values of both techniques are given in

Table 2.

Uncertainties are estimated (using a coverage factor $k = 2$) to: D_{pulse} : 3.5 %, D_{levi} : 1.6 %. (Reference data of Assael et al. [5] plotted in Figure 4 is given with an uncertainty of 1.7 %). Deviations due to a possible change of normal spectral emissivity during the liquid phase are not considered.

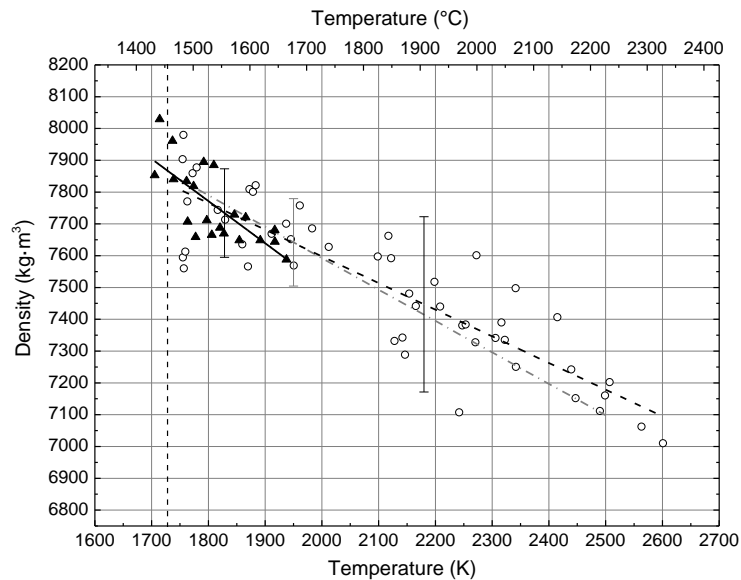


Figure 5: Density of liquid nickel as function of temperature. Open circles with respective dashed line: results for density with linear least square fit by using the pulse-heating technique. Full triangles with respective solid line: results for density with dedicated linear least square fit determined by the levitation method. Dash-dotted line in gray: literature data for comparison [5]. Vertical dashed line: temperature of phase transition, 1728 K (1455°C).

Table 2: Density results of liquid nickel determined with the pulse-heating technique (D_{pulse}) and the levitation technique (D_{levi}). And literature reference data (D_{ref}) of Assael et al. [5].

Data obtained by pulse-heating and levitating				Reference Data of Assael et al. [5]		
Temperature (K)	Temperature (°C)	D_{pulse} (kg·m ⁻³)	D_{levi} (kg·m ⁻³)	Temperature (K)	Temperature (°C)	D_{ref} (kg·m ⁻³)
1705	1432		7898			
1750	1477	7808	7838	1750	1477	7839
1800	1527	7766	7772	1800	1527	7790
1850	1577	7724	7706	1850	1577	7740
1900	1627	7682	7640	1900	1627	7691
1950	1677	7640	7573	1950	1677	7642
2000	1727	7598		2000	1727	7592
2050	1777	7556		2050	1777	7543
2100	1827	7514		2100	1827	7493
2150	1877	7472		2150	1877	7444
2200	1927	7430		2200	1927	7395
2250	1977	7389		2250	1977	7345
2300	2027	7347		2300	2027	7296
2350	2077	7305		2350	2077	7246
2400	2127	7263		2400	2127	7197
2450	2177	7221		2450	2177	7148
2500	2227	7179		2500	2227	7098
2550	2277	7137				
2600	2327	7095				

Discussion

The density results of copper, plotted in Figure 4 and nickel, plotted in Figure 5 show a good agreement with the literature reference compilations of Assael et al. [4,5] within the stated uncertainties.

Anyhow for copper the data obtained from pulse-heating show large scattering. The high electrical conductivity and low mechanical strength of copper demand large heating currents and high heating rates at pulse-heating to avoid bending of the wire-specimens (as described in chapter experimental). This leads to short experimental durations and less pronounced intensity profiles compared to the data obtained for nickel.

Data for nickel obtained by the levitation technique exhibit more spread compared to levitation data for copper. Reason is a more pronounced tendency to perform surface oscillations of the levitated droplet in case of nickel that can't be canceled out completely by averaging.

Comparing the data of the two used measuring techniques the different advantages offered by pulse-heating or electromagnetic levitating are apparent. Due to long experimental durations (compared with pulse-heating) data obtained by the levitation method exhibit low uncertainties. The pulse-heating technique in contrast offers the ability to obtain data in a temperature range unattainable to other

techniques, but in turn the sample is destroyed when reaching the boiling point (and exploding to a steam of nanometer sized particles).

The good concordance of pulse-heating data in comparison to results obtained by the levitation method and literature as well substantiate the assumption that no longitudinal expansion of the clamped wire specimen occurs during pulse-heating when using a sufficiently high heating rate. The increased thermal radial expansion occurring instead represents the thermal volume expansion of the specimen. More precise measurements are recommended to confirm this assumption to be definitely right (for instance through applying an image recording system with exposure times below 100 ns). Anyhow, calculating the volume expansion from the increased radial expansion is affirmed to be practicable for pulse-heating.

Conclusion

Density results of liquid copper and liquid nickel were presented using the two different investigation setups based on fast resistive pulse-heating and electromagnetic levitation and are compared to literature reference data. As literature data of density at high temperatures are scarce the extension of the respectively research at TU Graz to alloys as well as the further improvement of the measuring techniques are in process.

Acknowledgment

We are grateful for the interchange of scientific equipment between Institute of Materials Physics in Space, German Aerospace Center (DLR), Linder Höhe, 51147 Köln, Germany and Institute of Experimental Physics, Graz University of Technology, Petersgasse 16, 8010 Graz, Austria.

The project Measurement of surface tension and density by means of levitation is supported by the Austrian Science Fund (FWF) - Project P 23838-N20

References

- [1] E. Kaschnitz, G. Pottlacher and H. Jäger: *Int. Journal of Thermophysics*, 1992, vol 13 (4), pp. 699-710
- [2] B. Wilthan, C. Cagran and G. Pottlacher: *Int. Journal of Thermophysics*, 2005, vol 26, pp. 1017-1029
- [3] T. Hüpf, C. Cagran, G. Lohöfer and G. Pottlacher: *Journal of Physics/Condensed matter*, 2008, vol 98, pp. 82-85
- [4] M. J. Assael, A. E. Kalyva, K. D. Antoniadis, R. M. Banish, I. Egry, J. Wu, E. Kaschnitz and W. A. Wakeham: *Journal of Physical and Chemical Reference Data*, 2010, vol. 39 (3), pp. 033105 1-8
- [5] M. J. Assael, A. E. Kalyva, K. D. Antoniadis, R. M. Banish, I. Egry, J. Wu, E. Kaschnitz and W. A. Wakeham: *High Temp.-High Press.*, 2012, vol. 41, pp. 161-184
- [6] C. Cagran, T. Hüpf, B. Wilthan, G. Pottlacher: *High Temp.-High Press.*, 2008, vol. 37, pp. 205-219

- [7] C. Cagran, B. Wilthan, G. Pottlacher, B. Roebuck, M. Wickins and R. A. Harding: *Intermetallics*, 2003, vol. 11, pp. 1327-1334
- [8] H. Preston-Thomas: *Metrologia*, 1990, vol. 27, pp. 3-10
- [9] C. Cagran, C. Brunner, A. Seiffter and G. Pottlacher: *High Temp.-High. Press.*, 2002, vol. 34, pp. 669-679
- [10] T. Hüpf, C. Cagran, E. Kaschnitz and G. Pottlacher: *Thermochemica Acta*, 2009, vol. 494, pp. 40-44
- [11] T. Hüpf and G. Pottlacher: *Thermal Conductivity 30 – Thermal Expansion 18*, 2010, Ed. D. S. Gaal, ISBN No. 978-1-60595-015-0, pp. 192–206
- [12] C. Cagran: *Thermal Conductivity and Thermal Diffusivity of Liquid Copper*, 2000, Diploma Thesis, TU Graz
- [13] J. Brillo and I. Egry: *Int. Journal of Thermophysics*, 2003, vol. 24 (4), pp. 1155-1170
- [14] G. Lohöfer, J. Brillo and I. Egry: *Int. Journal of Thermophysics*, 2004, vol. 25 (5), pp. 1535-1550
- [15] K. Aziz, A. Schmon and G. Pottlacher: *High Temp.-High Press.*, 2014, vol. 43, pp. 193-200
- [16] D. R. Lide: *CRC Handbook of Chemistry and Physics 88th edition*, 2007

Publication:Thermophysical Properties of Manganin (Cu₈₆Mn₁₂Ni₂)
in the Solid and Liquid State

A. Schmon, K. Aziz, M. Luckabauer and G. Pottlacher

International Journal of Thermophysics, 36:1618–1626, 2015.

The following manuscript, belonging to this publication, describes a set of thermophysical properties of Manganin obtained by employing four different examination setups. Solidus and liquidus temperatures were determined using a differential thermal analysis system. In the solid, temperature dependent electrical resistivity was determined using a four-point probe setting positioned in a furnace. Density in the solid was measured applying a high-resolution two-beam laser dilatometer. Liquid phase properties of enthalpy, isobaric heat capacity, electrical resistivity, density, thermal conductivity and thermal diffusivity were determined using a fast resistive pulse-heating system.

The paper was written by the author of this thesis. Experiments regarding the investigations of the liquid phase were performed by the author of this thesis, as well as solid state investigations using the four-point probe setting. Differential thermal analysis experimentation was operated by K. Aziz and the author of this thesis. Experiments applying the two-beam laser dilatometer were performed by M. Luckabauer. G. Pottlacher was the supervisor in this project. Together with the author of this thesis K. Aziz and G. Pottlacher were involved in all decisions. The co-authors assisted the review of the final publication manuscript.

Thermophysical properties of Manganin (Cu₈₆Mn₁₂Ni₂) in the solid and liquid state

A. Schmon¹, K. Aziz¹, M. Luckabauer², G. Pottlacher¹

¹Institute of Experimental Physics, NAWI Graz, Graz University of Technology, 8010 Graz, Austria

²Institute of Materials Physics, NAWI Graz, Graz University of Technology, 8010 Graz, Austria

Email: alexander.schmon@tugraz.at

Abstract

Manganin is the trademark name of the alloy Cu₈₆Mn₁₂Ni₂. Despite its frequent usage in manufacturing processes literature data are scarce particularly at higher temperatures. This work presents a set of thermophysical data of this alloy in a temperature range above its classic area of application up to the end of its liquid phase.

For investigating the alloy four examination setups were employed. Using DTA solidus and liquidus temperatures were obtained. In the solid phase electrical resistivity as function of temperature was determined by a four-point-probe positioned in a furnace. Thermal expansion was measured with a high-resolution two beam laser-dilatometer based on Michelson-interferometry and thereby density was calculated.

The liquid state was investigated using a μ s-ohmic-pulse-heating setup. Wire shaped specimens were resistively volume heated as part of an electrical discharge circuit. Measured quantities were the current through the specimen, the voltage drop along the specimen, the surface radiance by a pyrometer and the thermal expansion with an adapted CCD camera system. On the basis of these measurements temperature-dependent thermophysical properties of enthalpy, isobaric heat capacity, electrical resistivity and density are obtained. Additionally thermal conductivity and thermal diffusivity are estimated in the high temperature range applying the Wiedemann-Franz law.

Introduction

The alloy Cu₈₆Mn₁₂Ni₂ (Manganin®¹) is a resistance alloy known for its virtually temperature independent electrical resistivity in the temperature range between 0°C and 100°C. The electrical resistivity - temperature curve shows a flat, slight parabolic shape with a maximum near room temperature. The low temperature coefficient of resistivity, long term

¹ trademark proprietor:
'Isabellenhütte Heusler GmbH & Co. KG'

stability and rather low thermal conductivity ($22 \text{ W}\cdot\text{m}^{-1}\cdot\text{K}^{-1}$ at 20°C) [1] make it a commonly used material for manufacturing ammeter shunts or measuring lines. Moreover this alloy shows a small relative Seebeck coefficient against copper [2] which minimizes disturbing influences caused by temperature differences at contact points.

Experimentation at high temperatures has to deal with difficulties such as chemical reactions, evaporation, heat transfer, loss of mechanical stability etc. One way to minimize interactions with the environment is to reduce the experimental duration. A fast resistive pulse-heating method is applied at TU Graz that facilitates investigations of electrically conducting samples in the high temperature range by performing short-term studies. Investigation times of only about $60 \mu\text{s}$ permit an examination of the specimen under containerless conditions and the determination of thermophysical properties up to temperatures of several thousand centigrade. This makes this method well suited for investigating the liquid state as contaminations of the specimens and heat losses can be considered negligible. For examining the solid phase the appliance of steady state techniques is more convenient as their large investigation times provide measurements of higher resolution.

Within this study, thermophysical properties of Manganin in the liquid phase like specific enthalpy, electrical resistivity, isobaric heat capacity and density have been measured using the pulse-heating technique. Electrical resistivity and density of the solid state were determined using the steady-state techniques of a four-point-probe setup and a two-beam laser-dilatometer respectively.

Experimental methods

The fast resistive pulse-heating technique is based on the approach to heat a sample due to its ohmic resistance by applying a high electrical current pulse. In the apparatus at TU Graz (schematic depicted in Figure 1) a wire shaped specimen is clamped (vertically aligned) in the center of a discharge chamber filled with an inert gas atmosphere (nitrogen, pressure of 2.3 bar), described in detail in [3, 4]. The passage of an electrical current of about 10,000 A leads to heating rates up to 10^8 K/s . Due to this rapid heating the specimen maintains its cylindrical shape even in the liquid phase until the boiling point is reached where the specimen explodes as result of the intense volume increase. [5, 6, 7]

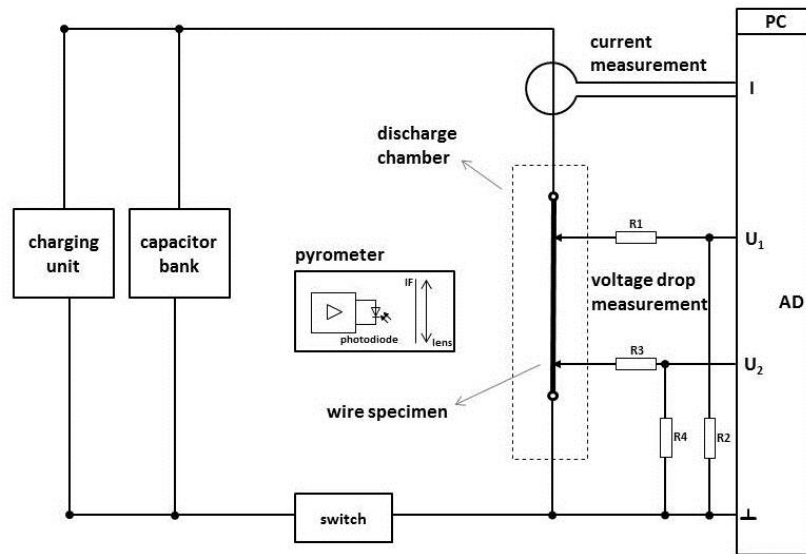


Figure 1: Schematic description of the pulse-heating setup. The capacitor bank (500 μF) is charged by a high voltage generator. The wire shaped specimen is resistively volume heated as part of the electrical discharge circuit. Current is measured by an induction coil, voltage drop is determined by two knife-edge contacts and surface radiance is detected using a pyrometer (working at 1570 nm).

During this process which typically takes between 40 μs and 60 μs several time-resolved quantities are measured simultaneously. The current through the wire sample is measured by an induction coil (from Person Electronics) with included real-time integration element. The voltage drop along a metered section of the wire is determined by two knife-edge contacts directly placed on the wire (both voltages are measured with respect to a known potential). For temperature determination (according to ITS-90 [8]) the surface radiance is detected using a pyrometer working at 1570 nm (bandwidth of approx. 85 nm). The melting plateau in the voltage output of the pyrometer (more precisely the mean of solidus and liquidus) is used as reference point and temperature is calculated assuming a constant normal spectral emissivity in the liquid phase (discussed in [9]). The thermal volume expansion of the specimen is recorded by an adapted CCD camera system consisting of a multi-channel-plate and CCD array combination [10]. The wire is backlit by a photoflash and shadowgraph images are recorded by the monitoring system about every 5 μs . For evaluation every image is displayed as an intensity profile and related to image series recorded prior starting the heating process. On the basis of the electrical measurements electrical resistivity and specific enthalpy can be calculated. From thermal volume expansion measurements density can be obtained.

The four-point-probe setup is used to perform accurate electrical resistivity measurements in the solid phase. Two pairs of electrodes are spot-welded onto a specimen of cylindrical shape. One pair of current carrying and one pair for voltage sensing arranged in between. Thereby wiring resistances and contact resistances are eliminated. The setting is constructed inside a radiation furnace under argon atmosphere. During a preset heating program a constant current of 300 mA with alternating direction of current is applied for voltage-drop metering. In this case a constant heating rate of 4 K/min was used.

The high-resolution laser dilatometer used, detailed description in [11], is based on a two-beam Michelson laser interferometer. Two laser beams (He-Ne laser, 632.8 nm) are reflected by two parallel, polished surfaces of a typically L-shaped specimen. The specimen is positioned in a radiation furnace to operate a preset heating program. For temperature control three thermocouples are spot-welded onto the specimen, which allow a monitoring of the temperature gradient along the specimen. By deploying a feedback temperature regulation using a supplemental furnace the temperature inhomogeneity along the specimen can be decreased below the accuracy limits of the thermocouples. Thereby a total length change measurement resolution of 10 nm can be achieved. The setting is placed in a vacuum chamber (pressure less than 10^{-6} mbar) equipped with a window to pass the laser beams. Dilatometric measurements in this case were performed applying a heating rate of 4 K/min.

Results and discussion

Solidus and liquidus temperatures were determined by differential thermal analysis (DTA), employing a STA 449 C Jupiter (Netzsch). Measurements, using a heating rate of 10 K/min, delivered a solidus temperature $T_s = 1177$ K and a liquidus temperature $T_l = 1269$ K (which agrees well with the manufacturer's data sheet stating a melting point of 1233 K [1]). For data evaluation additional a density at room temperature of 8400 kg m^{-3} was adopted [1].

Density:

Figure 2 presents the results of density as function of temperature obtained by laser dilatometer measurements in the solid and high-speed imaging during pulse-heating from the end of the solid to the end of the liquid phase. The linear least square fit in the solid phase (density expressed in $\text{kg}\cdot\text{m}^{-3}$) is

$$D_{\text{solid}}(T) = 8524 - 0.382 T - 0.135 \cdot 10^{-3} T^2 \quad 300 \text{ K} < T < 1070 \text{ K} \quad (1)$$

and in the liquid phase

$$D_{\text{liquid}}(T) = 8466 - 0.849 T \quad 1290 \text{ K} < T < 1860 \text{ K} \quad (2)$$

The resulting curves of the two measuring techniques match well at their point of encounter, at the end of the solid phase.

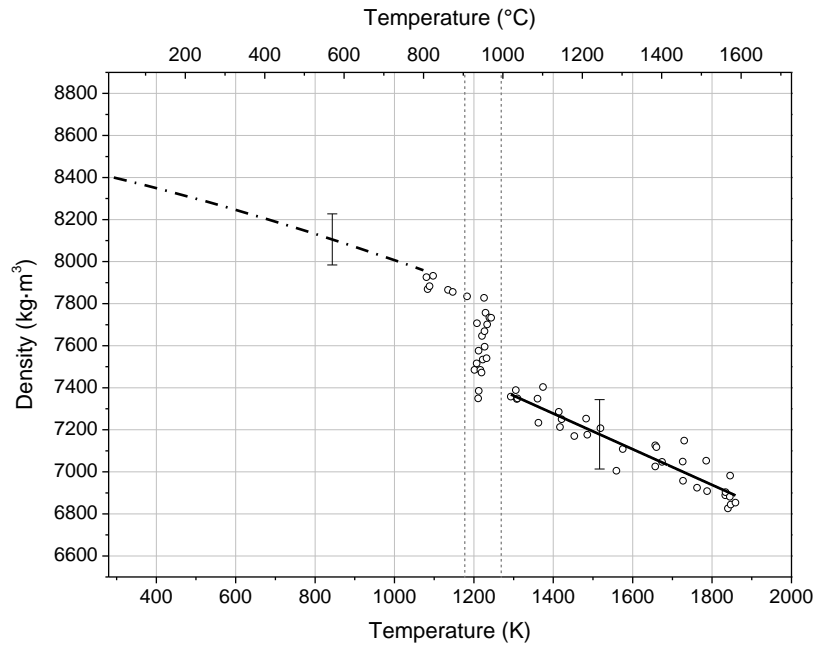


Figure 2: Density of Manganin as function of temperature. Open circles and solid line: results obtained by pulse-heating with respect linear least square fit in the liquid phase. Dash-dotted line: results obtained by dilatometer measurements. Vertical dashed lines: solidus temperature 1177 K and liquidus temperature 1269 K.

Electrical resistivity:

Electrical resistivity of Manganin as function of temperature is depicted in Figure 3. Four point probe measurements in the solid, from RT up to 1050 K, show a flat slightly decreasing resistance behaviour (dash-dotted line in the figure). The less pronounced temperature dependence of electrical resistivity, known from the vicinity of RT, is continued in the entire solid phase.

The polynomial least square fits, with resistivity expressed in $\mu\Omega\cdot\text{m}$, are:

$$\rho_{\text{solid}}(T) = 0.382 + 0.440 \cdot 10^{-3} T - 1.095 \cdot 10^{-6} T^2 + 0.834 \cdot 10^{-9} T^3 \quad 300 \text{ K} < T < 615 \text{ K} \quad (3)$$

$$\rho_{\text{solid}}(T) = 0.295 + 0.532 \cdot 10^{-3} T - 0.674 \cdot 10^{-6} T^2 + 0.276 \cdot 10^{-9} T^3 \quad 615 \text{ K} < T < 1050 \text{ K} \quad (4)$$

High temperature pulse-heating measurements deliver electrical data up to the end of the liquid phase. Electrical resistivity with initial specimen geometry ρ_{IG} (without considering thermal expansion) was calculated by:

$$\rho_{\text{IG}}(T) = \frac{U(T) r^2 \cdot \pi}{I(T) l} \quad (5)$$

with U : voltage drop, I : current, r : specimen radius at RT, l : specimen length at RT.

Taking into account thermal expansion of the specimen electrical resistivity in the liquid phase yields to (in $\mu\Omega\cdot\text{m}$):

$$\rho_{\text{liquid}}(T) = 0.412 + 0.587 \cdot 10^{-4} T \quad 1270 \text{ K} < T < 1860 \text{ K} \quad (6)$$

depicted by the solid line in Figure 3. During the melting transition $\rho_{\text{liquid}}(T)$ changes from $0.44 \mu\Omega\text{m}$ to $0.49 \mu\Omega\text{m}$, that is a change of resistivity of $\Delta\rho = 0.05 \mu\Omega\text{m}$.

In their region of overlap the results of four-point-probe and pulse-heating show a good agreement within the stated uncertainties.

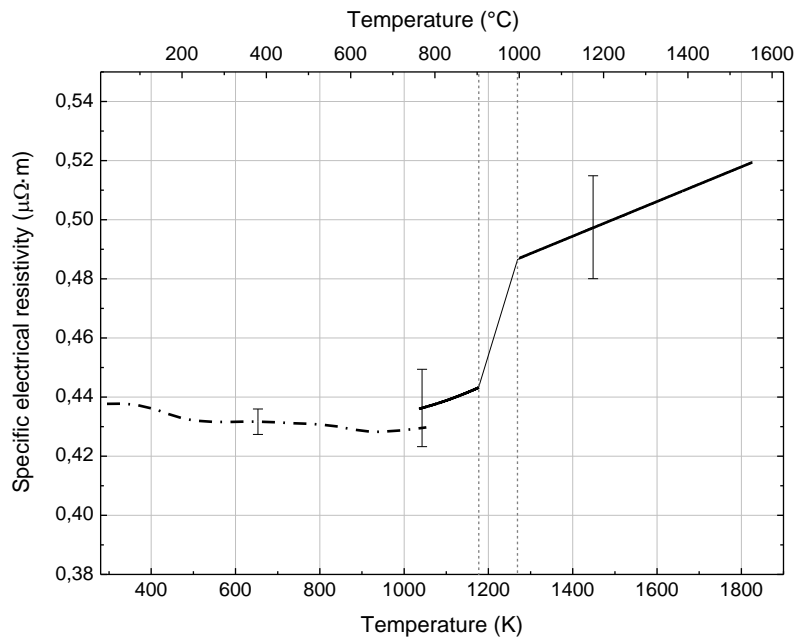


Figure 3: Electrical resistivity of Manganin as function of temperature. Solid line: results obtained by pulse-heating. Dash-dotted line: results obtained by four-point-probe measurements. Vertical dashed lines: solidus temperature 1177 K and liquidus temperature 1269 K.

Specific enthalpy:

Specific enthalpy as function of temperature can be calculated from the measured electrical signals during pulse-heating by:

$$H(t) = \frac{1}{m} \int U(t) \cdot I(t) dt \quad (5)$$

with m : mass of the specimen (obtained from geometry and density at RT), U : voltage drop along the specimen, I : current through the specimen.

Results of specific enthalpy are shown in Figure 4. Linear fit in the solid state (enthalpy expressed in $\text{kJ}\cdot\text{kg}^{-1}$) is

$$H_{\text{solid}}(T) = -247 + 0.581 T \quad 1050 \text{ K} < T < 1176 \text{ K} \quad (6)$$

and in liquid state

$$H_{\text{liquid}}(T) = -87 + 0.616 T \quad 1270 \text{ K} < T < 1860 \text{ K} \quad (7)$$

At the solidus enthalpy $H(T_s) = 436 \text{ kJ}\cdot\text{kg}^{-1}$ and at the liquidus $H(T_l) = 691 \text{ kJ}\cdot\text{kg}^{-1}$, yielding a heat of fusion $\Delta H = 255 \text{ kJ}\cdot\text{kg}^{-1}$. Isobaric heat capacity c_p can be obtained from the slope of the enthalpy-temperature function. Heat capacity in the solid state is obtained to $c_{p,s} = 581 \text{ J}\cdot\text{kg}^{-1}\cdot\text{K}^{-1}$ and in the liquid to $c_{p,l} = 616 \text{ J}\cdot\text{kg}^{-1}\cdot\text{K}^{-1}$. The heat capacity in the solid is limited to a small temperature range proximate near melting and should be considered as a rough estimate.

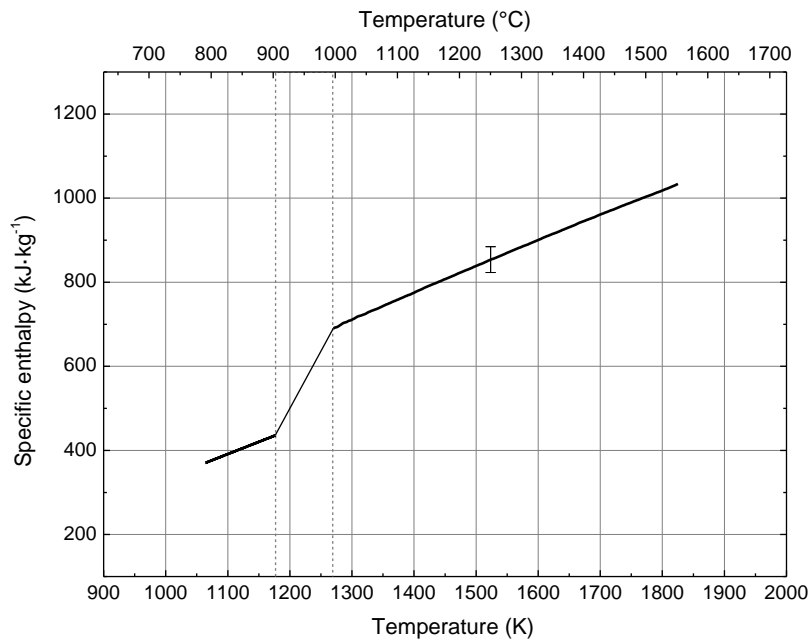


Figure 4: Specific enthalpy of Manganese as function of temperature obtained by the pulse-heating technique. The slope of the curve represents the isobaric heat capacity; the enthalpy change during melting describes the heat of fusion. Vertical dashed lines: solidus temperature 1177 K and liquidus temperature 1269 K

Thermal conductivity and thermal diffusivity:

Thermal conductivity λ is estimated applying the Wiedemann-Franz law which states that the ratio of thermal conductivity and electrical conductivity of a metal is proportional to temperature based on the free electron model (Drude model):

$$\lambda(T) = \frac{L \cdot T}{\rho(T)}$$

with L: Lorenz-number, $\rho(T)$: electrical resistivity.

The theoretical Lorenz-number of $2.45 \cdot 10^{-8} \text{ V}^2\text{K}^{-2}$ was used as approximation, although the Lorenz-number can vary for different metals and especially for alloys [12]. Results for thermal conductivity in the high temperature range are depicted in Figure 5. Linear fit in the solid state near melting (thermal conductivity expressed in $\text{W}\cdot\text{K}^{-1}\cdot\text{m}^{-1}$) is

$$\lambda_{\text{solid}}(T) = 7.875 + 4.864 \cdot 10^{-2} T \quad 1050 \text{ K} < T < 1176 \text{ K} \quad (8)$$

and in the liquid state

$$\lambda_{\text{liquid}}(T) = 13.476 + 3.991 \cdot 10^{-2} T \quad 1270 \text{ K} < T < 1860 \text{ K} \quad (9)$$

Thermal diffusivity a is estimated by:

$$a(T) = \frac{\lambda(T)}{c_p(T) \cdot D(T)}$$

with c_p : isobaric heat capacity, $D(T)$: density.

As the behaviour of thermal diffusivity is very similar to thermal conductivity, it is not depicted graphically. The linear fits in the solid and liquid states (thermal diffusivity expressed in $10^{-5} \text{ m}^2\cdot\text{s}^{-1}$) are:

$$a_{\text{solid}}(T) = 0.043 + 0.122 \cdot 10^{-2} T \quad 1050 \text{ K} < T < 1176 \text{ K} \quad (10)$$

$$a_{\text{liquid}}(T) = -0.009 + 0.111 \cdot 10^{-2} T \quad 1270 \text{ K} < T < 1860 \text{ K} \quad (11)$$

Since we obtain only one constant value for the isobaric heat capacity c_p in the solid phase the validity of thermal diffusivity in the solid is limited to a temperature range close to melting.

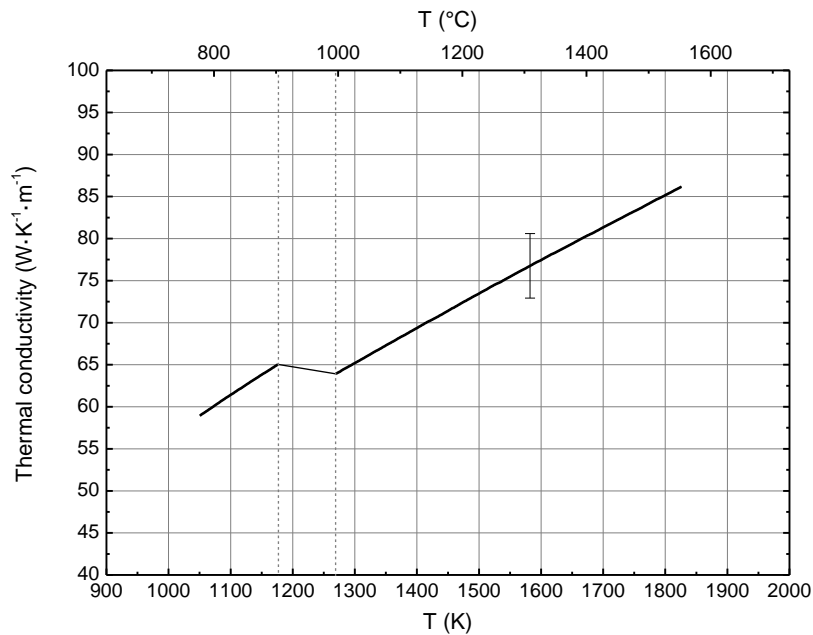


Figure 5: Thermal conductivity of Manganin as function of temperature estimated applying the Wiedemann-Franz law (with $L = 2.45 \cdot 10^{-8} \text{ V}^2 \text{K}^{-2}$). Vertical dashed lines: solidus temperature 1177 K and liquidus temperature 1269 K.

Uncertainty

Uncertainties are estimated according to GUM [13], using a coverage factor $k = 2$, to: solidus and liquidus temperatures $\Delta T: \pm 6 \text{ K}$; density $D_{\text{solid}}: 1.5 \%$ and $D_{\text{liquid}}: 2.2 \%$; specific electrical resistivity $\rho_{\text{solid}}: 1 \%$ and $\rho_{\text{liquid}}: 3.6 \%$, specific enthalpy $H_{\text{solid}}: 3.9 \%$ and $H_{\text{liquid}}: 3.5 \%$; thermal conductivity $\lambda: 5 \%$; thermal diffusivity: $\alpha: 8 \%$.

Conclusion

Pulse-heating, laser-dilatometer, four-point-probe and DTA measurements were performed to obtain thermophysical properties of Manganin. Among the presented results, density, specific electrical resistivity and specific enthalpy were given in the temperature range between 300 K and 1860 K. Although the high temperature range is not the classic area of application of this alloy, this work aims to improve the scarce literature database above RT up to higher temperatures.

References

- [1] Manganin® manufacturer's online datasheet, http://www.isabellenhuetten.de/uploads/media/MANGANIN_02.pdf, accessed Feb 10, 2015
- [2] K. D. D. Rathnayaka, *Journal of Physics E: Sci. Instrum.* **18**, 380 (1985)
- [3] E. Kaschnitz, G. Pottlacher, H. Jäger, *Int. Journal of Thermophysics* **13**, 699 (1992)
- [4] B. Wilthan, C. Cagran, C. Brunner, G. Pottlacher, *Thermochimica acta* **415**, 47-54 (2004)
- [5] B. Wilthan, C. Cagran, G. Pottlacher, *Int. Journal of Thermophysics* **26**, 1017 (2005)
- [6] C. Cagran, T. Hüpf, B. Wilthan, G. Pottlacher, *High Temp.-High Press.* **37**, 205 (2008)
- [7] C. Cagran, B. Wilthan, G. Pottlacher, B. Roebuck, M. Wickins, R. A. Harding, *Intermetallics* **11**, 1327 (2003)
- [8] H. Preston-Thomas, *Metrologia* **27**, 3 (1990)
- [9] C. Cagran, C. Brunner, A. Seifert, G. Pottlacher, *High Temp.-High. Press.* **34**, 660 (2002)
- [10] T. Hüpf, G. Pottlacher, *Thermal Conductivity 30 – Thermal Expansion 18*, Ed. D. S. Gaal, ISBN No. 978-1-60595-015-0, 192 (2010)
- [11] M. Luckabauer, U. Kühn, J. Eckert, W. Sprengel, *Phys. Rev. B.* **89**, 174113 (2014)
- [12] P. G. Klemens, R. K. Williams, *Int. Met. Rev.* **31**, 197 (1986)
- [13] ISO, *Guide to the Expression of Uncertainty in Measurement*, Geneva (1993)

Bibliography

- [1] S. D. Veazey and W. C. Roe. Review: Density measurements in liquid metals and liquid binary alloy systems - a survey. *Journal of Materials Science*, 7:445–466, 1972.
- [2] A. F. Crawley. Densities of liquid metals and alloys. *International Metallurgical Reviews*, 19(1):32–48, 1974.
- [3] J. W. Shaner. Thermal expansion of metals over the entire liquid range. In *Thermal Expansion 6*, pages 69–82. Springer, 1978.
- [4] T. Iida. The physical properties of liquid metals. *Clarendon Press Oxford*, pages 78–89, 1988.
- [5] J. Blumm and J. Henderson. Measurement of the volumetric expansion and bulk density of metals in the solid and molten regions. *High Temp.-High Press.*, 32(1):109–113, 2000.
- [6] L. W. Wang, Q. S. Mei, et al. Density measurement of liquid metals using dilatometer. *J. Mater. Sci. Technol.*, 22(4):569–571, 2006.
- [7] V. I. Kovalchuk and S. S. Dukhin. Dynamic effects in maximum bubble pressure experiments. *Colloids and Surfaces A: Physicochemical and Engineering Aspects*, 192(1):131–155, 2001.
- [8] I. Egry, E. Ricci, R. Novakovic, and S. Ozawa. Surface tension of liquid metals and alloys—recent developments. *Advances in colloid and interface science*, 159(2):198–212, 2010.
- [9] M. Hajirahimi, F. Mokhtari, and A. H. Fatollahi. New identities for sessile

- drops. *Applied Mathematics and Mechanics*, 36 (3), 2014.
- [10] S. Srinivasan, G. H. McKinley, and R. E. Cohen. Assessing the accuracy of contact angle measurements for sessile drops on liquid-repellent surfaces. *Langmuir*, 27(22):13582–13589, 2011.
- [11] R. W. Hyers and J. R. Rogers. A review of electrostatic levitation for materials research. *High Temperature Materials and Processes*, 27(6):461–474, 2008.
- [12] T. Ishikawa, J. T. Okada, Watanabe Y., et al. Thermophysical property measurements of high temperature melts using an electrostatic levitation method. *Japanese Journal of Applied Physics*, 50(11S):11RD03, 2011.
- [13] E. H. Trinh and K. Ohsaka. Measurement of density, sound velocity, surface tension, and viscosity of freely suspended supercooled liquids. *Int. Journal of Thermophysics*, 16(2):545–555, 1995.
- [14] D. M. Herlach, R. F. Cochrane, I. Egry, H. J. Fecht, and A. L. Greer. Containerless processing in the study of metallic melts and their solidification. *International Materials Reviews*, 38(6):273–347, 1993.
- [15] I. Egry. Containerless processing for thermophysical property measurements of liquid metals: review and outlook. *High Temp.-High Press.*, 40:203–214, 2011.
- [16] A. Goodwin, K. N. Marsh, and W. A. Wakeham. *Measurement of the thermodynamic properties of single phases*, volume 6. Elsevier, 2003.
- [17] J. Brillo, G. Lohoefer, F. Schmidt-Hohagen, and S. Schneider. Thermophysical property measurements of liquid metals by electromagnetic levitation. *International Journal of Materials and Product Technology*, 26(3):247–273, 2006.
- [18] I. Egry, G. Lohoefer, and S. Sauerland. Measurements of thermophysical properties of liquid metals by noncontact techniques. *Int. Journal of Thermophysics*, 14(3):573–584, 1993.

- [19] L. Wang, A. Xian, and H. Shao. Density measurement of liquid indium and zinc by the gamma-ray attenuation method. *High Temp. - High Press.*, 35/36:659–665, 2003/2007.
- [20] W. D. Drotning. Thermal expansion of iron, cobalt, nickel and copper at temperatures up to 600 K above melting. *High Temp. - High Press.*, 13:441–458, 1981.
- [21] E. Kaschnitz, G. Pottlacher, and H. Jaeger. A new microsecond pulse-heating system to investigate thermophysical properties of solid and liquid metals. *Int. Journal of Thermophysics*, 13(4):699–710, 1992.
- [22] B. Wilthan, C. Cagran, C. Brunner, and G. Pottlacher. Thermophysical properties of solid and liquid platinum. *Thermochimica Acta*, 415:47–54, 2004.
- [23] F. Sachsenhofer. Data evaluation for pulse heating experiments combined with emissivity measurements using a division-of-amplitude photopolarimeter. Master’s thesis, Institute of Experimental Physics, TU Graz, 2000.
- [24] B. Wilthan, C. Cagran, and G. Pottlacher. Combined dsc and pulse-heating measurements of electrical resistivity and enthalpy of tungsten, niobium, and titanium. *Int. Journal of Thermophysics*, 26(4):1017–1029, 2005.
- [25] C. Cagran, T. Huepf, B. Wilthan, and G. Pottlacher. Selected thermophysical properties of Hf-3%Zr from 2200K to 3500K obtained by a fast pulse-heating technique. *High Temp.-High Press.*, 37:205–219, 2008.
- [26] C. Cagran, B. Wilthan, G. Pottlacher, B. Roebuck, M. Wickins, and R.A. Harding. Thermophysical properties of a Ti-44%Al-8%Nb-1%B alloy in the solid and molten states. *Intermetallics*, 11:1327 – 1334, 2003.
- [27] C. Cagran. *Untersuchung des Emissionsverhaltens flüssiger Metalle mittels Photopolarimetrie und Mehrwellenlängenpyrometrie*. PhD thesis, TU Graz, 2004.
- [28] M. Kurz. Modifizierung eines Pyrometers für die Messung der Strahlungsin-

- tensität im Bereich der Schmelztemperatur von Aluminium. Master's thesis, TU Graz, 2012.
- [29] C. Claus, C. Brunner, A. Seifert, and Pottlacher G. Liquid-phase behaviour of normal spectral emissivity at 684.5 nm of some selected metals. *High Temp.-High Press.*, 34(6):669–679, 2002.
- [30] P. G. Klemens and R. K. Williams. Thermal conductivity of metals and alloys. *Int. Metals Reviews*, 31(5):197–215, 1986.
- [31] G. Pottlacher and T. Huepf. A review of expansion measurements for subsecond ohmic pulse-heating experiments. In *Thermal Conductivity 30: Thermal Expansion 18: Joint Conferences: August 29-September 2, 2009, Pittsburgh, Pennsylvania, USA*, volume 30, page 192. DEStech Publications, Inc, 2010.
- [32] T. Huepf. *Density Determination of Liquid Metals*. PhD thesis, TU Graz, 2010.
- [33] T. Macher. Modernisierung einer ohmschen Pulsheizapparatur zur Bestimmung thermophysikalischer Daten von Metallen in der flüssigen Phase. Master's thesis, TU Graz, 2014.
- [34] K. Aziz. *Surface Tension Measurements of Liquid Metals and Alloys by the Oscillating Drop Technique in Combination with an Electromagnetic Levitation Device*. PhD thesis, TU Graz, 2016.
- [35] K. Aziz, A. Schmon, and G. Pottlacher. Measurement of surface tension of liquid copper by means of electromagnetic levitation. *High Temp.-High Press.*, 43:193–200, 2014.
- [36] K. Aziz, A. Schmon, and G. Pottlacher. Measurement of surface tension of liquid nickel by the oscillating drop technique. *High Temp.-High Press.*, 44:475–481, 2015.
- [37] K. Aziz, A. Schmon, E. Kaschnitz, J. Rattenberger, and G. Pottlacher. Measurement of surface tension of Cu-5Sn by an oscillating drop - levitation technique. *Int. Journal of Thermophysics*, 37:1–8, 2016.

-
- [38] O. Muck, German patent no. 42204 (Oct. 30, 1923).
- [39] P. Rony. *The electromagnetic levitation of metals*. PhD thesis, University of California, 1964.
- [40] S. Y. Shiraishi and R. G. Ward. The density of nickel in the superheated and supercooled liquid states. *Canadian Metallurgical Quarterly*, 3:117–122, 1964.
- [41] E. Fromm and H. Jehn. Electromagnetic forces and power absorption in levitation melting. *Brit. J. Appl. Phys.*, 16:653–663, 1965.
- [42] D. L. Cummings and D. A. Blackburn. Oscillations of magnetically levitated aspherical droplets. *Journal of Fluid Mechanics*, 224:395–416, 1991.
- [43] P. V. R. Suryanarayana and Y. Bayazitoglu. Effect of static deformation and external forces on the oscillations of levitated droplets. *Physics of Fluids A*, 3:967–977, 1991.
- [44] S. Sauerland, G. Lohoefer, and I. Egry. Surface tension measurements on levitated liquid metal drops. *Journal of Non-Crystalline Solids*, 156:833–836, 1993.
- [45] G. Lohoefer, P. Neuhaus, and I. Egry. Tempus: a facility for measuring the thermophysical properties of undercooled liquid metals. *High Temp.-High Press.*, 23(3):333–342, 1991.
- [46] R. F. Brooks and K. C. Mills. Measurement of the thermophysical properties of melts by a levitated-drop method. *High Temp.-High Press.*, 25(6):657–664, 1993.
- [47] E. Gorges, L. M. Ruez, A. Schillings, and I. Egry. Density measurements on levitated liquid metal droplets. *Int. Journal of Thermophysics*, 17(5):1163–1172, 1996.
- [48] J. Brillo and I. Egry. Density determination of liquid copper, nickel, and their alloys. *Int. Journal of Thermophysics*, 24(4):1155–1170, 2003.

- [49] S. I. Bakhtiyarov and D. A. Siginer. Electromagnetic levitation part I: Theoretical and experimental considerations. *Fluid Dynamics and Materials Processing*, 4(2):99–112, 2008.
- [50] G. Lohoefer and S. Schneider. Heat balance in levitation melting: The influence of sample cooling by heat conduction. *High Temp.-High Press.*, 44:147–162, 2015.
- [51] S. Sauerland, K. Eckler, and I. Egry. High-precision surface tension measurements on levitated aspherical liquid nickel droplets by digital image processing. *Journal of Materials Science Letters*, 11(6):330–333, 1992.
- [52] D. R. Lide. CRC Handbook of Chemistry and Physics. *CRC Press*, 88th edition, 2007.
- [53] T. Huepf, C. Cagran, G. Lohoefer, and G. Pottlacher. Electrical resistivity of high temperature metallic melts - Hf-3% Zr, Re, Fe, Co, and Ni. *High Temp.-High Press.*, 37:239–246, 2008.
- [54] M. J. Assael, A. E. Kalyva, D. A. Konstantinos, R. M. Banish, I. Egry, J. Wu, E. Kaschnitz, and W. A. Wakeham. Reference data for the density and viscosity of liquid antimony, bismuth, lead, nickel and silver. *High Temp.-High Press.*, 41:161–184, 2012.
- [55] A. Schmon, K. Aziz, and G. Pottlacher. Density determination of liquid copper and liquid nickel by means of fast resistive pulse heating and electromagnetic levitation. *Metallurgical and Materials Transactions A*, 46(6):2674–2679, 2015.
- [56] H. Preston-Thomas. The international temperature scale of 1990 (ITS-90). *Metrologia*, 27:3–10, 1990.
- [57] C. Cagran, A. Seifert, and G. Pottlacher. Thermophysical properties of solid and liquid copper. *Schriften des Forschungszentrums Jülich, Series Energy Technology*, 15:763–766, 2000.
- [58] M. J. Assael, A. E. Kalyva, D. A. Konstantinos, R. M. Banish, I. Egry, J. Wu,

- E. Kaschnitz, and W. A. Wakeham. Reference data for the density and viscosity of liquid copper and liquid tin. *Journal of Physical and Chemical Reference Data*, 39(3):033105, 2010.
- [59] M. J. Assael, K. Kakosimos, R. M. Banish, J. Brillo, I. Egry, R. Brooks, P. N. Quested, K. C. Mills, A. Nagashima, Y. Sato, and W. A. Wakeham. Reference data for the density and viscosity of liquid aluminum and liquid iron. *Journal of Physical and Chemical Reference Data*, 35(1):285–300, 2006.
- [60] A. Schmon, K. Aziz, M. Luckabauer, and G. Pottlacher. Thermophysical properties of manganin (Cu₈₆Mn₁₂Ni₂) in the solid and liquid state. *Int. Journal of Thermophysics*, 36:1618–1626, 2015.
- [61] M. Boivineau, C. Cagran, D. Doytier, V. Eyraud, M. H. Nadal, B. Wilthan, and G. Pottlacher. Thermophysical properties of solid and liquid Ti-6Al-4V (TA6V) alloy. *Int. Journal of Thermophysics*, 27(2):507–529, 2006.
- [62] J. J. Z. Li, W. L. Johnson, and W.-K. Rhim. Thermal expansion of liquid Ti-6Al-4V measured by electrostatic levitation. *Applied Physics Letters*, 89:111913, 2006.
- [63] B. Wilthan. *Verhalten des Emissionsgrades und thermophysikalische Daten von Legierungen bis in die flüssige Phase mit einer Unsicherheitsanalyse aller Messgrößen*. PhD thesis, TU Graz, 2005.
- [64] G. Lohoefer. Nonuniform electric fields in pulse heated wires. *Int. Journal of Thermophysics*, 14(3):471–483, 1993.
- [65] C. Cagran. *Untersuchung des Emissionsverhaltens flüssiger Metalle mittels Photopolarimetrie und Mehrwellenlängenpyrometrie*. PhD thesis, TU Graz, 2004.

List of Figures

2.1	Depiction of the the Archimedean method	5
2.2	Depiction of the push-rod dilatometer functionality	7
2.3	Illustration of the maximum bubble pressure method	9
2.4	Depiction of a sessile drop profile	10
2.5	Depiction of a constraint drop	11
3.1	Experimental setup of the pulse-heating system	18
3.2	Circuit diagram of the pulse-heating setup	19
3.3	Pulse-heating wire specimen positioned in the sample holder	21
3.4	Schematic cross section of the pulse-heating pyrometer	23
3.5	Schematic depiction of the image intensifier arrangement	25
3.6	Image recording procedure at pulse-heating	26
3.7	Illustration of the storage area of the CCD array	27
3.8	Experimental time schedule at pulse-heating	28
3.9	Flow diagram illustrating the relationship between quantities	29
3.10	Pyrometersignal as function of experimental duration	34
3.11	Shadowgraph image sequence evaluation	36
3.12	Full width at half maximum evaluation	37
3.13	Wire expansion at different heating rates	39
3.14	Wire expansion for density determination	40
3.15	CCD images at different heating rates	42
3.16	Relationship specimen diameters and image widths	44
4.1	Illustration of electromagnetic levitating	48
4.2	Schematic depiction of the levitation apparatus	50
4.3	Picture of the built-up levitation apparatus	52
4.4	Picture of a typical levitation coil	53

4.5	Levitation coil construction	56
4.6	Schematic depiction of the thermal expansion measurement setting	57
4.7	Images of a levitated liquid sample	58
4.8	Schematic illustration of the individual pixel indication	60
4.9	Center of mass determination	61
4.10	Illustration of the edge curve evaluation	63
4.11	Depiction of the calculated equilibrium shape	64
4.12	Relationship volume in pixel to volume in mm	65
5.1	Density of nickel obtained by pulse-heating	70
5.2	Density of liquid nickel - comparison of results	72
5.3	Density of copper obtained by pulse-heating	75
5.4	Density of liquid copper - comparison of results	77
5.5	Density of aluminium obtained by pulse-heating	80
5.6	Density of liquid aluminium - comparison of results	82
5.7	Density of Manganin as function of temperature	85
5.8	Density of TiAl6V4 as function of temperature	90
6.1	Estimated expanded uncertainty with and without skin-effect . . .	94
6.2	Illustration of temperature uncertainty contribution	95